

Trends in Renewable Energy

Volume 3, Issue 1, June 2017



Cover image: a biogas plant, see article by Mézes, Bai *et al.* in this issue.



futureenergysp.com
thefutureenergy.org

Trends in Renewable Energy

ISSN: 2376-2136 (Print) ISSN: 2376-2144 (Online)

<http://futureenergysp.com/>

Trends in Renewable Energy is an open accessed, peer-reviewed semi-annual journal publishing reviews and research papers in the field of renewable energy technology and science.

The aim of this journal is to provide a communication platform that is run exclusively by scientists working in the renewable energy field. Scope of the journal covers: Bioenergy, Biofuel, Biomass, Bioprocessing, Biorefinery, Biological waste treatment, Catalysis for energy generation, Energy conservation, Energy delivery, Energy resources, Energy storage, Energy transformation, Environmental impact, Feedstock utilization, Future energy development, Green chemistry, Green energy, Microbial products, Physico-chemical process for Biomass, Policy, Pollution, Renewable energy, Smart grid, Thermo-chemical processes for biomass, etc.

The Trends in Renewable Energy publishes the following article types: peer-reviewed reviews, mini-reviews, technical notes, short-form research papers, and original research papers.

The article processing charge (APC), also known as a publication fee, is fully waived for the Trends in Renewable Energy.

Editorial Team of Trends in Renewable Energy

EDITOR-IN-CHIEF

Dr. Bo Zhang

P.E., Prof. of Chemical Engineering, Editor, Trends in Renewable Energy, United States

HONORARY CHAIRMEN

Dr. Yong Wang

Voiland Distinguished Professor, The Gene and Linda Voiland School of Chemical Engineering and Bioengineering, Washington State University, United States

Dr. Mahendra Singh Sodha

Professor, Lucknow University; Former Vice Chancellor of Devi Ahilya University, Lucknow University, and Barkatulla University; Professor/Dean/HOD/Deputy Director at IIT Delhi; Padma Shri Award; India Professor of Industrial Chemistry, CEO of Eurochem Engineering srl, Italy

Dr. Elio Santacesaria

VICE CHAIRMEN

Dr. Mo Xian

Prof., Assistant Director, Qingdao Institute of BioEnergy and Bioprocess Technology, Chinese Academy of Sciences, China

Dr. Changyan Yang

Prof., School of Chemical Engineering & Pharmacy, Wuhan Institute of Technology, China

EDITORS

Dr. Yiu Fai Tsang,

Associate Prof., Department of Science and Environmental Studies, The Education University of Hong Kong

Dr. Melanie Sattler

Dr. Syed Qasim Endowed Professor, Dept. of Civil Engineering, University of Texas at Arlington, United States

Dr. Attila Bai

Associate Prof., University of Debrecen, Hungary

Prof. Christophe Pierre Ménézo

University of Savoy Mont-Blanc, France

Dr. Moinuddin Sarker

MCIC, FICER, MInstP, MRSC, FARSS., VP of R & D, Head of Science/Technology Team, Natural State Research, Inc., United States Associate Prof., Biomass Processing Laboratory, Centre for Biofuel and Biochemical Research, Green Technology Mission Oriented Research, Universiti Teknologi PETRONAS, Malaysia

Dr. Suzana Yusup

University of Illinois at Urbana-Champaign, United States

Dr. Zewei Miao

Pfizer Inc., United States

Dr. Hui Wang

North Carolina Agricultural and Technical State University, United States

Dr. Shuangning Xiu

Associate Prof., Institute of Chemical Industry of Forest Products, China

Dr. Junming XU

Academy of Forest, China

Dr. Hui Yang

Prof., College of Materials Science and Engineering, Nanjing Tech University, China

Dr. Ying Zhang

Associate Prof., School of Chemistry and Materials Science, University of Science and Technology of China, China

Dr. Ming-Jun Zhu

Prof., Assistant Dean, School of Bioscience & Bioengineering, South China University of Technology, China

MANAGING EDITOR

Dr. Bo Zhang

P.E., Prof. of Chemical Engineering, Editor, Trends in Renewable Energy, United States

EDITORIAL BOARD

Dr. Elena Lucchi	Politecnico di Milano, Italy
Dr. Muhammad Mujtaba Asad	Faculty of Technical and Vocational Education, Universiti Tun Hussein Onn Malaysia, Malaysia
Dr. Afzal Sikander	Associate Prof., Department of Electrical Engineering, Graphic Era University, India
Dr. Padmanabh Thakur	Professor and Head, Department of Electrical Engineering, Graphic Era University, India
Dr. K. DHAYALINI	Professor, Department of Electrical and Electronics Engineering, K. Ramakrishnan College of Engineering, Tamilnadu, India
Shangxian Xie	Texas A&M University, United States
Dr. Tanmoy Dutta	Sandia National Laboratories, United States
Dr. Efstathios Stefanos	Pontifical Catholic University of Ecuador, Faculty of Exact and Natural Sciences, School of Physical Sciences and Mathematics, Ecuador
Dr. Xin Wang	Texas A&M University, United States
Dr. Rami El-Emam	Assist. Prof., Faculty of Engineering, Mansoura University, Egypt
Dr. Rameshprabu Ramaraj	School of Renewable Energy, Maejo University, Thailand
Dr. ZAFER ÖMER ÖZDEMİR	Kirklareli University, Technology Faculty, Turkey
Dr. Vijay Yeul	Chandrapur Super Thermal Power Station, India
Dr. Mohanakrishna Gunda	VITO - Flemish Institute for Technological Research, Belgium
Dr. Shuai Tan	Georgia Institute of Technology, United States
Shahabaldin Rezanian	Universiti Teknologi Malaysia (UTM), Malaysia
Dr. Madhu Sabnis	Contek Solutions LLC, Texas, United States
Dr. Qiangu (Jeremy) Yan	Mississippi State University, United States
Dr. Mustafa Tolga BALTA	Associate Prof., Department of Mechanical Engineering, Faculty of Engineering, Aksaray University, Turkey
Dr. María González Alriols	Associate Prof., Chemical and Environmental Engineering Department, University of the Basque Country, Spain
Dr. Nattaporn Chaiyat	Assist. Prof., School of Renewable Energy, Maejo University, Thailand
Dr. Nguyen Duc Luong	Institute of Environmental Science and Engineering, National University of Civil Engineering, Vietnam
Mohd Lias Bin Kamal	Faculty of Applied Science, Universiti Teknologi MARA, Malaysia
Dr. N.L. Panwar	Assistant Prof., Department of Renewable Energy Engineering, College of Technology and Engineering, Maharana Pratap University of Agriculture and Technology, India
Dr. Caio Fortes	BASF, Brazil
Dr. Flavio Praticco	Department of Methods and Models for Economics, Territory and Finance, Sapienza University of Rome, Italy
Dr. Wennan ZHANG	Docent (Associate Prof.) and Senior Lecturer in Energy Engineering, Mid Sweden University, Sweden
Dr. Ing. Stamatis S. Kalligeros	Assistant Prof., Hellenic Naval Academy, Greece
Carlos Rolz	Director of the Biochemical Engineering Center, Research Institute at Universidad del Valle, Guatemala
Ms. Liliash Makashini	Copperbelt University, Zambia
Dr. Ali Mostafaeipour	Assistant Prof., Industrial Engineering Department, Yazd University, Iran
Dr. Camila da Silva	Prof., Maringá State University, Brazil
Dr. Anna Skorek-Osikowska	Silesian University of Technology, Poland
Dr. Shek Atiqure Rahman	Sustainable and Renewable Energy Engineering, College of Engineering, University of Sharjah, Bangladesh
Dr. Emad J Elnajjar	Associate Prof., Department of Mechanical Engineering, United Arab Emirates University, United Arab Emirates
Dr. Xianglin Zhai	Poochon Scientific LLC, United States
Dr. Rui Li	North Carolina Agricultural and Technical State University, United States

Dr. Adam Elhag Ahmed	National Nutrition Policy Chair, Department of Community Services, College of Applied Medical Sciences, King Saud University, Saudi Arabia
Dr. Srikanth Mutnuri	Associate Prof., Department of Biological Sciences, Associate Dean for International Programmes and Collaboration, Birla Institute of Technology & Science, India
Dr. Bashar Malkawi	S.J.D., Associate Prof., College of Law, University of Sharjah, United Arab Emirates
Dr. Simona Silvia Merola	Istituto Motori - National Research Council of Naples, Italy
Dr. Hakan Caliskan	Faculty of Engineering, Department of Mechanical Engineering, Usak University, Turkey

Table of Contents

Volume 3, Issue No. 1, June 2017

Editorials

Our Journal is Moving Forward

Bo Zhang.....1

Articles

Power Systems Stability through Piecewise Monotonic Data Approximations – Part 1: Comparative Benchmarking of L1PMA, L2WPMA and L2CXCV in Overhead Medium-Voltage Broadband over Power Lines Networks

Athanasios G. Lazaropoulos2-32

Power Systems Stability through Piecewise Monotonic Data Approximations – Part 2: Adaptive Number of Monotonic Sections and Performance of L1PMA, L2WPMA, and L2CXCV in Overhead Medium-Voltage Broadband over Power Lines Networks

Athanasios G. Lazaropoulos33-60

Optimization of Raw Material Composition in an Agricultural Biogas Plant

Lili Mézes, Attila Bai, Dávid Nagy, István Cinka, Zoltán Gabnai.....61-75

A Comparison of Energy Consumption in Hydrothermal Liquefaction and Pyrolysis of Microalgae

Bo Zhang, Jinsheng Wu, Zhao Deng, Changyan Yang, Chang Cui, Yigang Ding.....76-85

Reviews

Characterization, Modification and Application of Biochar for Energy Storage and Catalysis: A

Review

Shuangning Xiu, Abolghasem Shahbazi, Rui Li86-101

Our Journal is Moving Forward

Happy New Year to all enthusiastic authors and editorial team members. The Trends in Renewable Energy (TRE) successfully concluded the second volume, and heading to another year. We deeply appreciate your support, and are looking forward to continuously working with all colleagues around the world.

The 2016 TRE Author of the Year Award goes to Dr. Athanasios G. Lazaropoulos at the National Technical University of Athens, Greece. Dr. Lazaropoulos contributed over 10 high quality papers to our journal during last two years. The great support of the authors encourages us to improve.

The 2016 TRE Paper of the Year goes to “A Review of Hydrothermal Carbonization of Carbohydrates for Carbon Spheres Preparation” (DOI: 10.17737/tre.2015.1.1.009). Within a short period of time, this paper received 6 citations including 3 external citations. Both the effort of authors and the power of open-access showed impacts to the renewable energy field.

During last two years, we have been accumulating knowledge of running a scientific journal. Now is the time to move forward. We are pursuing to be indexed in renowned indexes, such as the Directory of Open Access Journals (DOAJ), the Science Citation Index (SCI of Web of Science Core Collection), and Ei Compendex.

To prepare this journal to pass the evaluations conducted by multiple indexes, the journal is now an open accessed, peer-reviewed semi-annual journal with completely Free-of-Charge publication policy (*i.e.* no cost to authors and readers). We will continue the TRE’s mission to publish quality reviews, original research, and application-oriented papers, providing a communication platform that is run exclusively by scientists working in the renewable energy field. Papers are invited on any individual topic related to renewable energy or those that are interdisciplinary.

Bo Zhang
Editor in Chief
January 1, 2017



This work is licensed under a [Creative Commons Attribution 4.0 International License](https://creativecommons.org/licenses/by/4.0/).

Power Systems Stability through Piecewise Monotonic Data Approximations – Part 1: Comparative Benchmarking of L1PMA, L2WPMA and L2CXCVC in Overhead Medium-Voltage Broadband over Power Lines Networks

Athanasios G. Lazaropoulos*

*School of Electrical and Computer Engineering / National Technical University of Athens /
9 Iroon Polytechniou Street / Zografou, GR 15780*

Received October 20, 2016; Accepted November 11, 2016; Published January 1, 2017

This first paper assesses the performance of three well-known piecewise monotonic data approximations (*i.e.*, L1PMA, L2WPMA, and L2CXCVC) during the mitigation of measurement differences in the overhead medium-voltage broadband over power lines (OV MV BPL) transfer functions.

The contribution of this paper is triple. First, based on the inherent piecewise monotonicity of OV MV BPL transfer functions, L2WPMA and L2CXCVC are outlined and applied during the determination of theoretical and measured OV MVBPL transfer functions. Second, L1PMA, L2WPMA, and L2CXCVC are comparatively benchmarked by using the performance metrics of the percent error sum (PES) and fault PES. PES and fault PES assess the efficiency and accuracy of the three piecewise monotonic data approximations during the determination of transmission BPL transfer functions. Third, the performance of L1PMA, L2WPMA, and L2CXCVC is assessed with respect to the nature of faults —*i.e.* faults that follow either continuous uniform distribution (CUD) or normal distribution (ND) of different magnitudes—.

The goal of this set of two papers is the establishment of a more effective identification and restoration of the measurement differences during the OV MV BPL coupling transfer function determination that may significantly help towards a more stable and self-healing power system.

Keywords: Smart Grid; Intelligent Energy Systems; Broadband over Power Lines (BPL) networks; Power Line Communications (PLC); Faults; Fault Analysis; Fault Identification and Prediction; Power System Stability; Distribution Power Grids

1. Introduction

In recent years, the broadband over powerlines (BPL) technology has attracted significant popularity as a connectivity solution in homes and a provider of various smart grid related applications [1]. More specifically, the deployment of BPL networks across the vintage transmission and distribution power grids transforms them into an intelligent IP-based communications network further enhancing power system stability [2], [3]. Among the characteristics of this communications network, its low-cost deployment and potential of broadband last mile access through its wired/wireless interfaces render the

*Corresponding author: AGLazaropoulos@gmail.com

BPL technology both as a useful power grid complement and a strong telecommunications competitor to wireless networking solutions [4].

Thanks to the HomePlug Powerline Alliance, which is leading the standardization process of the BPL technology, more than 100 million BPL devices with an annual growth rate of 30% have already been deployed and are able to deliver high-bandwidth applications (e.g., HD video streaming and VoIP) with data rates that exceed 1Gbps [5]-[7]. To achieve these data rates, various inherent BPL deficiencies, such as high and frequency-selective channel attenuation and noise, should be overcome [8]-[13].

As the determination of the transfer functions of overhead medium-voltage (OV MV) BPL networks is concerned in this paper, the well-established hybrid method, which is employed to examine the behavior of various multiconductor transmission line (MTL) structures, is also adopted in this paper [2], [8]-[12], [14]-[25]. Given the OV MV BPL network topology, OV MV MTL configuration, and the applied coupling scheme as inputs, the hybrid method gives as an output the corresponding transfer function.

Despite the theoretical accuracy of the hybrid method during the determination of OV MV BPL transfer functions, a number of practical reasons and “real-life” conditions may create measurement differences between experimental and theoretical results. On the basis of six measurement difference categories, which are analyzed in [2], [24], [25], OV MV BPL transfer functions are significantly distorted critically affecting the monitoring and surveillance of the distribution power grid. To mitigate the aforementioned measurement differences and restore the undistorted OV MV BPL transfer function, a piecewise monotonic data approximation is applied [26]-[33]. Until now, only L1PMA has been applied and examined in transmission and distribution BPL networks [2], [24], [25]. Here, another two piecewise monotonic data approximations by Demetriou are first applied and comparatively benchmarked in comparison with the already validated L1PMA; say, L2WPMA [34] and L2CXCV [35].

The rest of this paper is organized as follows: In Sec. II, the OV MV MTL configuration and the respective indicative OV MV BPL topologies are presented. Sec. III synthesizes the principles of BPL signal propagation and transmission across OV MV BPL topologies. In Sec. IV, a brief presentation of the L1PMA is given. Also, L2WPMA and L2CXCV are analytically outlined. In the same Section, the percent error sum (PES) and fault PES, which are applied in order to benchmark L1PMA, L2WPMA, and L2CXCV, are reported. Sec. V discusses the simulations of various OV MV BPL networks intending to mark out the efficiency of L1PMA, L2WPMA, and L2CXCV and to mitigate the occurred measurement differences. Sec. VI concludes this paper.

2. Distribution Power Grids

2.1 OV MV MTL Configuration

The overhead MV distribution lines, which are examined in this paper, are shown in Fig. 1(a) of [2]. Overhead MV distribution line consists of:

- *Phase lines*: These lines with radii $r_{MV,p}$ are hung at typical heights h_{MV} above ground. The three phase conductors of the OV MV MTL configuration are further spaced by Δ_{MV} .
- *Neutral conductors*: There are no neutral conductors in the examined OV MV MTL configuration.

As regards the overhead MV distribution line configuration, it consists of ACSR three-phase conductors [8], [9], [17]. Exact values concerning conductor properties and configuration geometries are reported in [19].

In accordance with [21], [36]-[38], the ground with conductivity $\sigma_g = 5 \text{ mS/m}$ and relative permittivity $\epsilon_{rg} = 13$ is considered as the reference conductor. The aforementioned ground parameters define a realistic scenario during the following analysis while the impact of imperfect ground on broadband signal propagation via OV MV power lines was analyzed in [8], [9], [17], [19], [21], [39]-[41].

2.2 Indicative OV MV BPL Topologies

In accordance with [8]-[12], [14]-[22], [36], [42]-[44] and with reference to Fig. 1, average path lengths of the order of 1,000m are considered in OV MV BPL topologies. Hence, the following four indicative OV MV BPL topologies, concerning end-to-end connections of average path lengths, are examined, namely:

1. A typical urban topology (OV MV urban case) with $N=3$ branches ($L_1=500\text{m}$, $L_2=200\text{m}$, $L_3=100\text{m}$, $L_4=200\text{m}$, $L_{b1}=8\text{m}$, $L_{b2}=13\text{m}$, $L_{b3}=10\text{m}$).
2. A typical suburban topology (OV MV suburban case) with $N=2$ branches ($L_1=500\text{m}$, $L_2=400\text{m}$, $L_3=100\text{m}$, $L_{b1}=50\text{m}$, $L_{b2}=10\text{m}$).
3. A typical rural topology (OV MV rural case) with only $N=1$ branch ($L_1=600\text{m}$, $L_2=400\text{m}$, $L_{b1}=300\text{m}$).
4. The “LOS” transmission along the same end-to-end distance $L=L_1+\dots+L_{N+1}=1000\text{m}$ when no branches are encountered. This topology corresponds to Line of Sight transmission in wireless channels.

The four indicative OV MV BPL topologies are going to be used so that the accuracy of L1PMA, L2WPMA, and L2CXCVC is evaluated in Sec. V.

The assumptions for the circuital parameters of OV MV BPL topologies, which are concerned in this paper, are the same as [2], namely: (i) The branch lines are assumed identical to the transmission ones; (ii) The interconnections between the transmission and branch conductors of the lines are fully activated; (iii) The transmitting and the receiving ends are assumed to match the characteristic impedance of the modal channels; and (iv) The branch terminations are assumed to be open circuits.

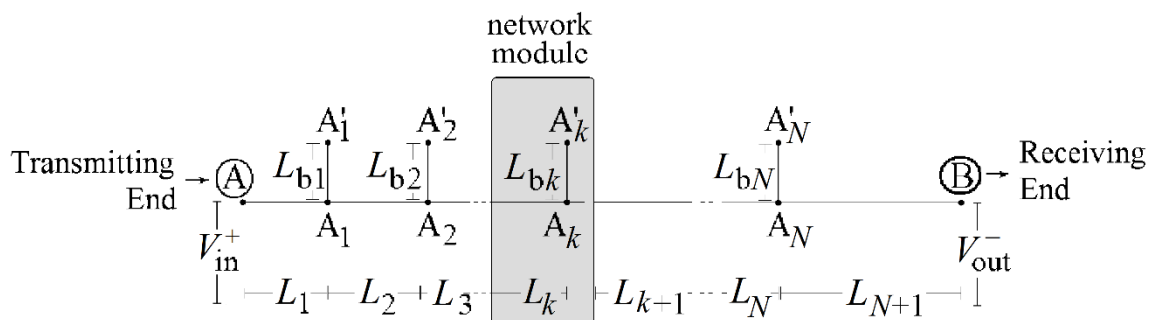


Figure 1. General OV MV BPL topology [2].

3. A Briefing of BPL Propagation and Transmission Analysis

3.1 Hybrid Method and Channel Transfer Function

The well-established hybrid method, which has been tested successfully in various transmission and distribution BPL networks [8]-[12], [14]-[23], [40]-[42], is also applied in this paper. Consisting of: (i) a bottom-up approach that is based on the MTL theory, eigenvalue decomposition (EVD), and singular value decomposition (SVD); and (ii) a top-down approach that is denoted as TM2 method and based on the concatenation of multidimensional chain scattering matrices, the hybrid method gives as an output the corresponding transfer function when the OV MV BPL network topology, OV MV MTL configuration and the applied coupling scheme are given as inputs.

3.2 MTL Theory, EVD and Channel Transfer Functions

As it has already been mentioned in [8]-[12], [14]-[18], [21], [36], the standard TL analysis can be extended to the MTL case through a matrix approach. Since the $n^{\text{OVMV}}+1$ conductors of the OV MV MTL configuration are laid parallel to the z axis, n^{OVMV} modes are supported by the MTL configuration. Through TM2 method, their spectral behavior is described by the $n^{\text{OVMV}} \times n^{\text{OVMV}}$ EVD modal transfer function matrix $\mathbf{H}^m \{\}$ whose elements $H_{i,j}^m \{\}$, $i, j = 1, \dots, n^{\text{OVMV}}$ are the EVD modal transfer functions where $H_{i,j}^m$ denotes the element of matrix $\mathbf{H}^m \{\}$ in row i of column j .

Since the EVD modal transfer function matrix is already evaluated, the $n^{\text{OVMV}} \times n^{\text{OVMV}}$ channel transfer function matrix $\mathbf{H} \{\}$ is determined by

$$\mathbf{H} \{\} = \mathbf{T}_V \cdot \mathbf{H}^m \{\} \cdot \mathbf{T}_V^{-1} \quad (1)$$

where \mathbf{T}_V is a $n^{\text{OVMV}} \times n^{\text{OVMV}}$ matrix that depends on the frequency, the OV MV MTL configuration and the physical properties of the cables [8]-[12], [14]-[18], [21], [36], [45].

3.3 Coupling Schemes and Coupling Transfer Functions

According to how signals are injected into OV MV lines, two categories of coupling schemes are mainly supported by the OV MV BPL networks, namely [2], [16], [18], [24], [25], [46]-[48]: (i) Wire-to-Ground (WtG) coupling schemes; and (ii) Wire-to-Wire (WtW) coupling schemes. Since the main interest of this paper is the comparative benchmark of the piecewise approximation methods, only one of the previous coupling schemes is going to be applied in the following analysis for the sake of clarity and terseness; say, WtG coupling scheme.

In the case of WtG coupling schemes, the coupling WtG channel transfer function $H^{\text{WtG}^s} \{\}$ is given from

$$H^{\text{WtG}^s} \{\} = [\mathbf{C}^{\text{WtG}}]^T \cdot \mathbf{T}_V \cdot \mathbf{H}^m \{\} \cdot \mathbf{T}_V^{-1} \cdot \mathbf{C}^{\text{WtG}} \quad (2)$$

where \mathbf{C}^{WtG} is a 3×1 coupling column vector with zero elements except in row s where the value is equal to 1. Note that WtG coupling schemes inject the signal onto the conductors, $s=1, \dots, 3$ while the signal returns via the ground. WtG coupling between conductor s and ground will be denoted as WtG^s , hereafter.

4. Presentation of L1PMA, L2WPMA, and L2CXCV

4.1 Introduction to Piecewise Monotonic Data Approximation Methods of Demetriou

Similarly to L1PMA, various monotonic data approximation methods have been proposed by Demetriou, such as L2WPMA and L2CXCV. Their application, which is theoretically presented and experimentally verified in [2], [24]-[31], successfully copes with problems that are derived from the presence of measurement differences during the OV MV BPL transfer function determination. Until now, only the efficiency of the best L1PMA to mitigate measurement differences during the determination of OV MV BPL transfer functions has been assessed [2], [24], [25]. In this paper, L2WPMA and L2CXCV are comparatively benchmarked against L1PMA when the mitigation of the occurred measurement differences during the OV MV BPL transfer function determination is required.

4.2 L1PMA

L1PMA exploits the piecewise monotonicity property that always occurs in transmission and distribution BPL transfer functions [2], [24], [25]. Actually, L1PMA decomposes the BPL transfer function into separate monotonous sections between its adjacent turning points (primary extrema) [28], [29]. Since the separate monotonous sections are identified, L1PMA separately handles them. On the basis of the minimization of the moduli sum of the measurement differences, L1PMA achieves to mitigate the uncorrelated measurement differences by neglecting the existence of few large ones [2], [49]. A detailed analysis concerning the application of L1PMA to distribution and distribution BPL transfer functions is given in [2], [24], respectively.

Apart from its sound theoretical background, another strong point of L1PMA is its easy and online software availability. In fact, the Fortran software package that is applied to implement the L1PMA has extensively been verified in various scientific fields [29], [31], [50]-[52] and is freely available online in [53]. In general terms, L1PMA software receives as inputs the measured OV MV BPL coupling transfer function, the measurement frequencies and the number of monotonic sections (*i.e.*, either user- or computer-defined) and gives as outputs the optimal primary extrema and the best fit of the measured OV MV BPL coupling transfer function.

4.3 L2WPMA

In accordance with [34], L2WPMA decomposes the examined BPL transfer function, which is contaminated by measurement differences, into separate monotonous sections between its primary extrema. Then, L2WPMA minimizes the weighted sum of the square of the measurement differences by requiring specific number of sign changes in the first divided measurement differences of the approximation. The number of sign changes is equal to the number of monotonic sections minus one where the number of monotonic sections is either user- or computer-defined.

Similarly to L1PMA, the Fortran software package that is applied to implement L2WPMA is freely available online in [34]. In fact, Fortran software employs a dynamic programming technique that divides the BPL transfer function data into disjoint sets of adjacent data and solves a problem of monotonic fit or isotonic regression for each set. The number of disjoint sets is at most equal to the defined number of monotonic sections. In comparison with the Fortran software of L1PMA, L2WPMA is characterized by

shorter computation times due to its lower complexity. In general terms, L2WPMA software receives the same inputs with the L1PMA one and gives as outputs a spline representation of the solution, the corresponding Lagrange multipliers and the best fit of the measured OV MV BPL coupling transfer function.

4.4 L2CXCVC

In accordance with [35], L2CXCVC smooths the OV MV transfer function data (in the least square error sense), which are contaminated with measurement differences. In fact, L2CXCVC smoothing is subject to one sign change in the second divided differences of the smoothed values. In contrast with L1PMA and L2WPMA, the number of monotonic sections is neither user- nor computer-defined since L2CXCVC partitions the data into two disjoint sets of adjacent data and calculates the required fit by solving a strictly convex quadratic programming problem for each set. The quadratic programming technique makes use of active sets and takes advantage of a B-spline representation of the smoothed values [35].

Similarly to L1PMA and L2WPMA, the entire Fortran code that is required to implement L2CXCVC is freely available online in [54]. In general, L2CXCVC receives as input the measured OV MV BPL coupling transfer function and gives as output the fit of the measured OV MV BPL coupling transfer function.

4.5 The Nature of Measurement Differences and the Mathematics of Piecewise Monotonic Data Approximation Methods

As already been mentioned, a set of practical reasons and “real-life” conditions create significant differences between experimental measurements and theoretical results during the transfer function determination of BPL networks. The reasons for these measurement differences can be grouped into six categories that are analytically reported in [2], [24], [25], [55]-[57]. The measured OV MV BPL coupling transfer function $\overline{H^{WtG}}\{\}$ is then determined by

$$\overline{H^{WtG}}(f_i) = H^{WtG}(f_i) + e(f_i), \quad i=1, \dots, u \quad (3)$$

where $f_i, i=1, \dots, u$ denotes the measurement frequency, $e(f_i)$ synthesizes the total measurement difference due to the aforementioned six categories and u is the number of subchannels in the examined frequency range.

Generalizing eq. (3), the measured OV MVBPL coupling transfer function column vector $\overline{\mathbf{H}^{WtG}}$ is then determined by

$$\overline{\mathbf{H}^{WtG}} \equiv \overline{\mathbf{H}^{WtG}}(\mathbf{f}) = \left[\overline{H^{WtG}}(f_1) \quad \dots \quad \overline{H^{WtG}}(f_i) \quad \dots \quad \overline{H^{WtG}}(f_u) \right]^T \quad (3)$$

where $\mathbf{f} = [f_1 \quad \dots \quad f_i \quad \dots \quad f_u]^T$ is the measurement frequency column vector and $f_i, i=1, \dots, u$ are the measurement frequencies. Similarly to the measured OV MV BPL coupling transfer function column vector $\overline{\mathbf{H}^{WtG}}$, the theoretical OV MV BPL coupling transfer function column vector \mathbf{H}^{WtG} can also be defined.

With reference to Secs. IV B-D, the measured OV MV BPL coupling transfer function column vector, the measurement frequency column vector and the number of monotonic sections (only for L1PMA and L2WPMA) are received by the three examined piecewise monotonic data approximation methods. With reference to Secs. IV B-D, each monotonic data approximation methods processes its inputs and gives as output the

approximated OV MV BPL coupling transfer function column vector $\overline{\mathbf{H}^{\text{WtG}}}(\mathbf{f})$ by applying its algorithm.

4.6 PES and Fault PES for L1PMA, L2WPMA and L2CXCV

As it has already been mentioned in Sec. IV E, to evaluate the approximation accuracy of the piecewise monotonic data approximation methods of this paper and, thus, to comparatively benchmark them, the performance metrics of [2] are used. More specifically, the PES expresses as a percentage the total sum of the relative differences between the approximated coupling transfer function and the theoretical coupling transfer function for all the used frequencies, namely

$$PES = 100\% \cdot \frac{\sum_{i=1}^u \left| \overline{\mathbf{H}^{\text{WtG}}}(f_i) - \mathbf{H}^{\text{WtG}}(f_i) \right|}{\sum_{i=1}^u \left| \mathbf{H}^{\text{WtG}}(f_i) \right|} \quad (4)$$

With respect to eq. (4), to assess the mitigation efficiency of the piecewise monotonic data approximation methods towards the faults, PES is compared against the fault PES that is given by

$$PES_{\text{fault}} = 100\% \cdot \frac{\sum_{i=1}^u \left| \overline{\mathbf{H}^{\text{WtG}}}(f_i) - \mathbf{H}^{\text{WtG}}(f_i) \right|}{\sum_{i=1}^u \left| \mathbf{H}^{\text{WtG}}(f_i) \right|} \quad (5)$$

5. Numerical Results and Discussion

5.1 Simulation Goals and Parameters

Various topologies of OV MV BPL networks are simulated with the purpose of comparatively benchmarking the approximation efficiency of the piecewise monotonic data approximation methods that are examined in this paper when various faults occur.

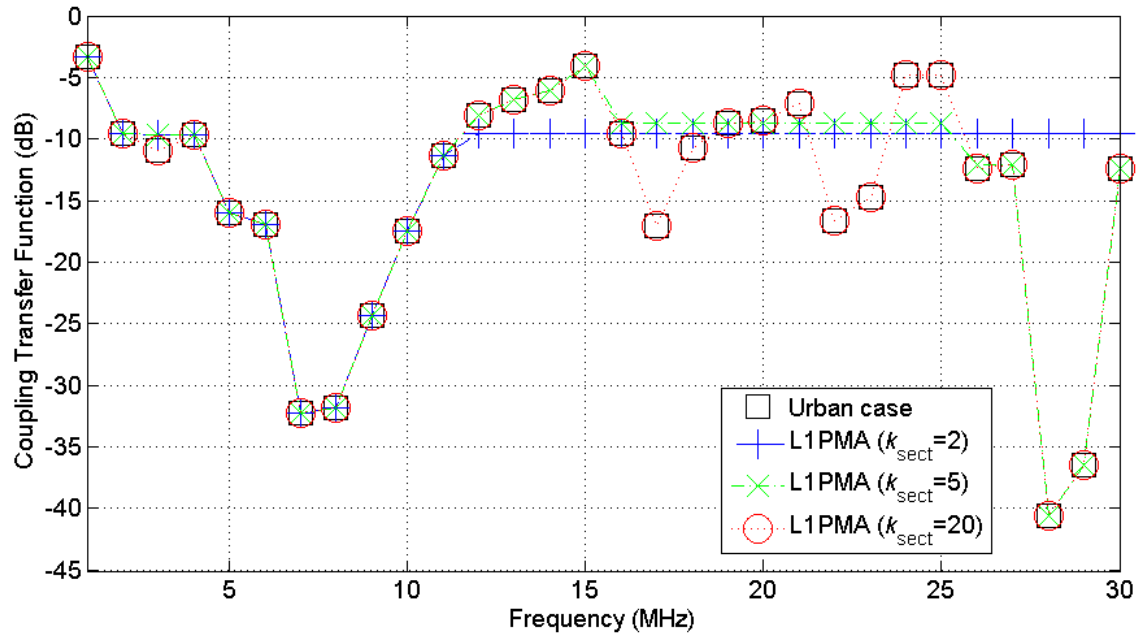
As regards the simulation specifications, those are the same with [2], [24], [25]. More specifically, the BPL frequency range and the flat-fading subchannel frequency spacing are assumed equal to 1-30MHz and 1MHz, respectively. Therefore, the number of subchannels in the examined frequency range is equal to 30. Arbitrarily, the WtG³ coupling scheme is applied during the following simulations. As it is usually done [12], [14], [15], [17], [19], [58], the selection of representative coupling schemes is a typical procedure for the sake of reducing manuscript size.

5.2 Theoretical and Approximated OV MV BPL Transfer Functions by Applying L1PMA, L2WPMA and L2CXCV

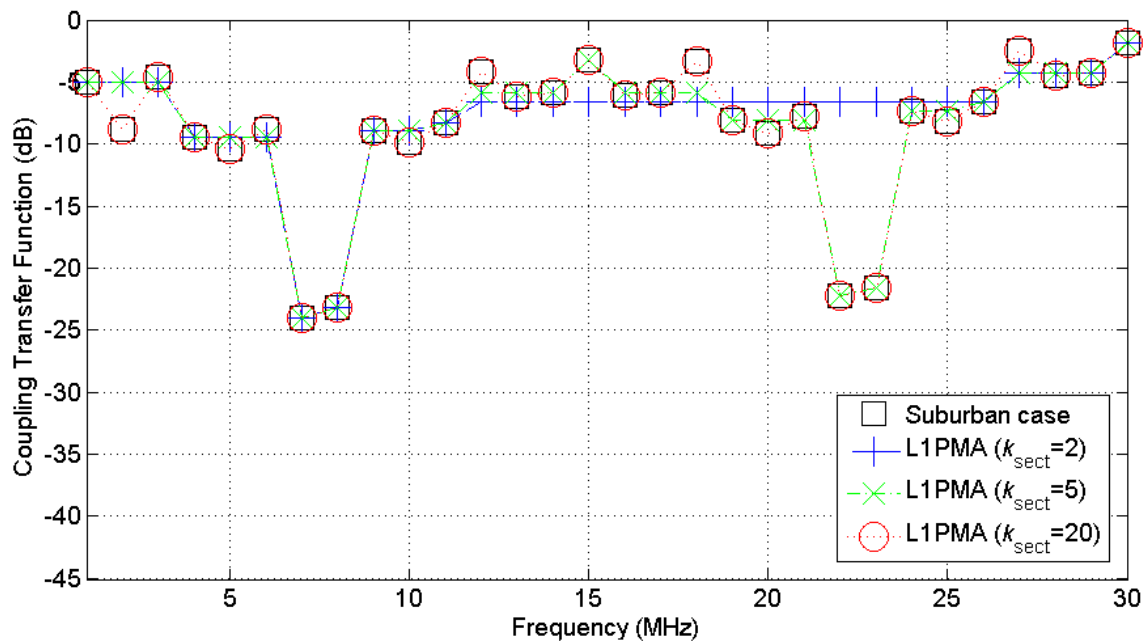
Prior to comparatively benchmarking L1PMA, L2WPMA, and L2CXCV, their overall performance against the mitigation of measurement differences during the determination of the OV MV BPL coupling transfer functions is presented in this subsection.

In Figs. 2(a)-(d), the theoretical coupling transfer function is plotted versus frequency for the four indicative OV MV BPL topologies, respectively, when WtG³

coupling scheme is applied. In each figure, L1PMA result is also plotted for a number of representative monotonic sections (*i.e.*, $k_{\text{sect}}=2$, $k_{\text{sect}}=5$, and $k_{\text{sect}}=20$). In Figs. 3(a)-(d) and Figs. 4(a)-(d), similar curves with Figs. 2(a)-(d) are shown for L2WPMA (same cases of monotonic sections) and L2CXCVC (no monotonic sections), respectively.



(a)



(b)

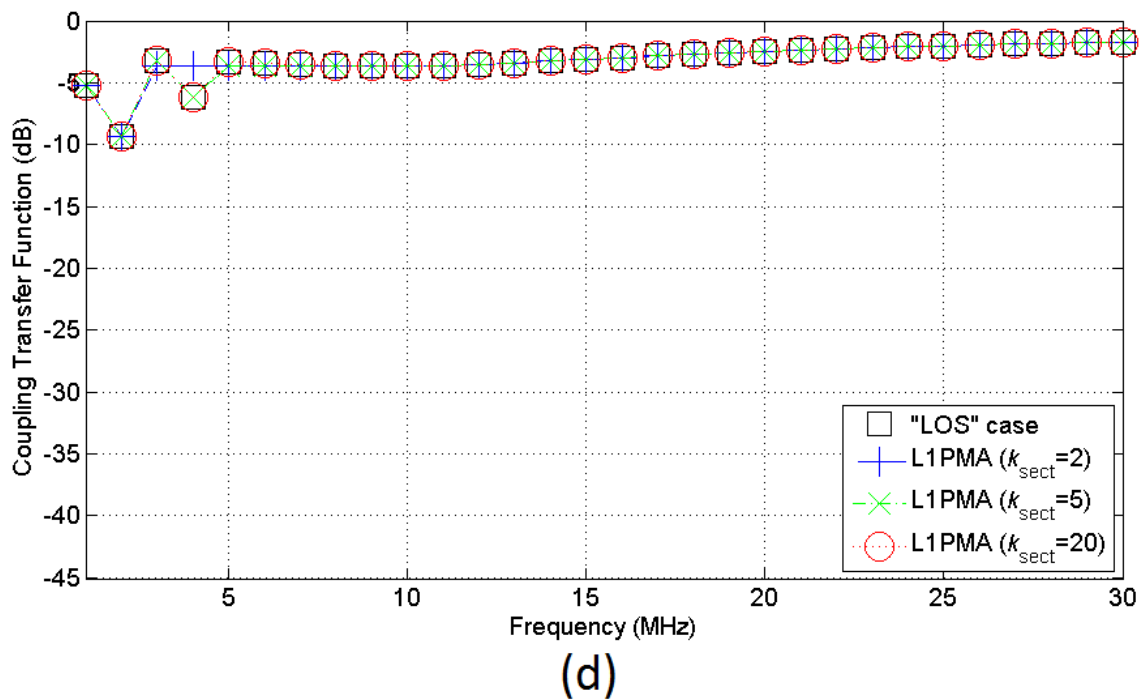
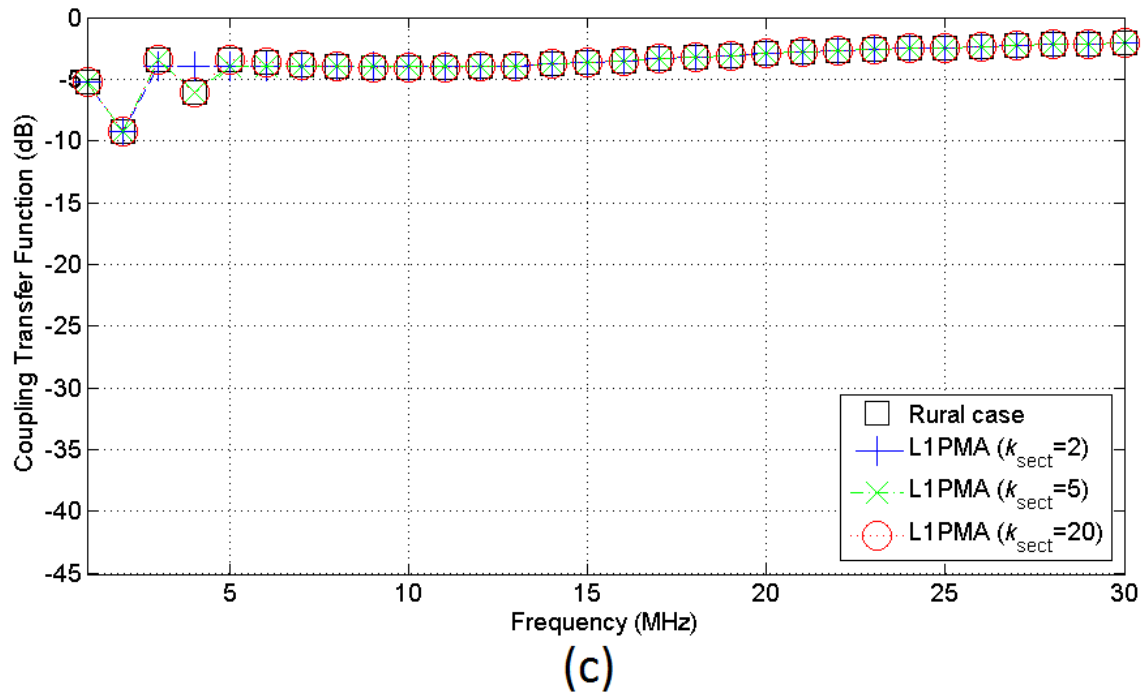
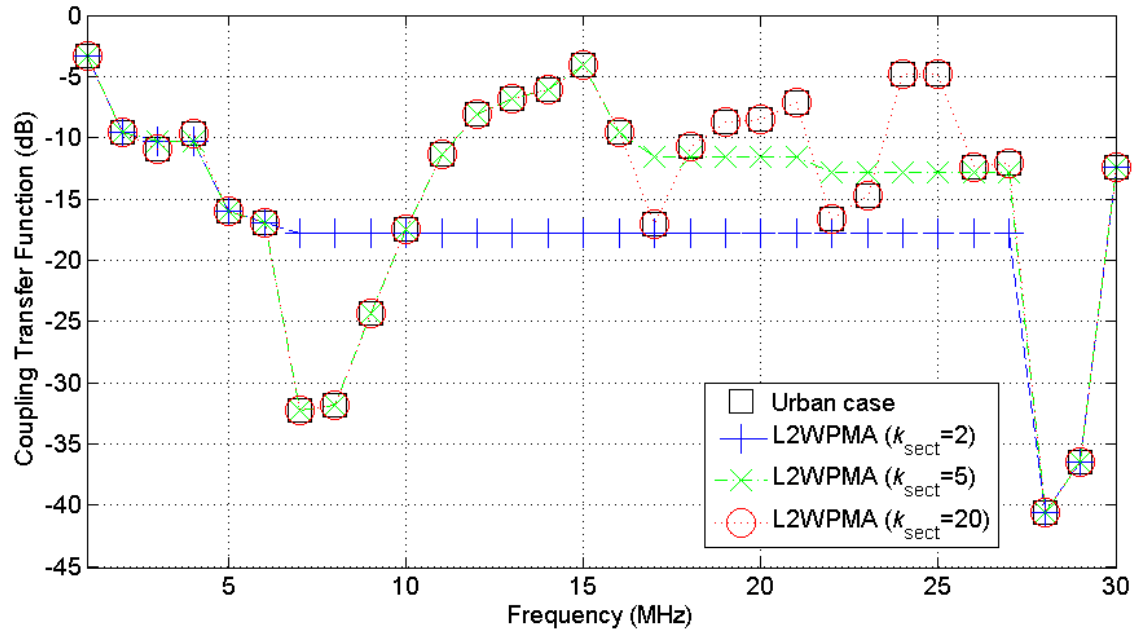
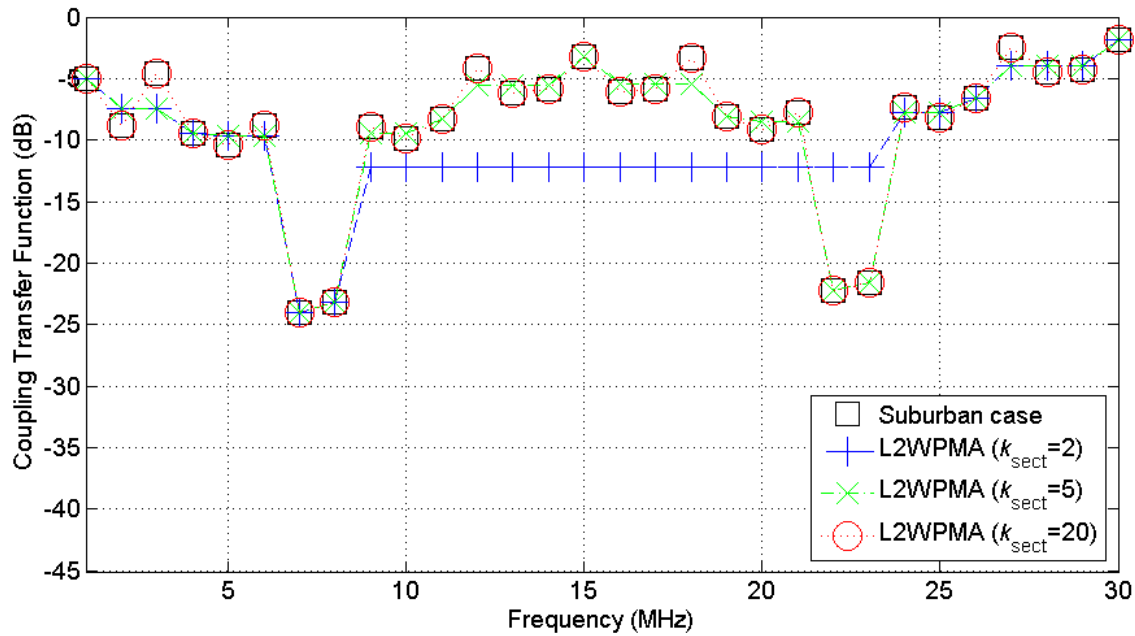


Figure 2. OV MV BPL Coupling transfer function when L1PMA is applied for three representative cases of monotonic sections. (a) Urban case. (b) Suburban case. (c) Rural case. (d) "LOS" case.



(a)



(b)

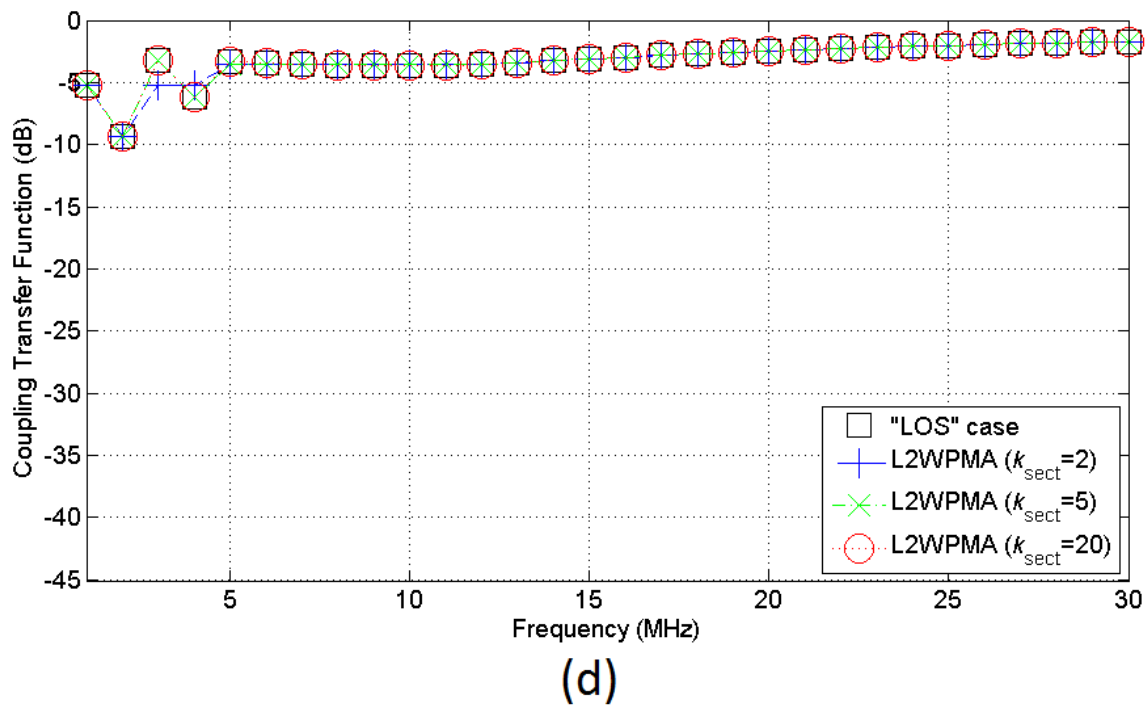
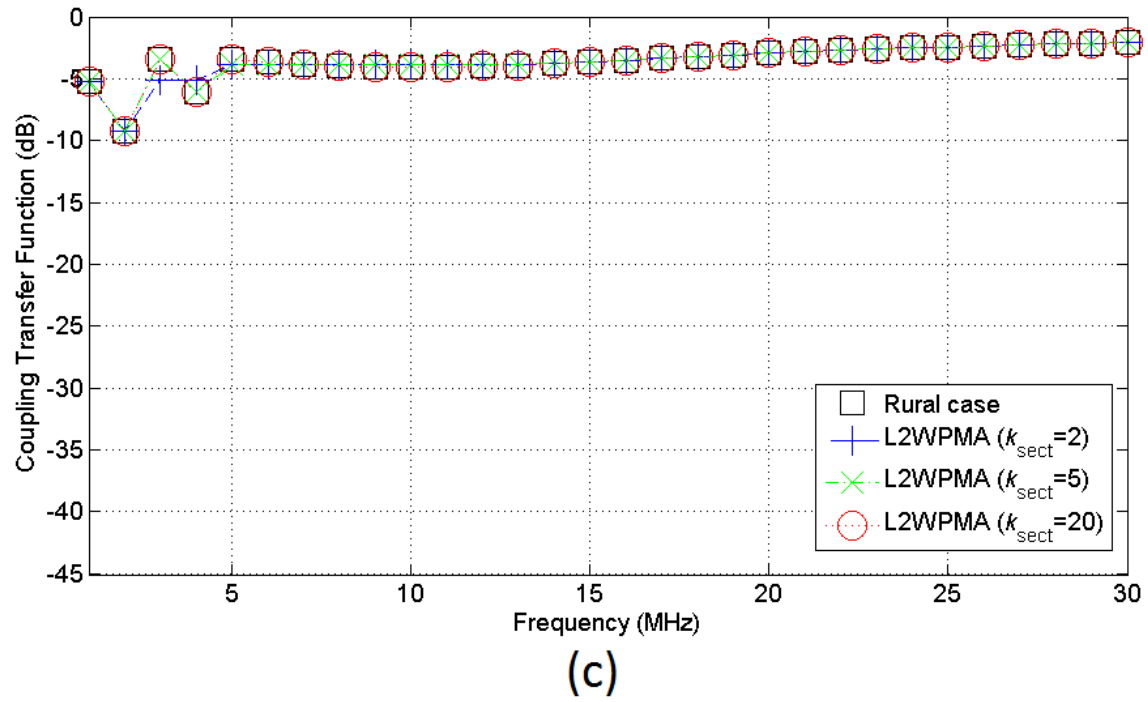
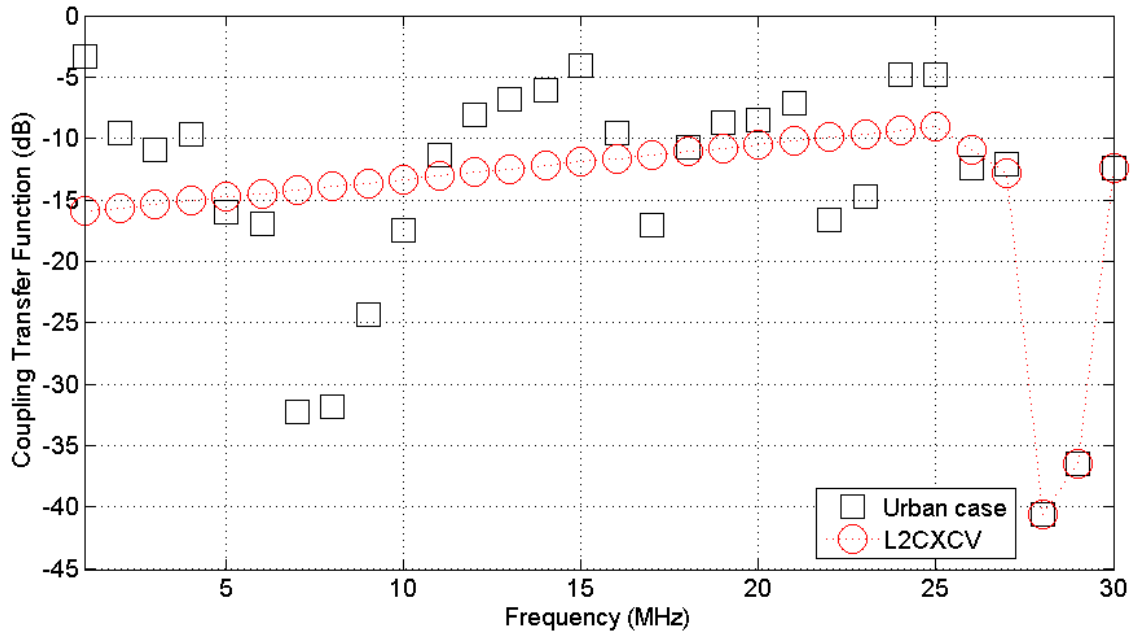
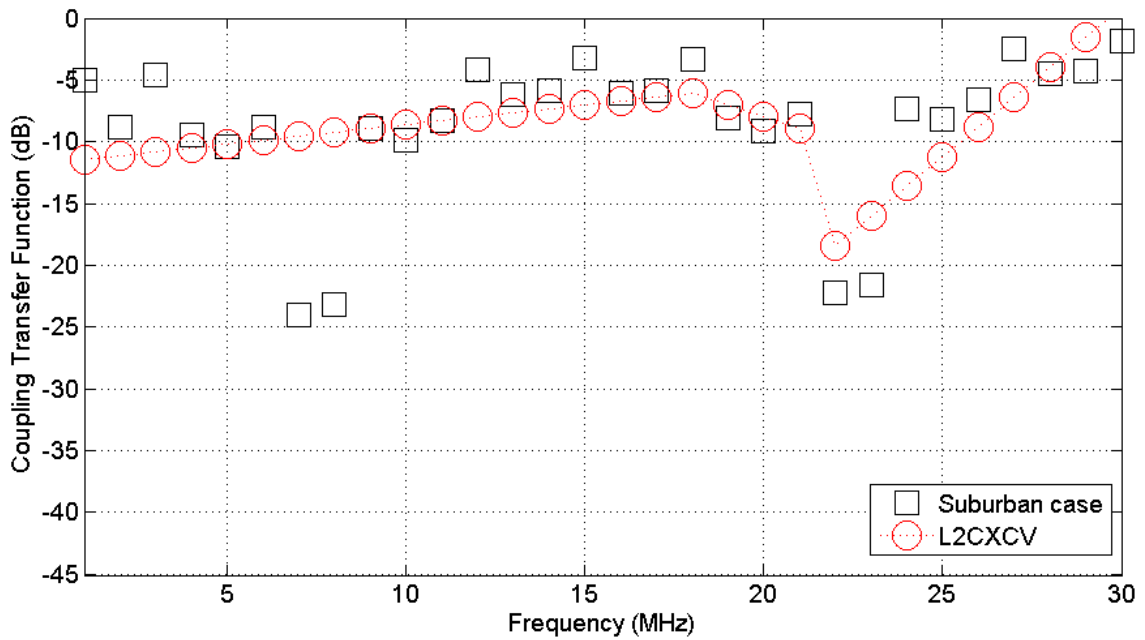


Figure 3. Same curves with Fig.2 but for L2WPMA for three representative cases of monotonic sections.



(a)



(b)

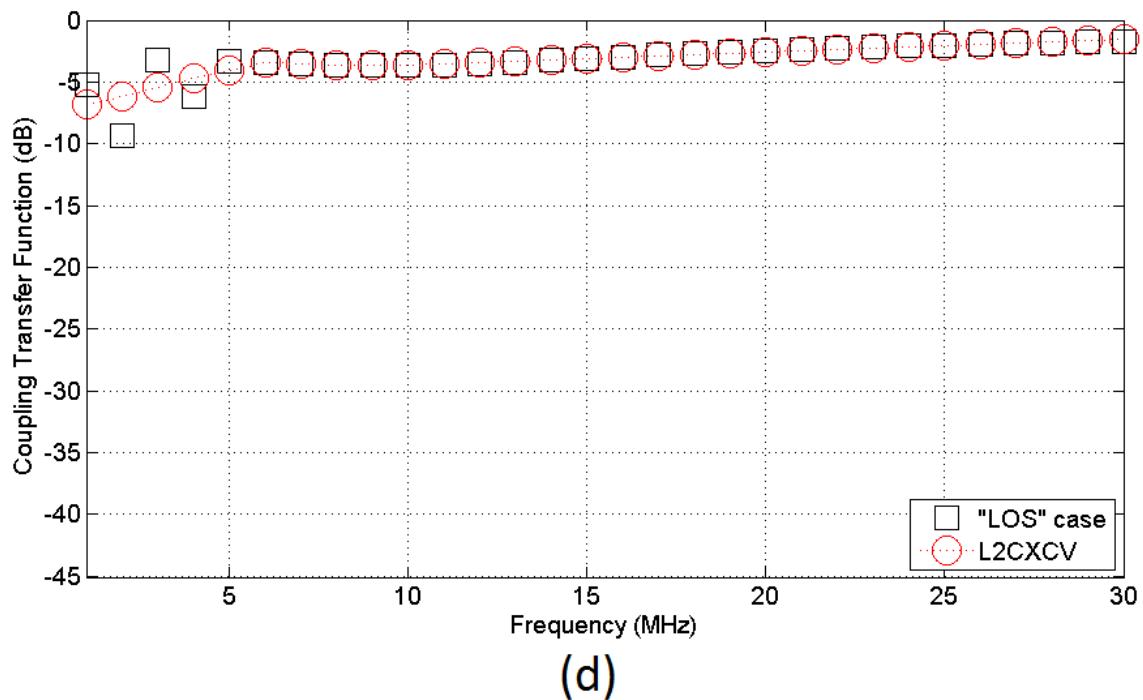
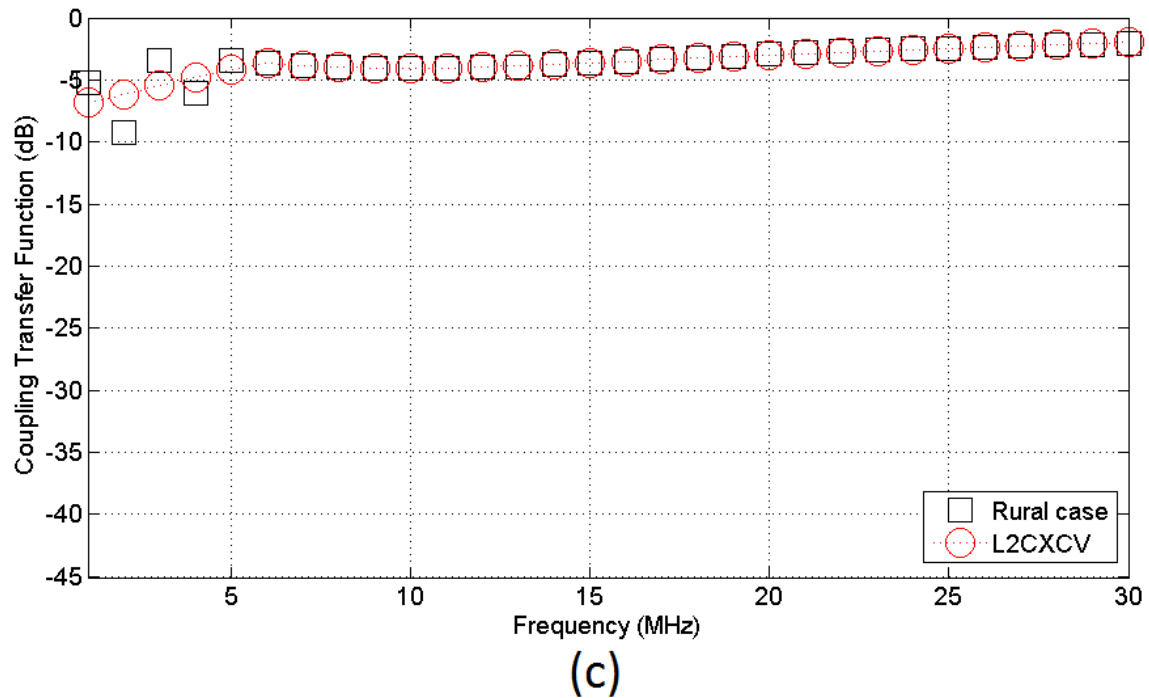


Figure 4. Same curves with Fig.2 but for L2CXCV.

From Figs. 2(a)-(d), 3(a)-(d), and 4(a)-(d), it is evident that L1PMA and L2WPMA very accurately approximate all the examined coupling transfer functions of the indicative OV MV BPL topologies while the number of monotonic sections remains high. As the number of monotonic sections decreases so does the accuracy of the approximation of L1PMA and L2WPMA. When the number of monotonic sections falls below three, all the three piecewise monotonic data approximations (*i.e.*, L1PMA, L2WPMA, and L2CXCV) present comparable results. In fact, if the number of

monotonic sections is equal to one or two, all the piecewise monotonic data approximations tend to approximate the coupling transfer function data closely to the linear approximation.

As it's already been mentioned in [2], the presence of branches along the end-to-end transmission path causes signal reflections, thus, creating a richer multipath environment that adds new spectral notches (extrema) across the coupling transfer function of "LOS" case. The new extrema that appear in the coupling transfer functions of these topologies (i.e., urban case) differ in depth and extent while they require additional monotonic sections so that the approximation may be accurate. Thanks to their adjustable number of monotonic sections, L1PMA and L2WPMA can improve their approximations so that a better accuracy is achieved and these new extrema can be embodied in their approximations –see approximations of $k_{sect}=20$ of Figs. 2(a) and 3(a). Indeed, not even one coupling transfer function data is outside the L1PMA and L2WPMA approximations of 20 monotonic sections in the two aforementioned figures. Conversely, L2CXCVC approximates the coupling transfer function data without the use of monotonic sections having several approximations of low accuracy as a result when OV MV BPL topologies are examined. As a matter of fact, L2CXCVC creates a general approximation rather than an approximation that tries to embody all the coupling transfer function data. To assess the performance of L1PMA, L2WPMA, and L2CXCVC, their PES is reported in Table 1 for the four indicative OV MV BPL topologies when different numbers of monotonic sections are applied and no measurement differences are assumed.

TABLE 1
PES between Theoretical and Approximated Coupling Transfer Functions when
L1PMA, L2WPMA, and L2CXCVC Are Applied

Number of Monotonic Sections	PES (%)											
	Urban case			Suburban case			Rural case			"LOS" case		
	L1PMA	L2WPMA	L2CXCVC									
1	37.53	48.02	34.55	44.10	74.16	36.64	24.68	30.54	9.45	29.51	40.74	11.39
2	27.06	41.05	34.55	22.45	38.66	36.64	3.79	3.92	9.45	3.93	3.99	11.39
3	15.14	16.57	34.55	22.45	37.04	36.64	3.79	3.92	9.45	3.93	3.99	11.39
4	8.50	9.60	34.55	6.00	6.44	36.64	1.24	1.36	9.45	0.77	0.83	11.39
5	8.50	9.60	34.55	6.00	6.44	36.64	1.24	1.36	9.45	0.77	0.83	11.39
6	3.37	4.26	34.55	4.38	4.81	36.64	7.36×10^{-6}	7.47×10^{-6}	9.45	7.37×10^{-6}	7.59×10^{-6}	11.39
7	3.37	4.26	34.55	4.38	4.81	36.64	7.36×10^{-6}	7.47×10^{-6}	9.45	7.37×10^{-6}	7.59×10^{-6}	11.39
8	0.35	0.35	34.55	3.35	3.59	36.64	7.36×10^{-6}	7.47×10^{-6}	9.45	7.37×10^{-6}	7.59×10^{-6}	11.39
9	0.35	0.35	34.55	3.35	3.59	36.64	7.36×10^{-6}	7.47×10^{-6}	9.45	7.37×10^{-6}	7.59×10^{-6}	11.39
10	0.07	0.07	34.55	2.56	3.01	36.64	7.36×10^{-6}	7.47×10^{-6}	9.45	7.37×10^{-6}	7.59×10^{-6}	11.39
11	0.07	0.07	34.55	2.56	3.01	36.64	7.36×10^{-6}	7.47×10^{-6}	9.45	7.37×10^{-6}	7.59×10^{-6}	11.39
12	1.21×10^{-5}	1.17×10^{-5}	34.55	1.79	2.11	36.64	7.36×10^{-6}	7.47×10^{-6}	9.45	7.37×10^{-6}	7.59×10^{-6}	11.39
13	1.21×10^{-5}	1.17×10^{-5}	34.55	1.79	2.11	36.64	7.36×10^{-6}	7.47×10^{-6}	9.45	7.37×10^{-6}	7.59×10^{-6}	11.39
14	1.21×10^{-5}	1.17×10^{-5}	34.55	1.21	1.57	36.64	7.36×10^{-6}	7.47×10^{-6}	9.45	7.37×10^{-6}	7.59×10^{-6}	11.39
15	1.21×10^{-5}	1.17×10^{-5}	34.55	1.21	1.57	36.64	7.36×10^{-6}	7.47×10^{-6}	9.45	7.37×10^{-6}	7.59×10^{-6}	11.39
16	1.21×10^{-5}	1.17×10^{-5}	34.55	0.67	0.67	36.64	7.36×10^{-6}	7.47×10^{-6}	9.45	7.37×10^{-6}	7.59×10^{-6}	11.39
17	1.21×10^{-5}	1.17×10^{-5}	34.55	0.67	0.67	36.64	7.36×10^{-6}	7.47×10^{-6}	9.45	7.37×10^{-6}	7.59×10^{-6}	11.39
18	1.21×10^{-5}	1.17×10^{-5}	34.55	0.31	0.31	36.64	7.36×10^{-6}	7.47×10^{-6}	9.45	7.37×10^{-6}	7.59×10^{-6}	11.39
19	1.21×10^{-5}	1.17×10^{-5}	34.55	0.31	0.31	36.64	7.36×10^{-6}	7.47×10^{-6}	9.45	7.37×10^{-6}	7.59×10^{-6}	11.39
20	1.21×10^{-5}	1.17×10^{-5}	34.55	7.16×10^{-6}	7.28×10^{-6}	36.64	7.36×10^{-6}	7.47×10^{-6}	9.45	7.37×10^{-6}	7.59×10^{-6}	11.39

The previous remarks concerning Figs. 2(a)-(d), 3(a)-(d), and 4(a)-(d) are reflected on the results of Table 1. Actually, the number of monotonic sections determines the approximation accuracy of L1PMA and L2WPMA to the coupling transfer functions of OV MV BPL networks. In contrast, L2CXCV performance remains stable and relatively poor regardless of the number of monotonic sections since this piecewise data approximation method does not include this property during the computation of its approximation. Further comparing L1PMA and L2WPMA performance, their approximation behavior remains nearly the same when different OV MV BPL topologies are examined and different number of monotonic sections is assumed. Actually, L1PMA presents slightly lower PES results than the respective ones of L2WPMA in the majority of the cases examined.

Already been identified for L1PMA in [2], there is an optimal number of monotonic sections above which the PES improvement remains marginal and uniquely describes the pattern of an OV MV BPL topology. This optimal number mainly depends on the OV MV BPL topology and remains the same either for L1PMA or for L2WPMA. In fact, as the OV MV BPL topology comprises more branches the optimal number of monotonic sections generally increases. From Table 1, the optimal number of monotonic sections is equal to 12, 20, 6, and 6 for the urban, suburban, rural, and “LOS” case, respectively.

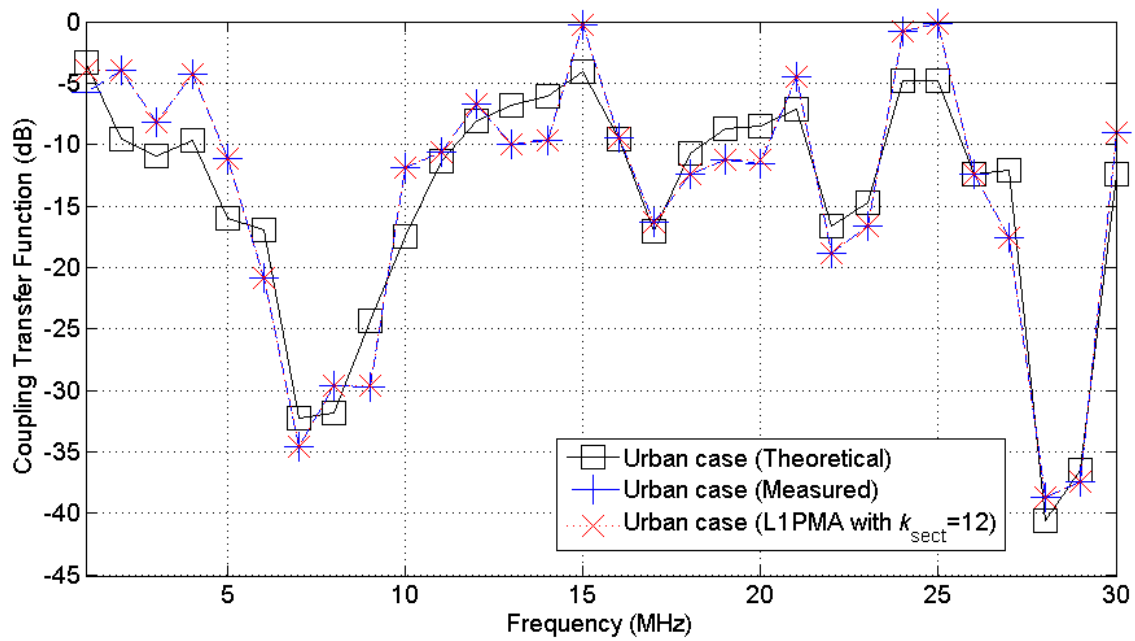
On the basis of its identity characteristics, the optimal number of monotonic sections also acts as an efficient countermeasure technique against the measurement differences. Since the optimal number of monotonic sections remains the same for given OV MV BPL topology, the presence of measurement differences can be mitigated for the sake of the preservation of the number of monotonic sections. To validate this concept, the performance of L1PMA, L2WPMA, and L2CXCV is assessed as a measurement difference mitigation technique in the following subsection.

5.3 L1PMA, L2WPMA and L2CXCV against Measurement Differences

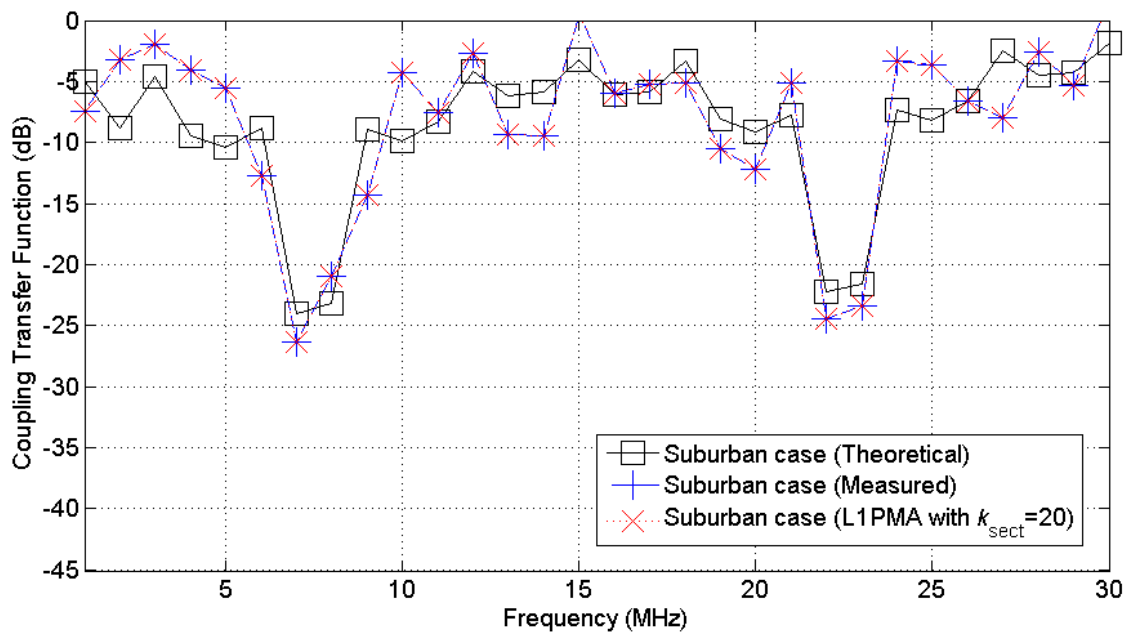
In accordance with [2], [24], [25], the six categories of measurement differences can create significant differences between experimental measurements and theoretical results during the determination of OV MV BPL coupling transfer functions. The total measurement difference can be assumed to follow either CUD with minimum value $-\alpha_{\text{CUD}}$ and maximum value α_{CUD} or ND with mean μ_{ND} and standard deviation σ_{ND} . Since the conclusions concerning the performance of piecewise monotonic data approximations have been verified to remain almost the same either CUD or ND is applied [2], [25], only one of the previous measurement difference distributions is adopted in the following analysis; say, CUD.

Piecewise monotonic data approximations achieve to mitigate the additive measurement differences by simply maintaining the monotonicity pattern of each OV MV BPL coupling transfer function. To examine the impact of measurement differences on the determination of OV MV BPL coupling transfer functions and the potential of counterbalancing the measurement differences, in Figs. 5(a)-(d), the theoretical and measured coupling transfer functions are plotted versus frequency for the four indicative OV MV BPL topologies, respectively. Note that the measured coupling transfer function corresponds to CUD of $\alpha_{\text{CUD}}=6\text{dB}$ when the corresponding optimal number of monotonic sections for each OV MV BPL topology is assumed. In each figure, the approximated coupling transfer function of the measured one is also drawn when L1PMA is applied.

In Figs. 6(a)-(d) and 7(a)-(d), same plots are given with Figs. 5(a)-(d) but for the application of L2WPMA and L2CXCXV, respectively.



(a)



(b)

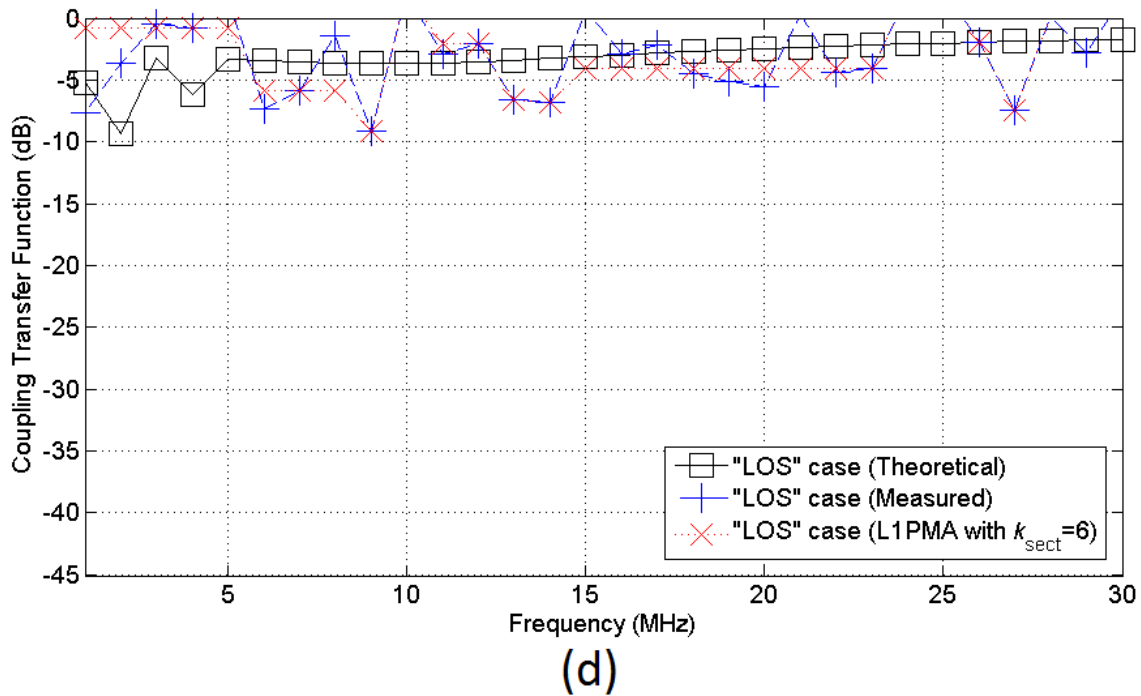
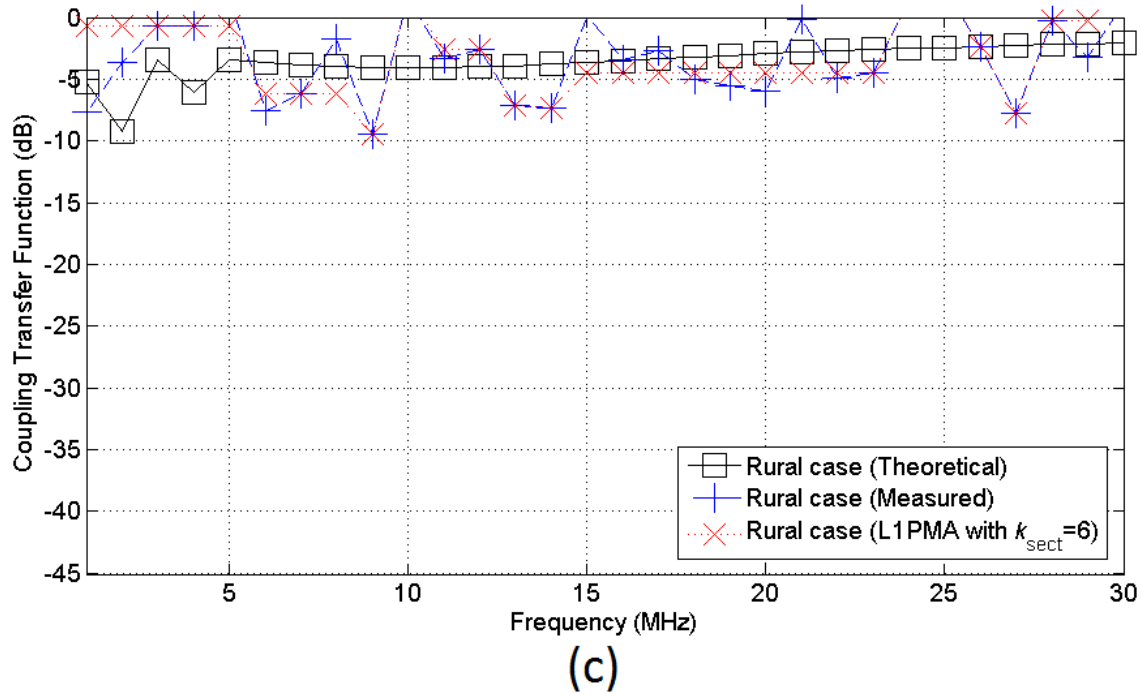
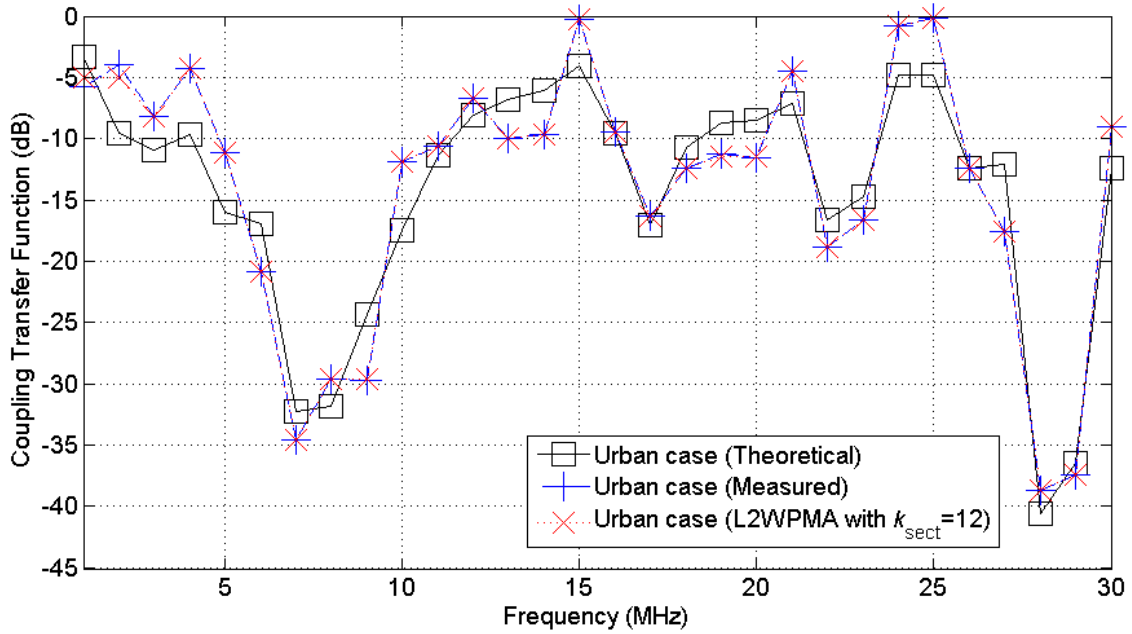
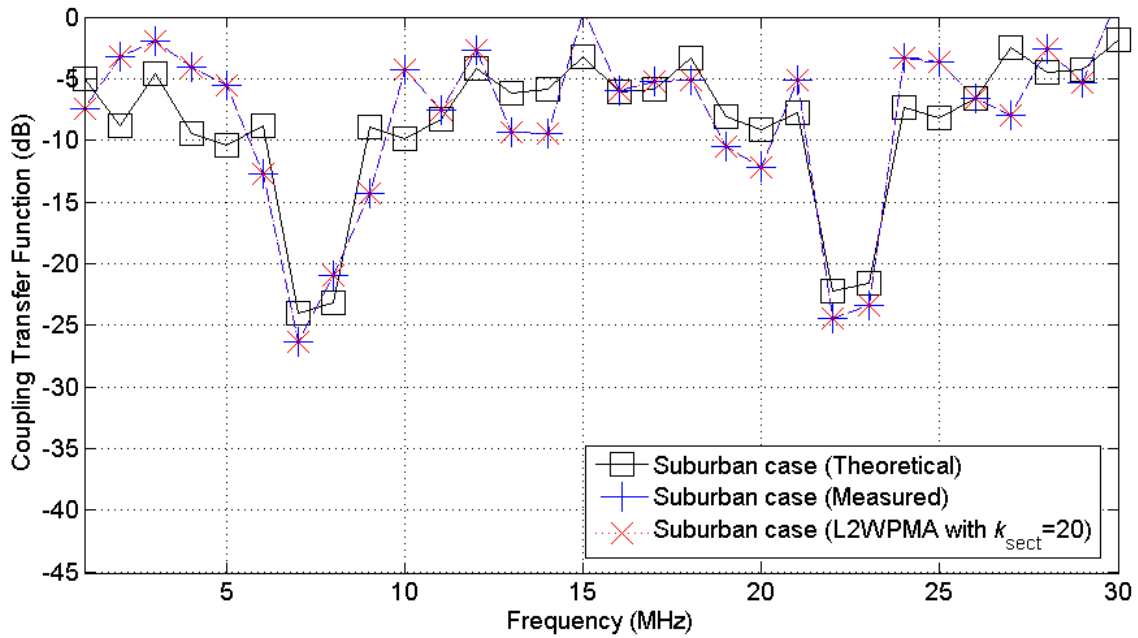


Figure 5. Theoretical, measured, and approximated OV MV BPL coupling transfer function when L1PMA is applied for the indicative measurement difference CUD of $\alpha_{\text{CUD}}=6\text{dB}$. (a) Urban case –the optimal number of monotonic sections is equal to 12–. (b) Suburban case –the optimal number of monotonic sections is equal to 20–. (c) Rural case –the optimal number of monotonic sections is equal to 6–. (d) “LOS” case –the optimal number of monotonic sections is equal to 6–.



(a)



(b)

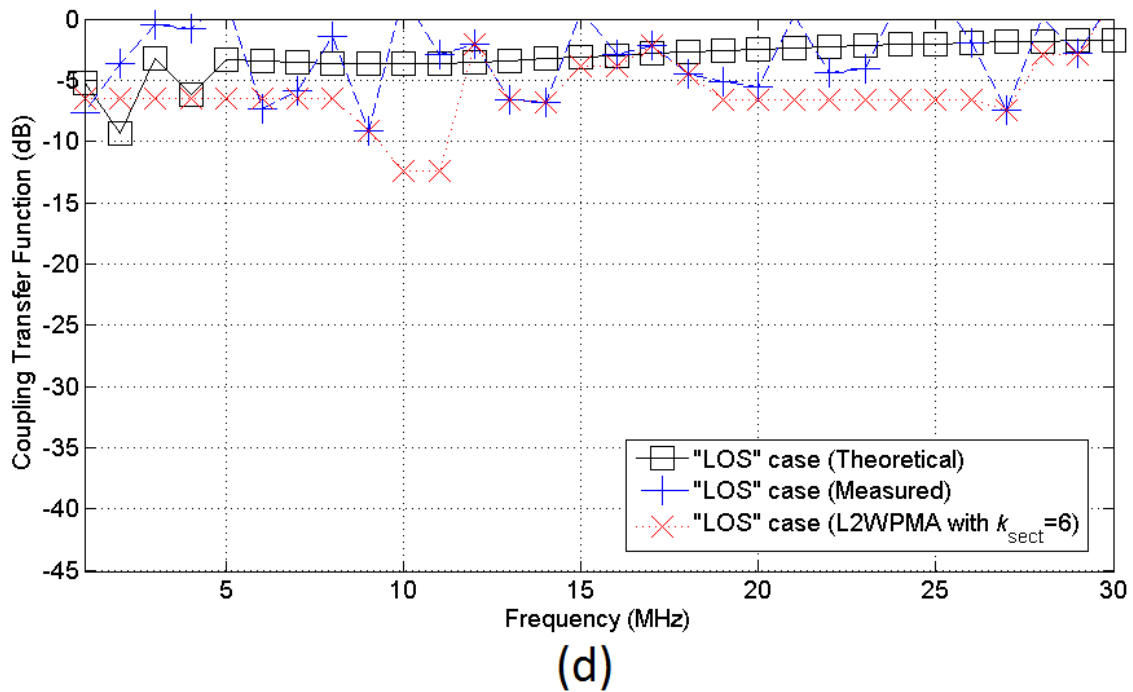
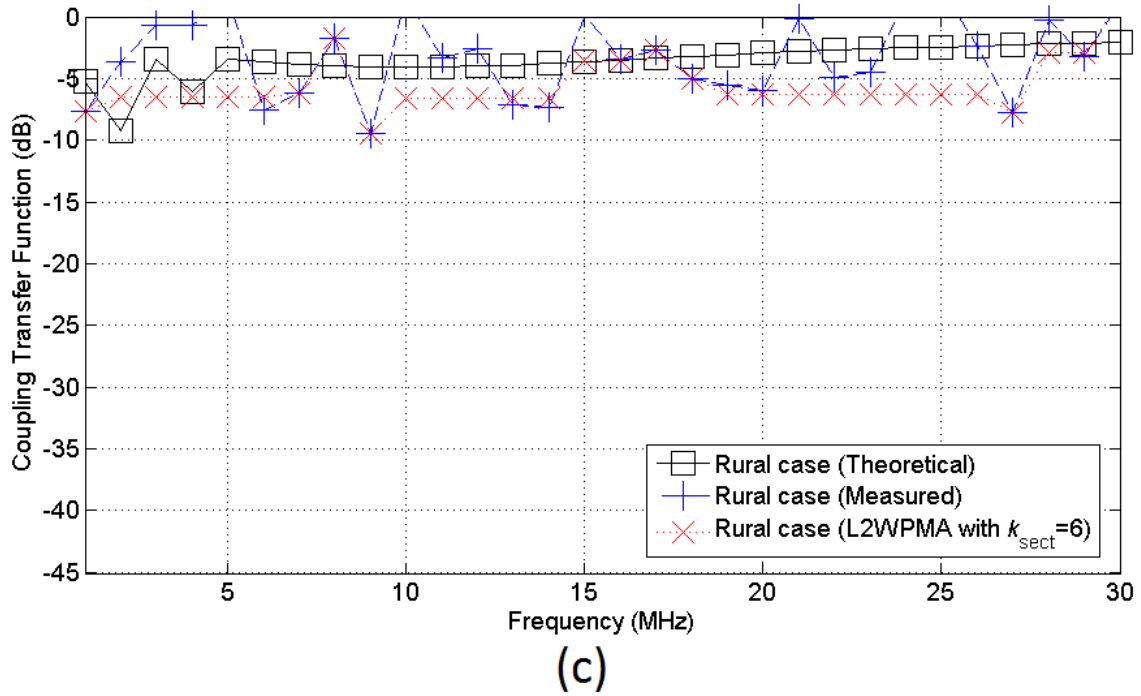
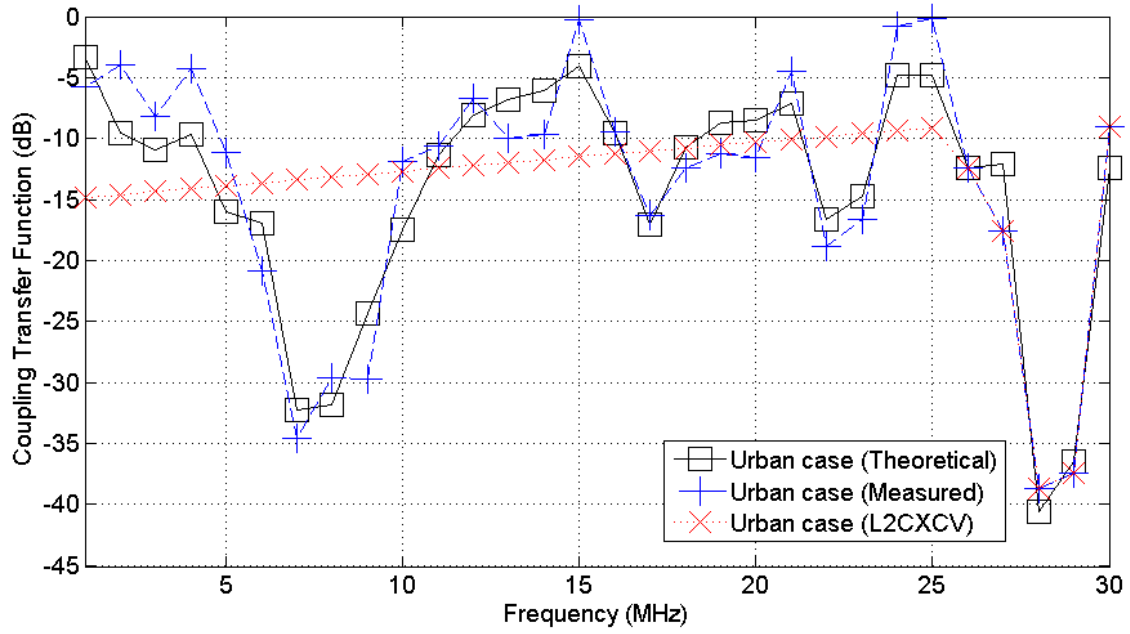
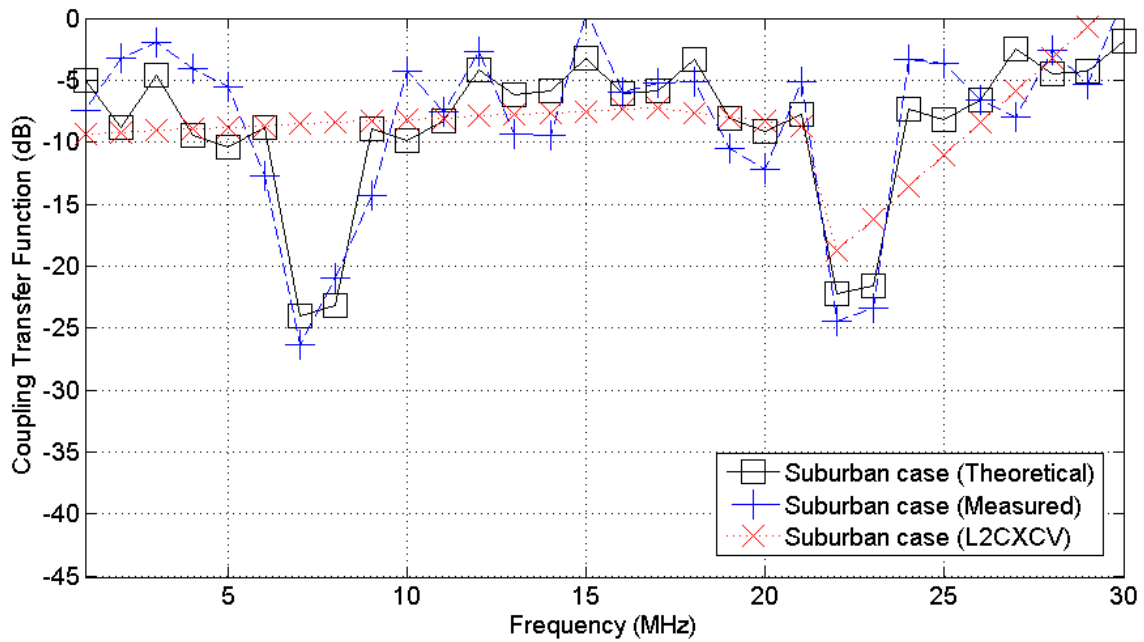


Figure 6. Same curves with Fig.5 but for L2WPMA.



(a)



(b)

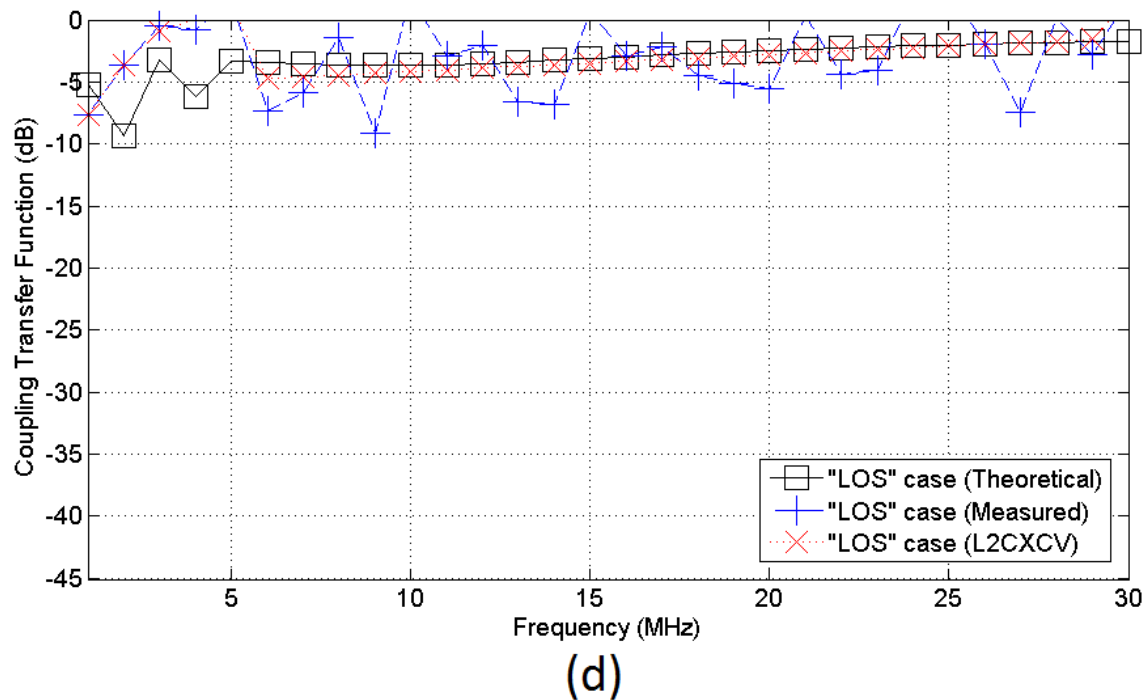
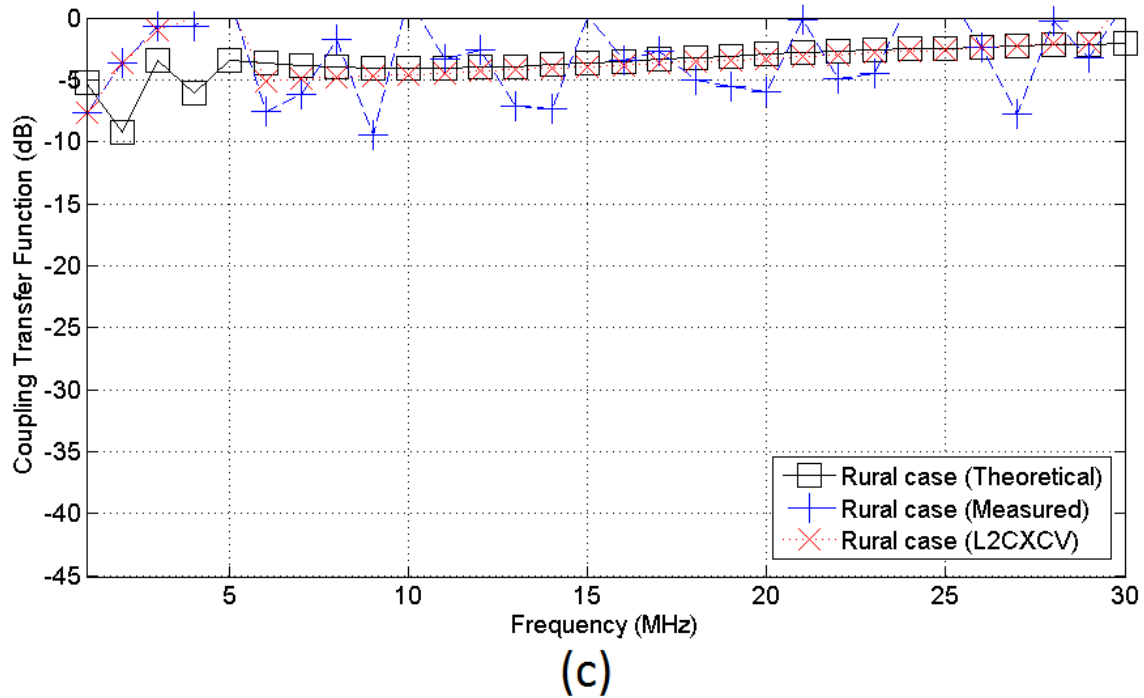


Figure 7. Same curves with Fig.2 but for L2CXCVC.

From Figs. 5(a)-(d), 6(a)-(d), and 7(a)-(d), it is clearly demonstrated that all the examined piecewise monotonic data approximations are attempting to identify the primary extrema of the measured OV MV BPL transfer functions and, then, interpolate the coupling transfer function data at these extrema. In the case of L1PMA and L2WPMA, the low optimal number of monotonic sections poses restrictions so that high fluctuations due to the high magnitudes of measurement differences, which distort the

monotonicity pattern and exceed the optimal number of monotonic sections, can be mitigated. Hence, both L1PMA and L2WPMA very efficiently approximate the OV MV BPL coupling transfer functions of rural and “LOS” cases. However, when aggravated OV MV BPL topologies are examined (*e.g.*, urban and suburban case), the need for high number of monotonic sections is required so that the depth and the extent of spectral notches of the theoretical OV MV BPL coupling transfer function are successfully included. The high optimal number of monotonic sections gives sufficient freedom to fit the measured OV MV BPL coupling transfer function data without excluding measurement differences of high magnitude. Conversely, L2CXCVC creates an average approximation that remains almost stable reducing the influence of gross measurement differences. Exploiting the CUD measurement difference nature, L2CXCVC approximation generally follows the theoretical OV MV BPL coupling transfer functions in all the indicative OV MV BPL topologies examined.

To comparatively benchmark L1PMA, L2WPMA, and L2CXCVC when measurement differences of different maximum CUD values occur, PES of each piecewise data approximation method as well as the PES_{fault} of indicative urban OV MV BPL topology are demonstrated in Table 2 when different maximum CUD values are applied. In Table 3, 4, and 5, same reports with Table 2 are presented but for the suburban, rural, and “LOS” case, respectively. Note that the optimal number of monotonic sections, which is presented in Table 1, is used for each indicative OV MV BPL topology.

TABLE 2
 PES_{fault} and PES for the Indicative Urban OV MV BPL Topology when
 L1PMA, L2WPMA, and L2CXCVC Are Applied for Different Maximum CUD Value

Maximum CUD Value (dB)	Urban Topology			
	PES_{fault} (%)	PES (%)		
		L1PMA	L2WPMA	L2CXCVC
1	3.51	3.51	3.51	34.65
2	7.51	7.61	7.03	35.91
3	9.63	9.79	9.39	35.35
4	13.27	13.86	12.94	35.58
5	16.27	15.72	16.30	36.58
6	18.76	18.68	17.95	34.51
7	20.22	20.17	20.22	38.06
8	24.70	24.59	24.67	36.72
9	27.31	27.15	27.15	37.66
10	36.17	34.64	36.89	41.56

TABLE 3
 PES_{fault} and PES for the Indicative Suburban OV MV BPL Topology when
 L1PMA, L2WPMA, and L2CXCV Are Applied for Different Maximum CUD Value

Maximum CUD Value (dB)	Suburban Topology			
	PES _{fault} (%)	PES (%)		
		L1PMA	L2WPMA	L2CXCV
1	5.74	5.74	5.74	36.77
2	12.27	12.27	12.27	36.71
3	15.74	15.74	15.74	36.21
4	21.69	21.69	21.69	37.46
5	26.61	26.56	25.13	38.27
6	30.68	30.68	30.68	36.01
7	33.07	33.07	33.07	40.07
8	40.39	40.39	40.39	39.78
9	44.66	44.66	44.66	40.60
10	59.14	59.14	59.14	58.34

TABLE 4
 PES_{fault} and PES for the Indicative Rural OV MV BPL Topology when
 L1PMA, L2WPMA, and L2CXCV Are Applied for Different Maximum CUD Value

Maximum CUD Value (dB)	Rural Topology			
	PES _{fault} (%)	PES (%)		
		L1PMA	L2WPMA	L2CXCV
1	14.00	11.27	8.97	11.49
2	29.92	24.28	22.93	18.18
3	38.38	34.01	29.50	26.35
4	52.87	49.09	39.60	36.22
5	64.86	53.43	67.39	35.09
6	74.79	56.11	81.51	35.34
7	80.60	73.22	100.46	34.22
8	98.45	85.31	187.02	49.86
9	108.85	101.03	184.77	60.06
10	144.16	145.50	300.00	75.71

TABLE 5
 PES_{fault} and PES for the Indicative “LOS” OV MV BPL Topology when L1PMA, L2WPMA, and L2CXCV Are Applied for Different Maximum CUD Value

Maximum CUD Value (dB)	“LOS” Topology			
	PES_{fault} (%)	PES (%)		
		L1PMA	L2WPMA	L2CXCV
1	15.57	11.66	9.74	13.45
2	33.28	25.90	26.67	20.77
3	42.69	37.87	32.82	29.80
4	58.82	54.80	50.82	40.76
5	72.16	59.28	86.18	39.34
6	83.21	60.95	108.25	39.51
7	89.68	91.99	123.44	38.58
8	109.52	95.25	276.60	55.97
9	121.10	112.46	228.31	66.99
10	160.38	161.53	413.36	84.38

- From Tables 2-5, a plethora of interesting conclusions can be revealed as follows:
- When the PES of a piecewise monotonic data approximation is lower than the respective PES_{fault} of the examined OV MV BPL topology for a given maximum CUD value, this implies that the approximated OV MV BPL coupling transfer function resembles more to the corresponding theoretical OV MV BPL transfer function than the measured one. Therefore, the mitigation of measurement differences may occur in the cases where the examined piecewise monotonic data approximations present lower PES than the corresponding PES_{fault} . Indeed, comparing PES_{fault} with PES of L1PMA, L2WPMA, and L2CXCV, at least one of the aforementioned piecewise monotonic data approximations achieves to mitigate the occurred measurement differences in 33 of the 40 cases examined, which is equivalent to 82.5%. Schematically, these 33 cases are illustrated with green background color in Tables 2-5.
 - Further analyzing the cases where a measurement difference mitigation can be achieved, the following analytics can be pointed out:
 - L1PMA presents the best PES in 4 of the 33 examined cases, say 12.12%.
 - L2WPMA presents the best PES in 6 of the 33 examined cases, say 18.18%.
 - L2CXCV presents the best PES in 22 of the 33 examined cases, say 66.67%.
 - L1PMA and L2WPMA present the same best PES in 1 of the 33 examined cases, say 3.03%.
 - Correlating the previous piecewise monotonic data approximation analytics with the examined OV MV BPL topologies, it is observed that:
 - During the OV MV BPL coupling transfer function approximation of topologies with low number of branches, such as “LOS” and rural cases, the spectral notches that observed in coupling transfer functions are

shallow and rare. Hence, OV MV BPL coupling transfer functions present wide ranges of flat spectral behavior while the optimal number of monotonic sections remains low. The measurement differences create fluctuations that can be counterbalanced by a simple approximation method, such as L2CXCVC, that maintains a steady monotonicity pattern. Therefore, it is obvious that L2CXCVC presents the best PES in comparison with L1PMA and L2WPMA when “LOS” and rural cases are examined.

- As the branch complexity of the OV MV BPL topologies raises so does the extent and the depth of spectral notches across the coupling transfer functions. Since an intense multipath environment is investigated, the need for including more primary and secondary extrema requires higher optimal number of monotonic sections. In these cases, the simple approximations, such as L2CXCVC, fail to describe the richness of the notches cancelling the efficiency of these approximations. Here, L1PMA and L2WPMA are able to catch the complexity of the OV MV BPL coupling transfer functions. Indeed, L1PMA and L2WPMA can almost equivalently mitigate the measurement differences of the examined urban OV MV BPL topology.
- Relating the previous piecewise monotonic data approximation analytics with the different applied maximum CUD values, it can be pointed out that:
 - When the maximum CUD value remains low, *i.e.*, below 6-7dB, the measured OV MV BPL coupling transfer functions little differ from the theoretical ones due to the weak fluctuations. Based on the optimal number of monotonic sections, L1PMA and L2WPMA approximate the measured OV MV BPL coupling transfer functions near the theoretical one by omitting the weak fluctuations.
 - As the maximum CUD value increases, the measurement differences become important and comparable to the spectral notches of OV MV BPL coupling transfer functions. On the basis of the optimal number of monotonic sections, L1PMA and L2WPMA approximate the data through the prism of specific monotonic sections. Here, the high optimal number of monotonic sections may permit the overfit of L1PMA and L2WPMA during the approximations rendering unable the rejection of the extrema due to measurement differences. Conversely, L2CXCVC produces a simple approximation, which tries to create an average fit neglecting the general fluctuations, that avoids the deficiency of the overfit of L1PMA and L2WPMA.
- To exploit the strong points of each of the aforementioned piecewise monotonic data approximations, an adaptive countermeasure technique against measurement differences should be proposed, as follows:
 - When the examined OV MV BPL topology is characterized by significant number of branches of short length (*i.e.*, urban topologies), L1PMA and L2WPMA should be adopted due to their proneness to easily adapt to the versatility of the coupling transfer functions of these topologies.
 - In contrast, when the examined OV MV BPL topologies consist of few long branches, a simple approximation, such as L2CXCVC, is required to give an overall and more general picture of the measured OV MV BPL coupling transfer function. Since the theoretical OV MV BPL coupling

transfer functions present shallow spectral notches, their behavior is close to the approximation generated by the L2CXCVCV.

- The most crucial role during the comparative benchmarking of the previous piecewise monotonic data approximations plays the selection of the optimal number of monotonic sections. In fact, the optimal number of monotonic sections determines: (i) the accuracy of L1PMA and L2WPMA that is expressed by PES; and (ii) the result of the comparison between piecewise monotonic data approximations of monotonic sections (*e.g.*, L1PMA and L2WPMA) and the approximations without monotonic sections (*e.g.*, L2CXCVCV). Also, comparing PES results of this paper with those of [2], it is obvious that even if same OV BPL topologies are examined the PES results are differentiated because of the different applied coupling schemes and the optimal number of monotonic sections. Here, additional investigation should be made in order to clarify the impact of specific factors, such as the applied coupling scheme, the examined OV MV BPL topology, and maximum CUD value, on the optimal number of monotonic sections. Identifying this need for PES performance improvement of piecewise monotonic data approximations that are based on the number of monotonic sections, a detailed analysis of the influence of the previous factors on the PES performance of OV MV BPL topologies is given in the companion paper of [59].

Conclusions

In this paper, the performance of L1PMA, L2WPMA, and L2CXCVCV against the measurement differences, which can occur during the determination of OV MV BPL coupling transfer functions, has been assessed in terms of PES and PES_{fault} .

From the various PES comparisons among the examined piecewise monotonic data approximations and the measurement differences, it has been pointed out that the mitigation of measurement differences is possible in the vast majority of the OV MV BPL cases examined regardless of the occurred magnitudes of the measurement difference distributions. In fact, piecewise monotonic data approximations that are based on the optimal number of monotonic sections (*i.e.*, L1PMA and L2WPMA) better cope with the measurement differences in OV MV BPL topologies of intense multipath environments (*i.e.*, urban topologies) whereas piecewise monotonic data approximations without monotonic sections better deal with the measurement differences of OV MV BPL topologies of “quiet” multipath environments (*i.e.*, suburban, rural, and “LOS” topologies). Depending on the examined OV MV BPL topology, a versatile measurement difference mitigation technique, which is going to use: (i) L2CXCVCV for the rural and “LOS” cases; and (ii) L1PMA or L2WPMA for the suburban and urban cases; could exploit all the 82.5% potential of mitigating measurement differences.

However, L1PMA and L2WPMA may further be enhanced if the selection of the optimal number of monotonic sections is further studied. The companion paper of [59] strengthens the PES efficiency of L1PMA and L2WPMA of this paper.

Conflicts of Interest

The author declares that there is no conflict of interests regarding the publication of this paper.

References

- [1] K. Ali, I. Pefkianakis, A. X. Liu, and K. H. Kim, "Boosting PLC Networks for High-Speed Ubiquitous Connectivity in Enterprises," arXiv preprint arXiv:1608.06574, 2016, [Online]. Available: <http://arxiv.org/pdf/1608.06574v1.pdf> (Accessed on 11/25/2016)
- [2] A. G. Lazaropoulos, "Best L1 Piecewise Monotonic Data Approximation in Overhead and Underground Medium-Voltage and Low-Voltage Broadband over Power Lines Networks: Theoretical and Practical Transfer Function Determination," *Hindawi Journal of Computational Engineering*, vol. 2016, Article ID 6762390, 24 pages, 2016. DOI: 10.1155/2016/6762390.
- [3] C. Cano, A. Pittolo, D. Malone, L. Lampe, A. M. Tonello, and A. Dabak, "State-of-the-art in Power Line Communications: From the Applications to the Medium," *IEEE J. Sel. Areas Commun.*, vol. 34, pp. 1935-1952, 2016.
- [4] L. Lampe, A. M. Tonello, and T. G. Swart, *Power Line Communications: Principles, Standards and Applications from Multimedia to Smart Grid*. John Wiley & Sons, 2016.
- [5] Homeplug, Technology Gains Momentum, 2013, [Online]. Available: <http://www.businesswire.com> (Accessed on 11/25/2016)
- [6] Homeplug, AV Whitepaper, 2007, [Online]. Available: <http://www.homeplug.org/techresources/resources/> (Accessed on 11/25/2016)
- [7] Homeplug, AV2 Whitepaper, 2011, [Online]. Available: <http://www.homeplug.org/techresources/resources/> (Accessed on 11/25/2016)
- [8] A. G. Lazaropoulos and P. G. Cottis, "Transmission characteristics of overhead medium voltage power line communication channels," *IEEE Trans. Power Del.*, vol. 24, no. 3, pp. 1164-1173, Jul. 2009.
- [9] A. G. Lazaropoulos and P. G. Cottis, "Capacity of overhead medium voltage power line communication channels," *IEEE Trans. Power Del.*, vol. 25, no. 2, pp. 723-733, Apr. 2010.
- [10] A. G. Lazaropoulos and P. G. Cottis, "Broadband transmission via underground medium-voltage power lines-Part I: transmission characteristics," *IEEE Trans. Power Del.*, vol. 25, no. 4, pp. 2414-2424, Oct. 2010.
- [11] A. G. Lazaropoulos and P. G. Cottis, "Broadband transmission via underground medium-voltage power lines-Part II: capacity," *IEEE Trans. Power Del.*, vol. 25, no. 4, pp. 2425-2434, Oct. 2010.
- [12] A. G. Lazaropoulos, "Broadband transmission characteristics of overhead high-voltage power line communication channels," *Progress in Electromagnetics Research B*, vol. 36, pp. 373-398, 2012. DOI: 10.2528/PIERB11091408
- [13] A. G. Lazaropoulos, "Capacity Performance of Overhead Transmission Multiple-Input Multiple-Output Broadband over Power Lines Networks: The Insidious Effect of Noise and the Role of Noise Models," *Trends in Renewable Energy*, vol. 2, no. 2, pp. 61-82, Jan. 2016. DOI: 10.17737/tre.2016.2.2.0023
- [14] A. G. Lazaropoulos, "Factors Influencing Broadband Transmission Characteristics of Underground Low-Voltage Distribution Networks," *IET Commun.*, vol. 6, no. 17, pp. 2886-2893, Nov. 2012.
- [15] A. G. Lazaropoulos, "Towards broadband over power lines systems integration: Transmission characteristics of underground low-voltage distribution power lines," *Progress in Electromagnetics Research B*, 39, pp. 89-114, 2012. DOI: 10.2528/PIERB12012409

- [16] A. G. Lazaropoulos, "Broadband transmission and statistical performance properties of overhead high-voltage transmission networks," *Hindawi Journal of Computer Networks and Commun.*, 2012, article ID 875632, 2012. DOI: 10.1155/2012/875632
- [17] A. G. Lazaropoulos, "Towards modal integration of overhead and underground low-voltage and medium-voltage power line communication channels in the smart grid landscape: model expansion, broadband signal transmission characteristics, and statistical performance metrics (Invited Paper)," *ISRN Signal Processing*, vol. 2012, Article ID 121628, 17 pages, 2012. DOI: 10.5402/2012/121628
- [18] A. G. Lazaropoulos, "Review and Progress towards the Common Broadband Management of High-Voltage Transmission Grids: Model Expansion and Comparative Modal Analysis," *ISRN Electronics*, vol. 2012, Article ID 935286, pp. 1-18, 2012. DOI: 10.5402/2012/935286
- [19] A. G. Lazaropoulos, "Review and Progress towards the Capacity Boost of Overhead and Underground Medium-Voltage and Low-Voltage Broadband over Power Lines Networks: Cooperative Communications through Two- and Three-Hop Repeater Systems," *ISRN Electronics*, vol. 2013, Article ID 472190, pp. 1-19, 2013. DOI: 10.1155/2013/472190
- [20] A. G. Lazaropoulos, "Green Overhead and Underground Multiple-Input Multiple-Output Medium Voltage Broadband over Power Lines Networks: Energy-Efficient Power Control," *Journal of Global Optimization*, vol. 57, no. 3, pp 997–1024, Nov. 2013. DOI: 10.1007/s10898-012-9988-y
- [21] P. Amirshahi and M. Kavehrad, "High-frequency characteristics of overhead multiconductor power lines for broadband communications," *IEEE J. Sel. Areas Commun.*, vol. 24, no. 7, pp. 1292-1303, Jul. 2006.
- [22] T. Sartenaer, "Multiuser communications over frequency selective wired channels and applications to the powerline access network" Ph.D. dissertation, Univ. Catholique Louvain, Louvain-la-Neuve, Belgium, Sep. 2004.
- [23] T. Calliacoudas and F. Issa, "Multiconductor transmission lines and cables solver," An efficient simulation tool for plc channel networks development," presented at the *IEEE Int. Conf. Power Line Communications and Its Applications*, Athens, Greece, Mar. 2002.
- [24] A. G. Lazaropoulos, "Measurement Differences, Faults and Instabilities in Intelligent Energy Systems –Part 1: Identification of Overhead High-Voltage Broadband over Power Lines Network Topologies by Applying Topology Identification Methodology (TIM)," *Trends in Renewable Energy*, vol. 2, no. 3, pp. 85 – 112, Oct. 2016. DOI: 10.17737/tre.2016.2.3.0026
- [25] A. G. Lazaropoulos, "Measurement Differences, Faults and Instabilities in Intelligent Energy Systems – Part 2: Fault and Instability Prediction in Overhead High-Voltage Broadband over Power Lines Networks by Applying Fault and Instability Identification Methodology (FIIM)," *Trends in Renewable Energy*, vol. 2, no. 3, pp. 113 – 142, Oct. 2016. DOI: 10.17737/tre.2016.2.3.0027
- [26] I. C. Demetriou and M. J. D. Powell, "Least squares smoothing of univariate data to achieve piecewise monotonicity," *IMA J. of Numerical Analysis*, vol. 11, pp. 411-432, 1991.
- [27] I. C. Demetriou and V. Koutoulidis, "On Signal Restoration by Piecewise Monotonic Approximation", in *Lecture Notes in Engineering and Computer*

- Science: *Proceedings of The World Congress on Engineering 2013*, London, U.K., Jul. 2013, pp. 268-273.
- [28] I. C. Demetriou, "An application of best L_1 piecewise monotonic data approximation to signal restoration," *IAENG International Journal of Applied Mathematics*, vol. 53, no. 4, pp. 226-232, 2013.
- [29] I. C. Demetriou, "L1PMA: A Fortran 77 Package for Best L_1 Piecewise Monotonic Data Smoothing," *Computer Physics Communications*, vol. 151, no. 1, pp. 315-338, 2003.
- [30] I. C. Demetriou, "Data Smoothing by Piecewise Monotonic Divided Differences," *Ph.D. Dissertation*, Department of Applied Mathematics and Theoretical Physics, University of Cambridge, Cambridge, 1985.
- [31] I. C. Demetriou, "Best L_1 Piecewise Monotonic Data Modelling," *Int. Trans. Opt Res.*, vol. 1, no. 1, pp. 85-94, 1994.
- [32] C. de Boor, *A Practical Guide to Splines*. Revised Edition, NY: Springer-Verlag, Applied Mathematical Sciences, vol. 27, 2001.
- [33] M. Holschneider, *Wavelets. An Analysis Tool*, Oxford: Clarendon Press, 1997.
- [34] I. C. Demetriou, "Algorithm 863: L2WPMA, a Fortran 77 package for weighted least-squares piecewise monotonic data approximation," *ACM Transactions on Mathematical Software (TOMS)*, vol. 33, no.1, pp. 6, 2007.
- [35] I. C. Demetriou, "L2CXCV: A Fortran 77 package for least squares convex/concave data smoothing," *Computer physics communications*, vol. 174, no.8, pp. 643-668, 2006.
- [36] P. Amirshahi, "Broadband access and home networking through powerline networks" Ph.D. dissertation, Pennsylvania State Univ., University Park, PA, May 2006. [Online]. Available: <http://etda.libraries.psu.edu/theses/approved/WorldWideIndex/ETD-1205/index.html> (Accessed on 11/25/2016)
- [37] M. D'Amore and M. S. Sarto, "Simulation models of a dissipative transmission line above a lossy ground for a wide-frequency range-Part I: Single conductor configuration," *IEEE Trans. Electromagn. Compat.*, vol. 38, no. 2, pp. 127-138, May 1996.
- [38] M. D'Amore and M. S. Sarto, "Simulation models of a dissipative transmission line above a lossy ground for a wide-frequency range-Part II: Multi-conductor configuration," *IEEE Trans. Electromagn. Compat.*, vol. 38, no. 2, pp. 139-149, May 1996.
- [39] A. Milioudis, G. T. Andreou, and D. P. Labridis, "Detection and location of high impedance faults in multiconductor overhead distribution lines using power line communication devices," *IEEE Trans. on Smart Grid*, vol. 6, no. 2, pp. 894-902, 2015.
- [40] A. G. Lazaropoulos, "Designing Broadband over Power Lines Networks Using the Techno-Economic Pedagogical (TEP) Method – Part I: Overhead High Voltage Networks and Their Capacity Characteristics," *Trends in Renewable Energy*, vol. 1, no. 1, pp. 16-42, Mar. 2015. DOI: 10.17737/tre.2015.1.1.002
- [41] A. G. Lazaropoulos, "Designing Broadband over Power Lines Networks Using the Techno-Economic Pedagogical (TEP) Method – Part II: Overhead Low-Voltage and Medium-Voltage Channels and Their Modal Transmission Characteristics," *Trends in Renewable Energy*, vol. 1, no. 2, pp. 59-86, Jun. 2015. DOI: 10.17737/tre.2015.1.2.006

- [42] T. Sartenaer and P. Delogne, "Deterministic modelling of the (Shielded) outdoor powerline channel based on the multiconductor transmission line equations," *IEEE J. Sel. Areas Commun.*, vol. 24, no. 7, pp. 1277-1291, Jul. 2006.
- [43] OPERA1, D5: Pathloss as a function of frequency, distance and network topology for various LV and MV European powerline networks. IST Integrated Project No 507667, Apr. 2005.
- [44] OPERA1, D44: Report presenting the architecture of plc system, the electricity network topologies, the operating modes and the equipment over which PLC access system will be installed, IST Integr. Project No 507667, Dec. 2005.
- [45] A. G. Lazaropoulos, "The Impact of Noise Models on Capacity Performance of Distribution Broadband over Power Lines (BPL) Networks," *Hindawi Computer Networks and Communications*, vol. 2016, Article ID 5680850, 14 pages, 2016. DOI: 10.1155/2016/5680850.
- [46] A. G. Lazaropoulos, "Policies for Carbon Energy Footprint Reduction of Overhead Multiple-Input Multiple-Output High Voltage Broadband over Power Lines Networks," *Trends in Renewable Energy*, vol. 1, no. 2, pp. 87-118, Jun. 2015. DOI: 10.17737/tre.2015.1.2.0011
- [47] A. G. Lazaropoulos, "Wireless Sensor Network Design for Transmission Line Monitoring, Metering and Controlling: Introducing Broadband over PowerLines-enhanced Network Model (BPLeNM)," *ISRN Power Engineering*, vol. 2014, Article ID 894628, 22 pages, 2014. DOI: 10.1155/2014/894628.
- [48] A. G. Lazaropoulos, "Wireless Sensors and Broadband over PowerLines Networks: The Performance of Broadband over PowerLines-enhanced Network Model (BPLeNM) (Invited Paper)," *ICAS Publishing Group Transaction on IoT and Cloud Computing*, vol. 2, no. 3, pp. 1-35, 2014.
- [49] M. J. D. Powell, *Approximation Theory and Methods*. Cambridge, U.K.: Cambridge University Press, 1981.
- [50] A. G. Lazaropoulos, *Engineering the Art through the Lens of LIPMA: A Tribute to the Modern Greek Painters*, Art Book ISSUU Digital Publishing Platform, Oct. 2014. [Online]. Available: <http://issuu.com/lazaropoulos/docs/l1pma> (Accessed on 11/25/2016)
- [51] A. G. Lazaropoulos, *ReEngineering the Art through the Lens of L2WPMA: A Tribute to Leonardo da Vinci's Inventions: Flying Machines, War Machines, Architect/Innovations and Water Land Machines*, Art Book ISSUU Digital Publishing Platform, Nov. 2014. [Online]. Available: <http://issuu.com/lazaropoulos/docs/l2wpma> (Accessed on 11/25/2016)
- [52] A. G. Lazaropoulos, *ReEngineering the Art through the Lens of LIPMA L2WPMA: The Eternal Youth of the Parthenon Art, Architecture, Marble Sculpture, Metallurgy Pottery*, Art Book ISSUU Digital Publishing Platform, Dec. 2014. [Online]. Available: http://issuu.com/lazaropoulos/docs/l1pma_l2wpma (Accessed on 11/25/2016)
- [53] <http://cpc.cs.qub.ac.uk/summaries/ADRF> (Accessed on 11/25/2016)
- [54] http://www.cpc.cs.qub.ac.uk/summaries/ADX_M_v1_0.html (Accessed on 11/25/2016)
- [55] T. Banwell and S. Galli, "A novel approach to accurate modeling of the indoor power line channel—Part I: Circuit analysis and companion model," *IEEE Trans. Power Del.*, vol. 20, no. 2, pp. 655-663, Apr. 2005.

- [56] S. Galli and T. Banwell, "A novel approach to accurate modeling of the indoor power line channel — Part II: Transfer function and channel properties," *IEEE Trans. Power Del.*, vol. 20, no. 3, pp. 1869-1878, Jul. 2005.
- [57] S. Galli and T. Banwell, "A deterministic frequency-domain model for the indoor power line transfer function," *IEEE J. Sel. Areas Commun.*, vol. 24, no. 7, pp. 1304-1316, Jul. 2006.
- [58] A. G. Lazaropoulos, "Deployment Concepts for Overhead High Voltage Broadband over Power Lines Connections with Two-Hop Repeater System: Capacity Countermeasures against Aggravated Topologies and High Noise Environments," *Progress in Electromagnetics Research B*, vol. 44, pp. 283-307, 2012. DOI: 10.2528/PIERB12081104
- [59] A. G. Lazaropoulos, "Power Systems Stability through Piecewise Monotonic Data Approximations – Part 2: Adaptive Number of Monotonic Sections and Performance of L1PMA, L2WPMA, and L2CXCV in Overhead Medium-Voltage Broadband over Power Lines Networks," *Trends in Renewable Energy*, vol. 3, no. 1, 33-60, Jan. 2017. DOI: 10.17737/tre.2017.3.1.0030

Article copyright: © 2017 Athanasios G. Lazaropoulos. This is an open access article distributed under the terms of the [Creative Commons Attribution 4.0 International License](https://creativecommons.org/licenses/by/4.0/), which permits unrestricted use and distribution provided the original author and source are credited.



Power Systems Stability through Piecewise Monotonic Data Approximations – Part 2: Adaptive Number of Monotonic Sections and Performance of L1PMA, L2WPMA, and L2CXCV in Overhead Medium-Voltage Broadband over Power Lines Networks

Athanasios G. Lazaropoulos*

*School of Electrical and Computer Engineering / National Technical University of Athens /
9 IroonPolytechniou Street / Zografou, GR 15780*

Received October 20,2016; Accepted November 11, 2016; Published January 1, 2017

This second paper investigates the role of the number of monotonic sections during the mitigation of measurement differences in overhead medium-voltage broadband over power lines (OV MV BPL) transfer functions. The performance of two well-known piecewise monotonic data approximations that are based on the number of monotonic sections (*i.e.*, L1PMA and L2WPMA) is assessed in comparison with the occurred measurement differences and L2CXCV, which is a piecewise monotonic data approximation without considering monotonic sections.

The contribution of this paper is double. First, further examination regarding the definition of the optimal number of monotonic section is made so that the accuracy of L1PMA can be significantly enhanced. In fact, the goal is to render piecewise monotonic data approximations that are based on the optimal number of monotonic sections as the leading approximation against the other ones without monotonic sections. Second, a generic framework concerning the definition of an adaptive number of monotonic sections is proposed for given OV MV BPL topology.

Keywords: Smart Grid; Intelligent Energy Systems; Broadband over Power Lines (BPL) networks; Power Line Communications (PLC); Faults; Power System Stability; Fault Analysis; Fault Identification and Prediction; Distribution Power Grids

1. Introduction

More than 100 million BPL devices with annual growth rate of 30% have already been deployed, being able to deliver high-bandwidth applications (*e.g.*, HD video streaming and VoIP) with data rates that exceed 1Gbps [1]-[3]. However, higher data rates can be achieved if the inherent BPL deficiencies, such as high and frequency-selective channel attenuation, noise, faults and measurement differences, are counterbalanced [4]-[9].

As the determination of channel attenuation and the identification of faults and measurement differences are concerned [10], the well-established hybrid method is employed as the suitable theoretical basis for describing BPL signal propagation and

*Corresponding author: AGLazaropoulos@gmail.com

transmission [4]-[8], [11]-[23]. Actually, the hybrid method, which is employed to examine the behavior of various multiconductor transmission line (MTL) structures, gives as output the corresponding transfer function for given OV MV BPL network topology, OV MV MTL configuration, and applied coupling scheme.

Although the hybrid method is notably accurate, a number of practical reasons and “real-life” conditions create measurement differences between experimental and theoretical results influencing the broadband performance of BPL networks and affecting the overall network design. On the basis of six measurement difference categories, which are analyzed in [21]-[23], piecewise monotonic data approximations can be applied in order to mitigate the measurement differences and restore the broadband performance [10], [22]-[31]. So far, three piecewise monotonic data approximations have been examined that are divided into two groups: (i) *Piecewise monotonic data approximations with predefined monotonic sections*: L1PMA and L2WPMA have been defined in [26], [27], [32] and their performance regarding the mitigation of measurement differences in transmission and distribution BPL networks has been assessed in [10], [21]-[23]. Already been identified, the performance of L1PMA and L2WPMA mainly depends on the predefined number of monotonic sections. In fact, the best performance against measurement differences is achieved when a specific number of monotonic sections is identified and applied; and (ii) *Piecewise monotonic data approximations without predefined monotonic sections*: L2CXCV has been defined in [33] and its performance concerning the mitigation of measurement differences in transmission BPL networks has been assessed in [10]. L2CXCV performance depends neither on user- nor on computer-defined number of monotonic sections. In accordance with [10], the right selection of the number of monotonic sections plays the key role during the application of L1PMA and L2WPMA and the comparative benchmark analysis between the aforementioned groups. In this companion paper, the selection of an adaptive number of monotonic sections is extended from the traditional definition of the optimal number of monotonic sections [10], [21]-[23] to the proposed adaptive one with regards to the maximization of the percent error sum (PES), which is treated as a metric of the mitigation performance of piecewise monotonic data approximations against measurement differences [10], [21].

The rest of this paper is organized as follows: In Sec. II, a brief presentation of L1PMA, L2WPMA, and L2CXCV is given as well as the suitable metrics of PES and fault PES, which are applied in order to identify the optimal number of monotonic sections. Sec. III discusses the simulations of various OV MV BPL networks intending to identify the generic framework concerning the definition of an adaptive number of monotonic sections to mitigate the occurred measurement differences. Sec. IV concludes this paper.

2. Brief Presentation of L1PMA, L2WPMA, L2CXCV and PESs

A set of piecewise monotonic data approximations has already been comparatively benchmarked concerning its mitigation behavior against measurement differences during the OV MV BPL transfer function determination [10], [21]-[23]. L1PMA, L2WPMA, and L2CXCV have been assessed with regards to: (i) their relative PES; and (ii) their PES against fault PES. As already been shown in [10], piecewise monotonic data approximations that are based on the optimal number of monotonic sections (*i.e.*, L1PMA and L2WPMA) better cope with the measurement differences in

OV MV BPL topologies of intense multipath environments (*i.e.*, urban topologies) whereas piecewise monotonic data approximations without predefined monotonic sections (*i.e.*, L2CXCVC) better deal with the measurement differences of OV MV BPL topologies of “quiet” multipath environments (*i.e.*, suburban, rural, and “LOS” topologies). However, significant PES improvement of L1PMA and L2WPMA can be achieved if a careful study concerning the optimal number of monotonic sections is carried out.

2.1 Piecewise Monotonic Data Approximations with Predefined Monotonic Sections (L1PMA and L2WPMA)

L1PMA and L2WPMA exploit their piecewise monotonicity property by decomposing BPL coupling transfer function data into separate monotonous data sections between adjacent turning points (primary extrema). Then, L1PMA and L2WPMA separately handle the monotonous sections by proposing suitable regression approximation [21]-[23]. In general terms, L1PMA and L2WPMA software receives as inputs the measured OV MV BPL coupling transfer function data, the measurement frequencies and the number of monotonic sections (*i.e.*, either user- or computer-defined) and gives as outputs the optimal primary extrema and the best fit of the measured OV MV BPL coupling transfer function data. The mitigation performance of L1PMA and L2WPMA against measurement differences mainly depends on the number of monotonic sections while the best performance is achieved when a critical number of monotonic sections is adopted.

2.2 Piecewise Monotonic Data Approximations without Predefined Monotonic Sections (L2CXCVC)

L2CXCVC smooths the OV MV transfer function data in the least square error sense by assuming one sign change in the second divided differences of the smoothed values [33]. In contrast with L1PMA and L2WPMA, the number of monotonic sections is neither user- nor computer-defined since L2CXCVC computes the required fit by solving a strictly convex quadratic programming problem for each set. Since L2CXCVC better deals with the measurement differences of OV MV BPL topologies of “quiet” multipath environments, it acts as the benchmark for the evaluation of the improved L1PMA (see Sec. III).

2.3 PES, Fault PES and Δ PES

As it has already been mentioned in [10] and [21], to evaluate the mitigation performance of the piecewise monotonic data approximation methods against the presented measurement differences, the performance metrics of PES, fault PES, and Δ PES are applied.

More specifically, PES expresses as a percentage the total sum of the relative differences between the approximated coupling transfer function and the theoretical coupling transfer function for all the used frequencies, namely

$$PES = 100\% \cdot \frac{\sum_{i=1}^u \left| \overline{\mathbf{H}^{WtG}}(f_i) - \mathbf{H}^{WtG}(f_i) \right|}{\sum_{i=1}^u \left| \mathbf{H}^{WtG}(f_i) \right|} \quad (1)$$

where $\mathbf{H}^{\text{WtG}}(f_i)$ is the $u \times 1$ theoretical OV MV BPL coupling transfer function column vector for given WtG coupling scheme and measurement frequency f_i , $i=1, \dots, u$, $\overline{\mathbf{H}^{\text{WtG}}}(f_i)$ is the respective measured OV MV BPL coupling transfer function, $\overline{\overline{\mathbf{H}^{\text{WtG}}}}(f_i)$ is the respective approximated OV MV BPL coupling transfer function and u is the number of the assumed flat-fading subchannels in the examined frequency band of operation. With respect to eq. (1), to evaluate the mitigation efficiency of the piecewise monotonic data approximation methods towards the measurement differences, PES of eq.(1) is compared against the fault PES that is given by

$$PES_{\text{fault}} = 100\% \cdot \frac{\sum_{i=1}^u |\overline{\mathbf{H}^{\text{WtG}}}(f_i) - \mathbf{H}^{\text{WtG}}(f_i)|}{\sum_{i=1}^u |\mathbf{H}^{\text{WtG}}(f_i)|} \quad (2)$$

Indeed, with reference to eq. (1) and (2), the proposed ΔPES metric that is determined by

$$\Delta PES = -(PES - PES_{\text{fault}}) \quad (3)$$

expresses the difference between PES and fault PES. ΔPES achieves to assess the mitigation efficiency of the examined piecewise monotonic data approximation method; if ΔPES is positive then the piecewise monotonic data approximation method counterbalances the measurement differences. Note that the measurement differences, which are applied during the simulations of Sec. III, follow continuous uniform distributions (CUDs) with variable maximum value a_{CUD} as already done in [10], [21].

3. Numerical Results and Discussion

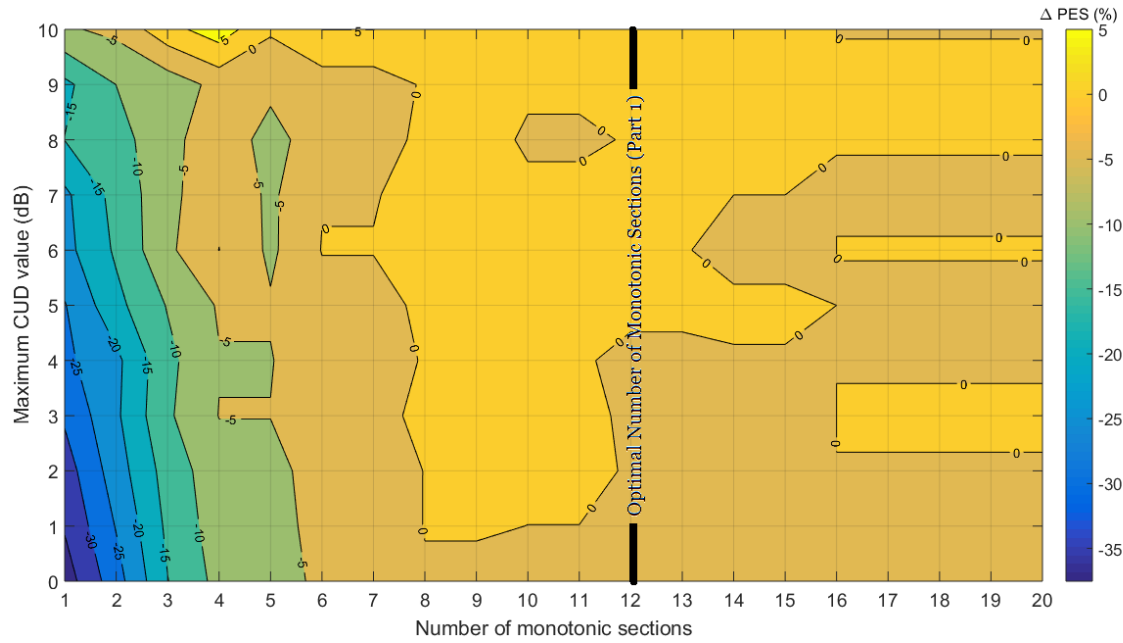
Various configurations of OV MV BPL networks are simulated with the purpose of assessing the mitigating performance of the piecewise monotonic data approximation methods of this paper against the occurred measurement differences. In fact, different OV MV BPL topologies and WtG coupling schemes are tested for various maximum CUD values.

As the simulation specifications are regarded, those are the same with [10]; the BPL frequency range and flat-fading subchannel frequency spacing are assumed to be equal to 1-30MHz and 1MHz, respectively. Therefore, the number of subchannels in the examined frequency range is equal to 30. The OV MV BPL topologies, which have been presented in Sec. IIB of [10], are also used in this paper while all the available WtG coupling schemes, say WtG^i , $i=1, \dots, 3$, that may be supported by the OV MV MTL configurations are investigated during the following simulations. Finally, the maximum CUD values that are examined range from 0dB to 10dB with 1dB step.

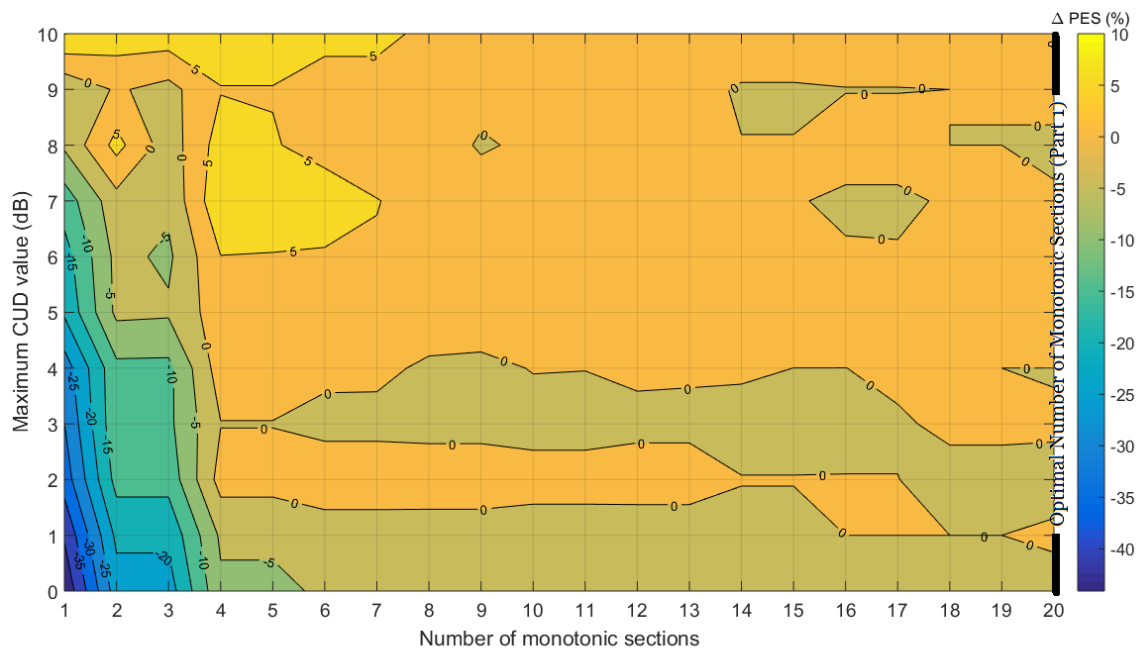
3.1 Optimal Number of Monotonic Sections and Different OV MV BPL Topologies and Coupling Schemes

In Fig. 1(a), ΔPES is plotted versus the maximum CUD value and the number of monotonic sections. In this figure, urban case is examined when WtG^1 coupling scheme and L1PMA are applied. The optimal number of monotonic sections that is analytically reported in [10], which is equal to 12 for the indicative urban case, is also drawn in the figure as a vertical line. In Figs. 1(b)-(d), same plots with Fig. 1(a) are given but for the

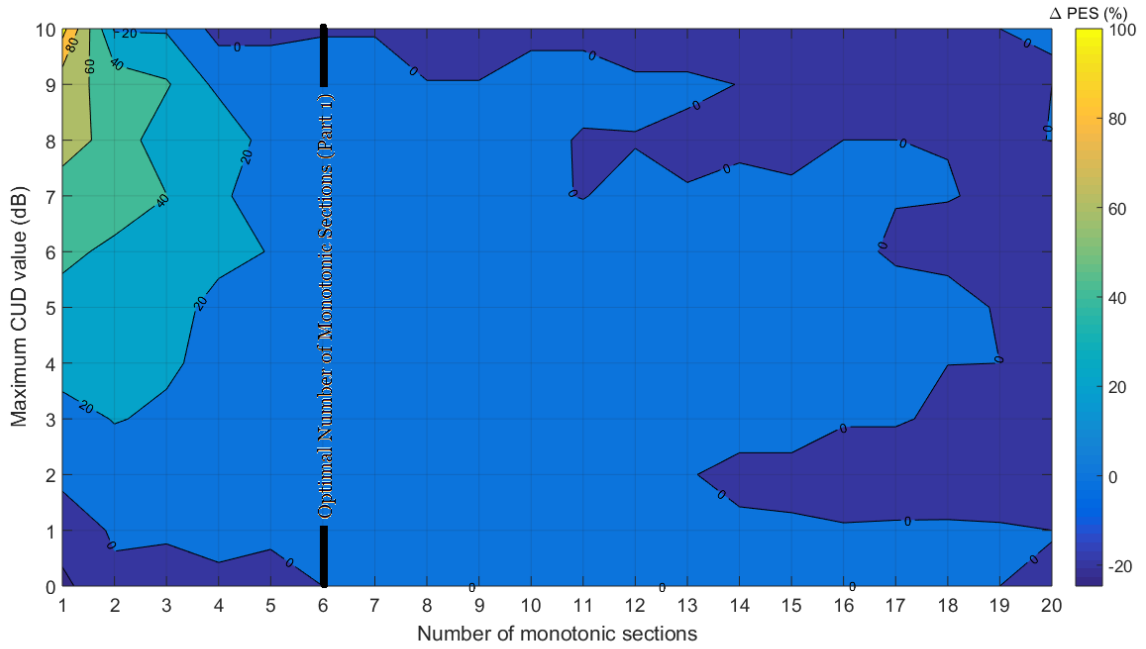
case of suburban, rural, and “LOS” case. Figs. 1(e)-(h) are the same with the respective Figs. 1(a)-(d) but for the application of L2WPMA. In Figs. 2(a)-(h) and Figs. 3(a)-(h), same plots with Figs. 1(a)-(h) are drawn but for WtG² and WtG³ coupling schemes, respectively.



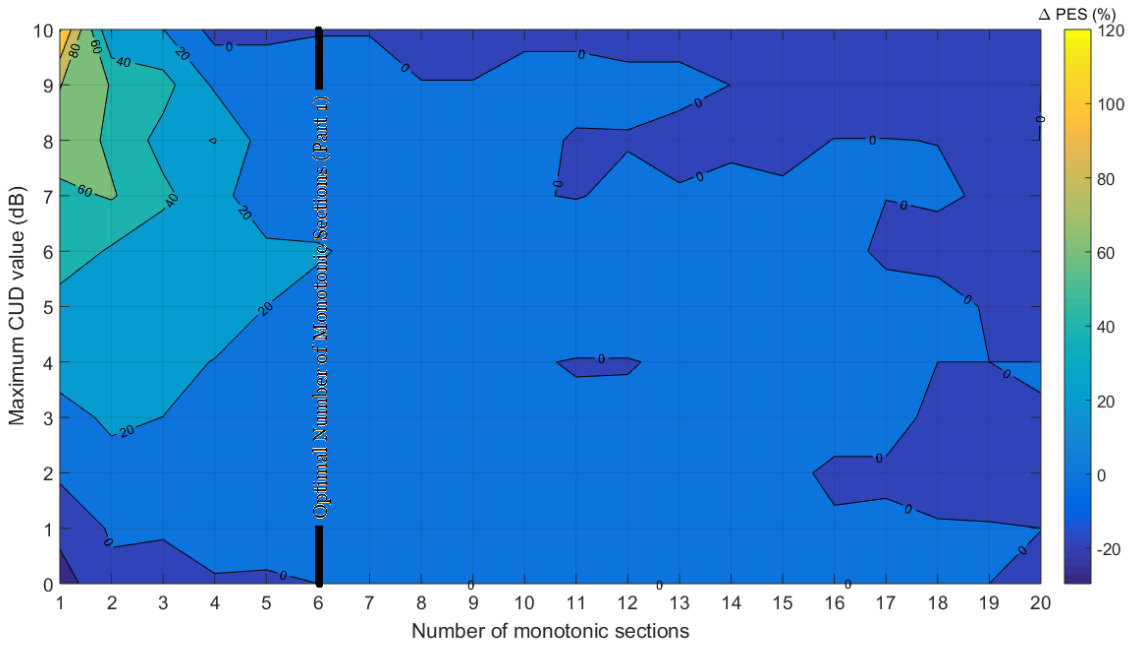
(a)



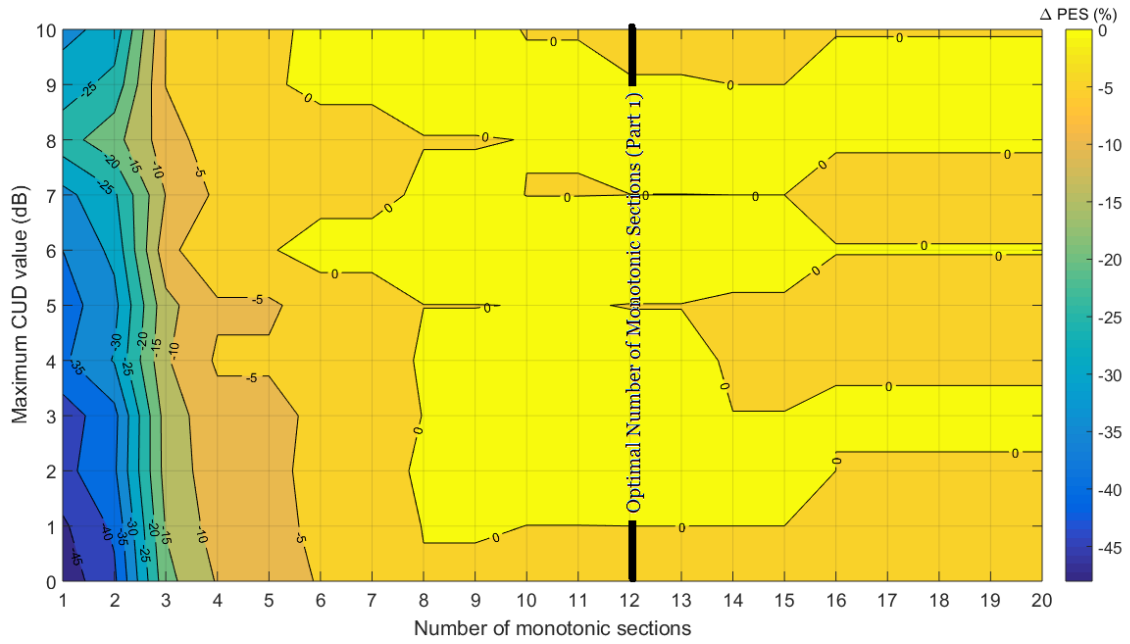
(b)



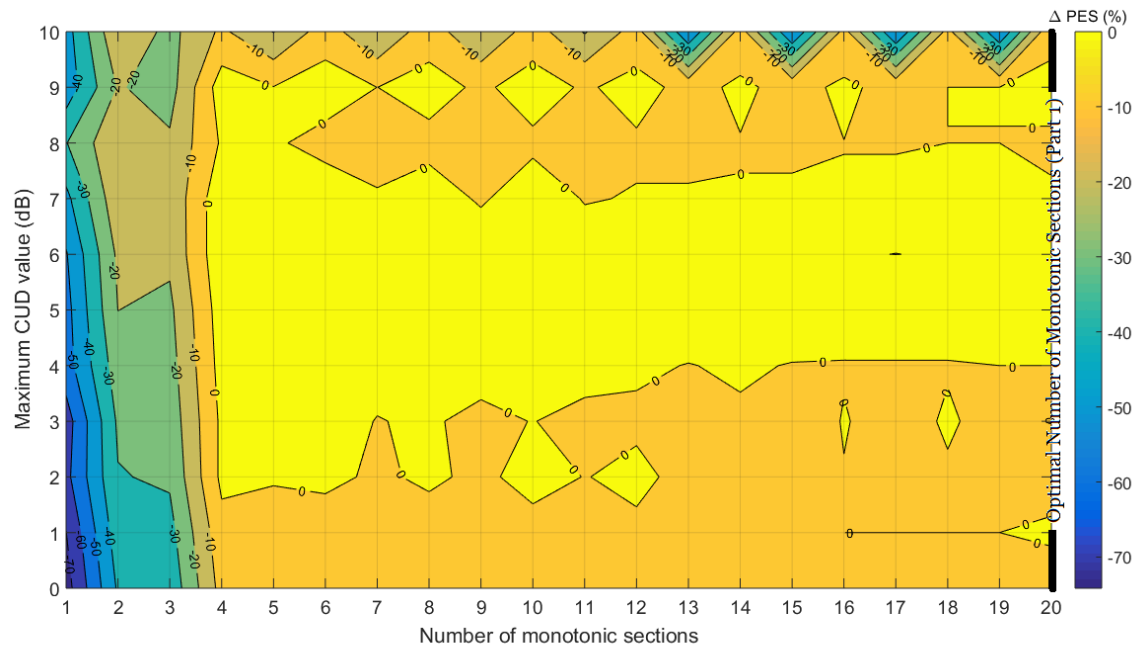
(c)



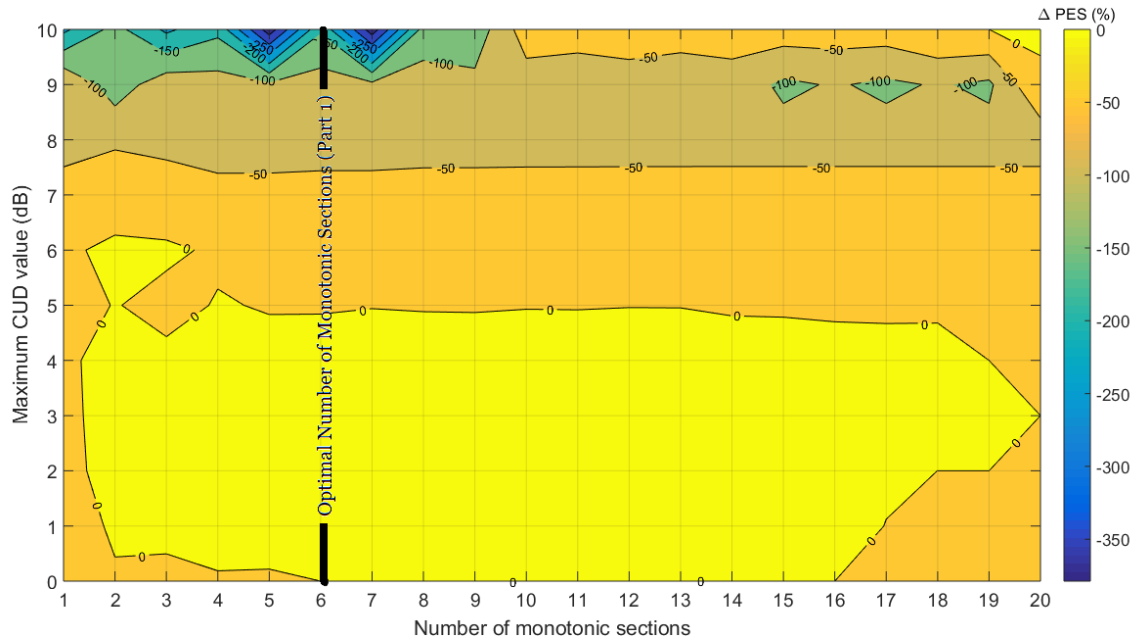
(d)



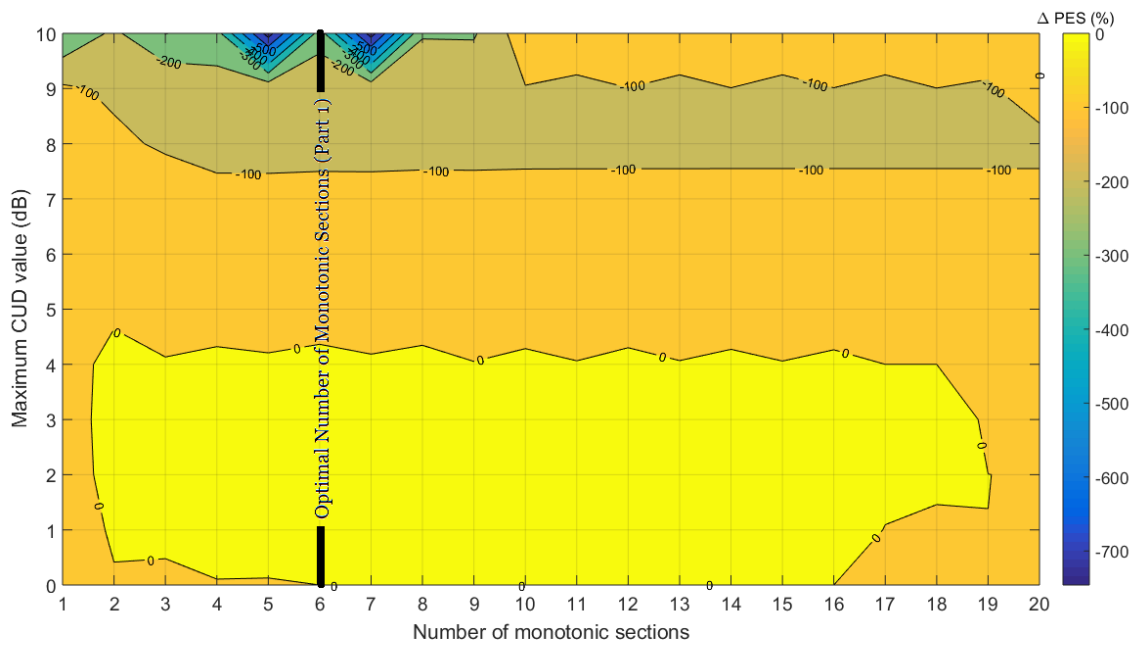
(e)



(f)

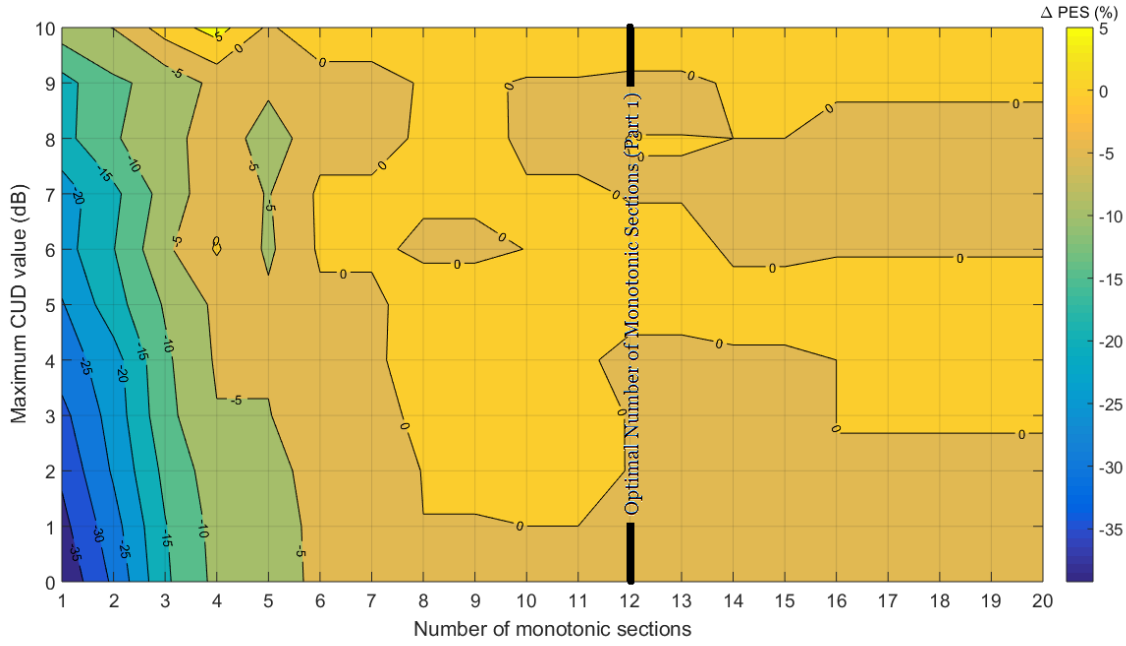


(g)

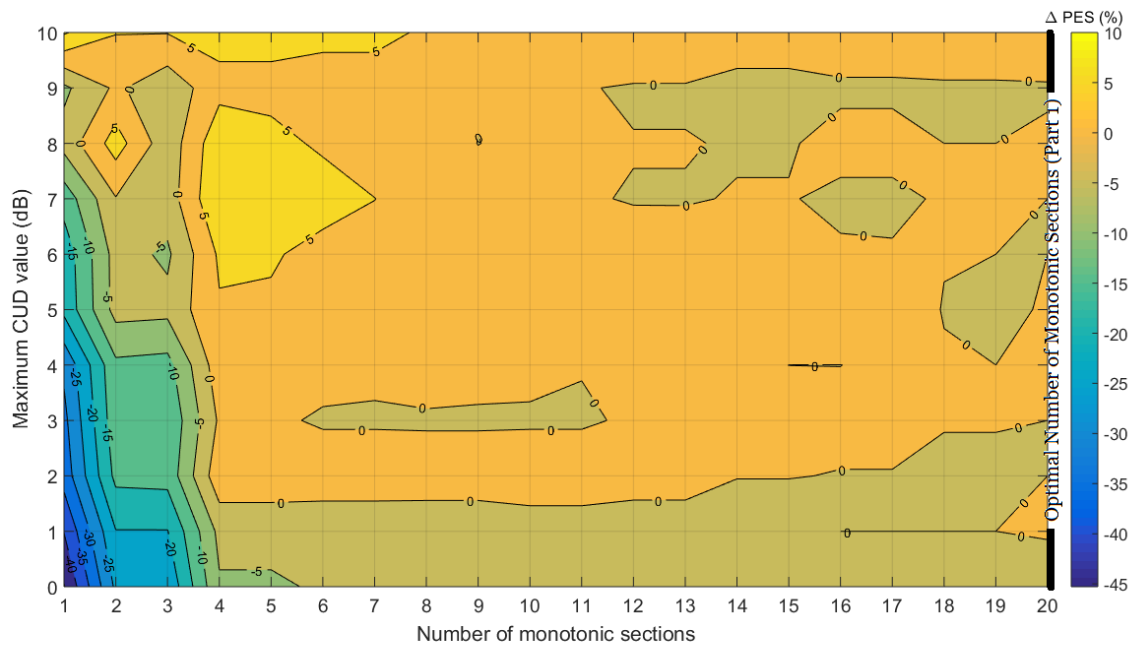


(h)

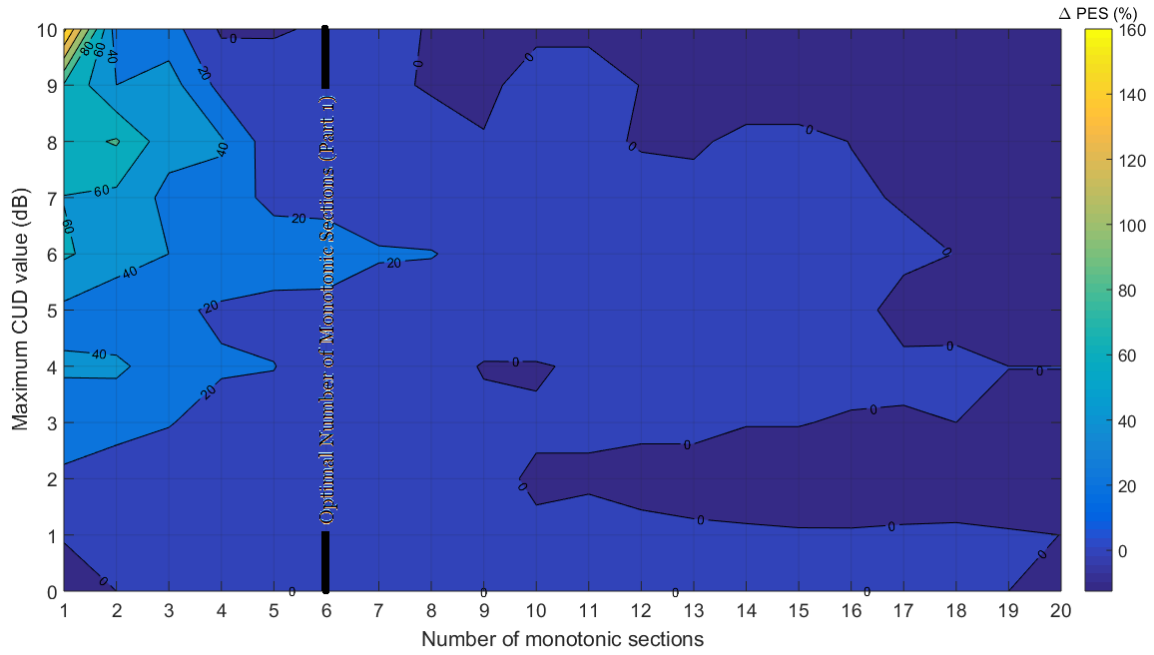
Figure 1. Δ PES is plotted for various indicative OV MV BPL topologies with respect to the maximum CUD value and number of monotonic sections (WtG¹ coupling scheme is applied and the vertical line of the optimal number of monotonic sections is shown). (a) Urban case / L1PMA. (b) Suburban case / L1PMA. (c) Rural case / L1PMA. (d) “LOS” case / L1PMA. (e) Urban case / L2WPMA. (f) Suburban case / L2WPMA. (g) Rural case / L2WPMA. (h) “LOS” case / L2WPMA.



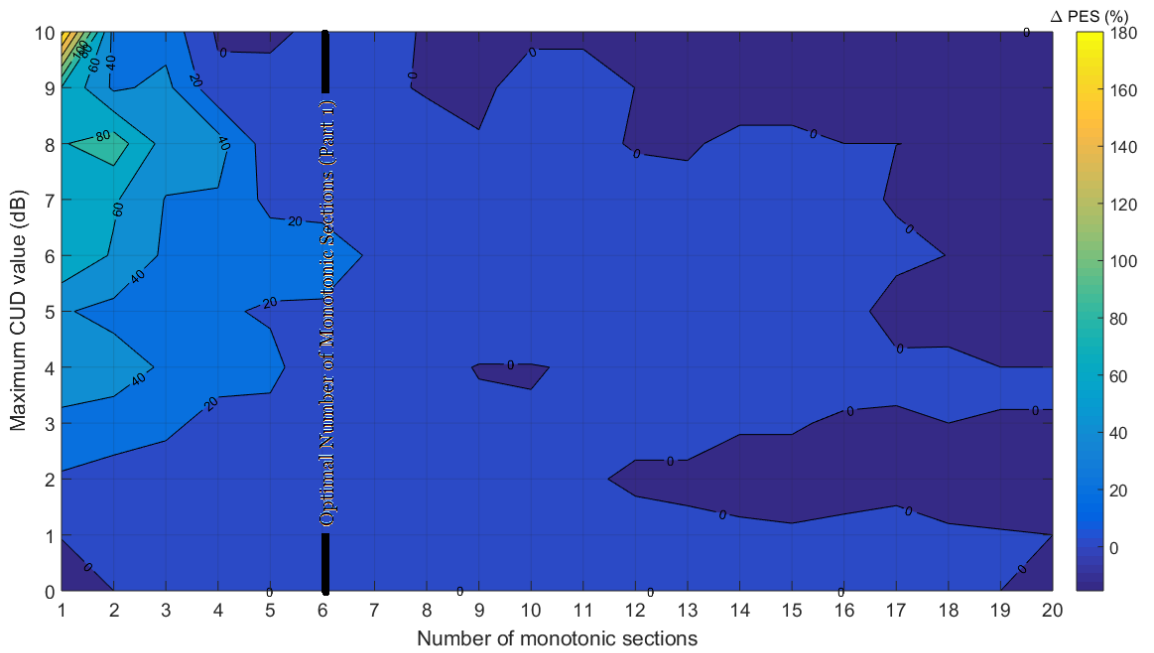
(a)



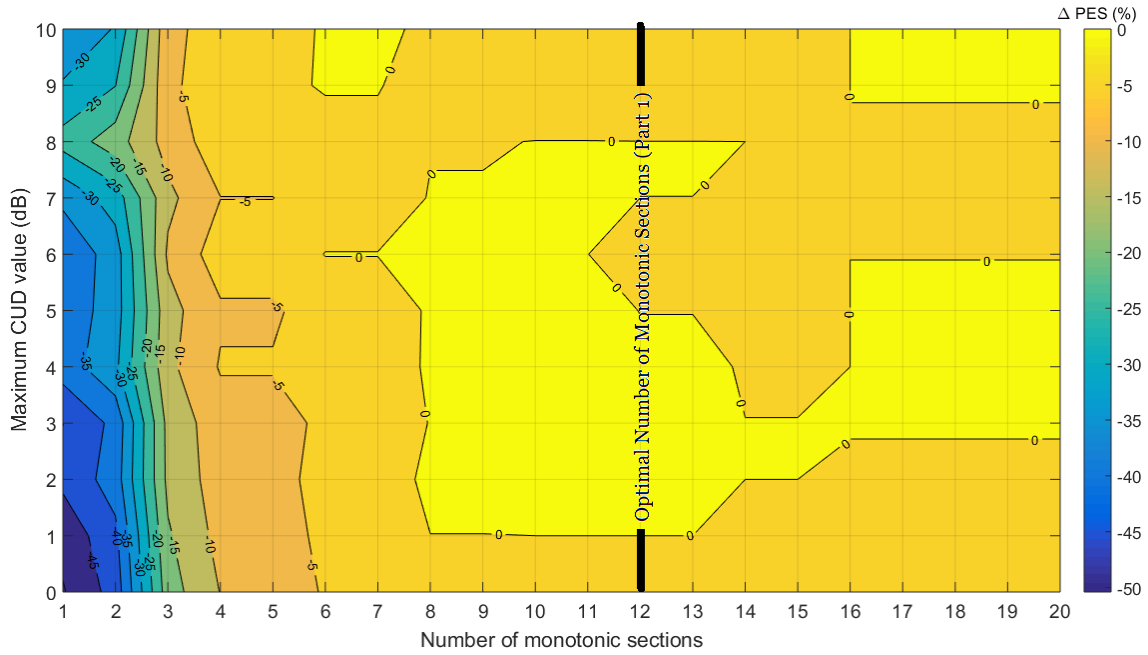
(b)



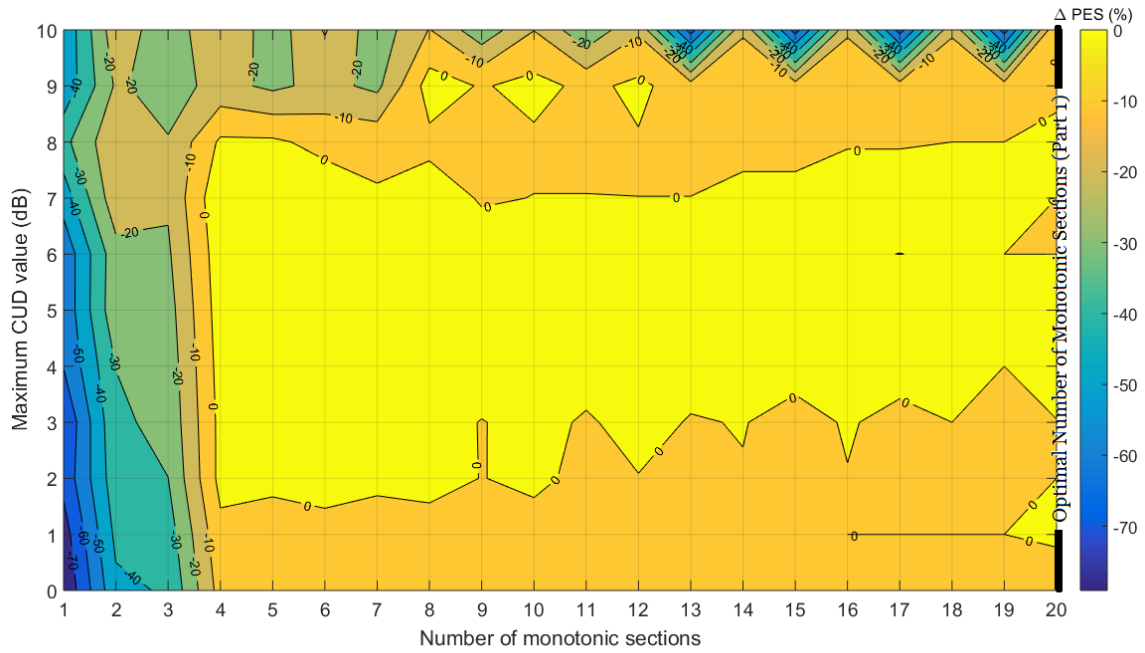
(c)



(d)



(e)



(f)

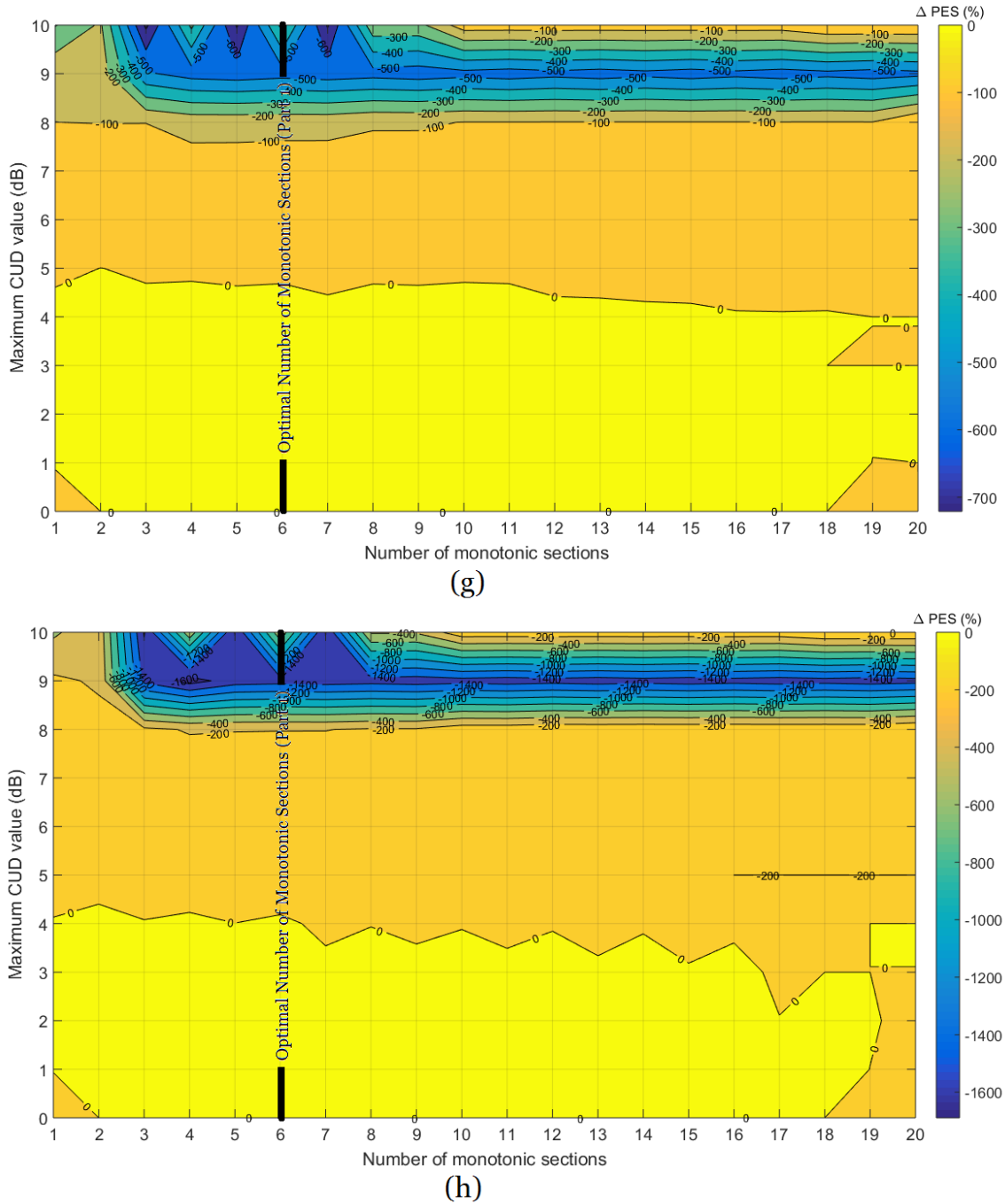
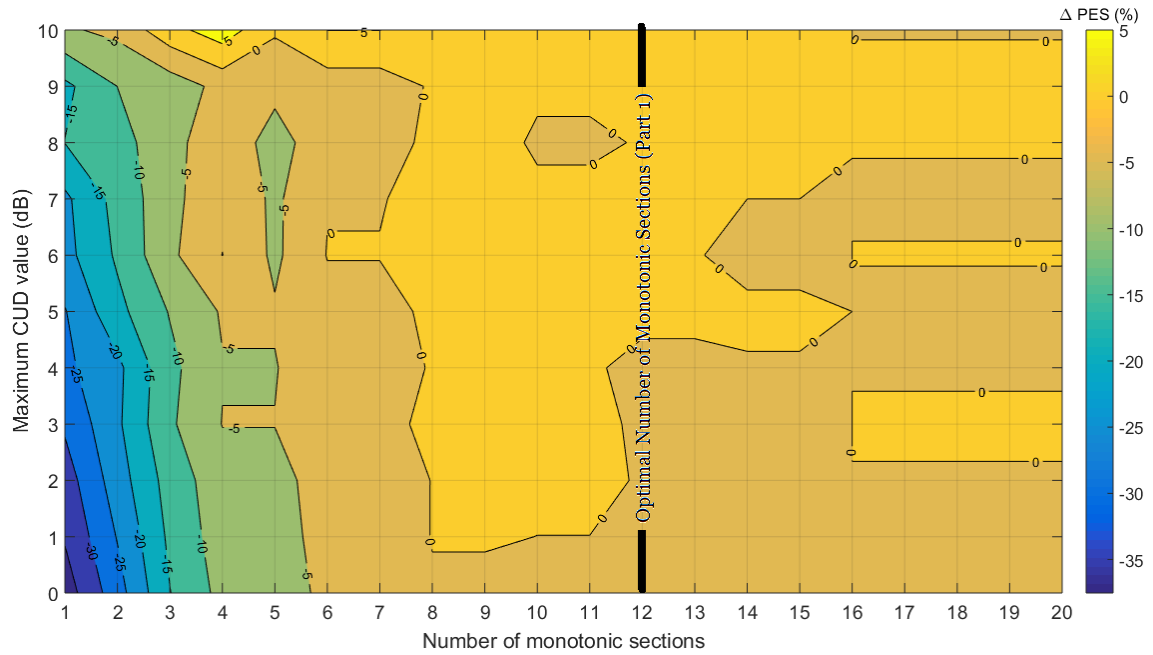
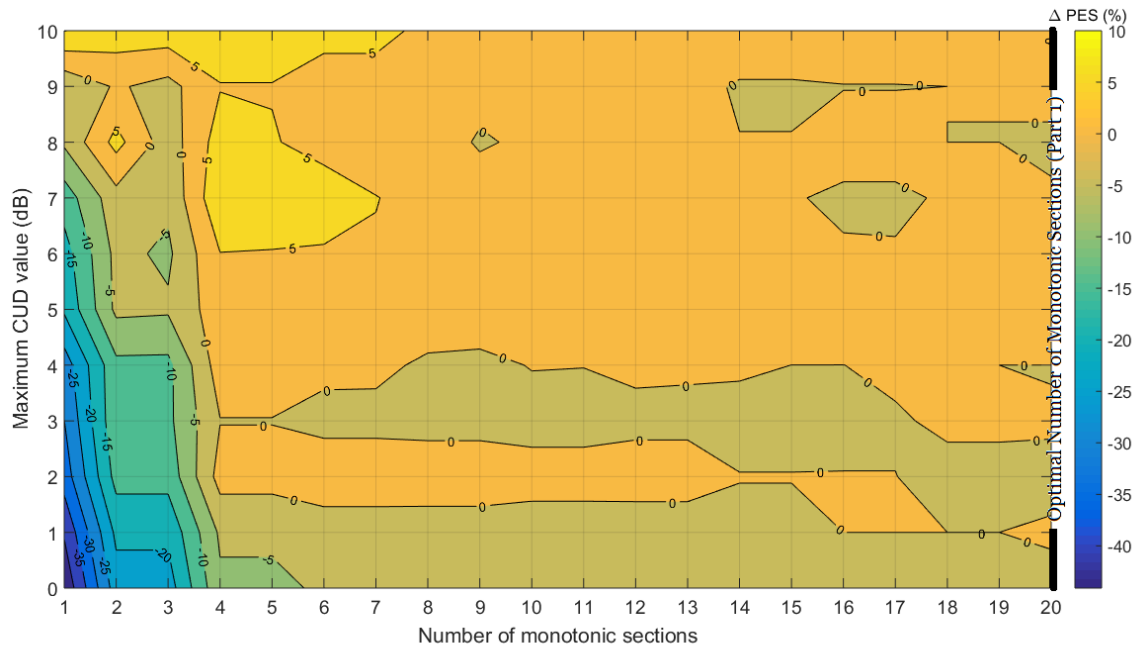


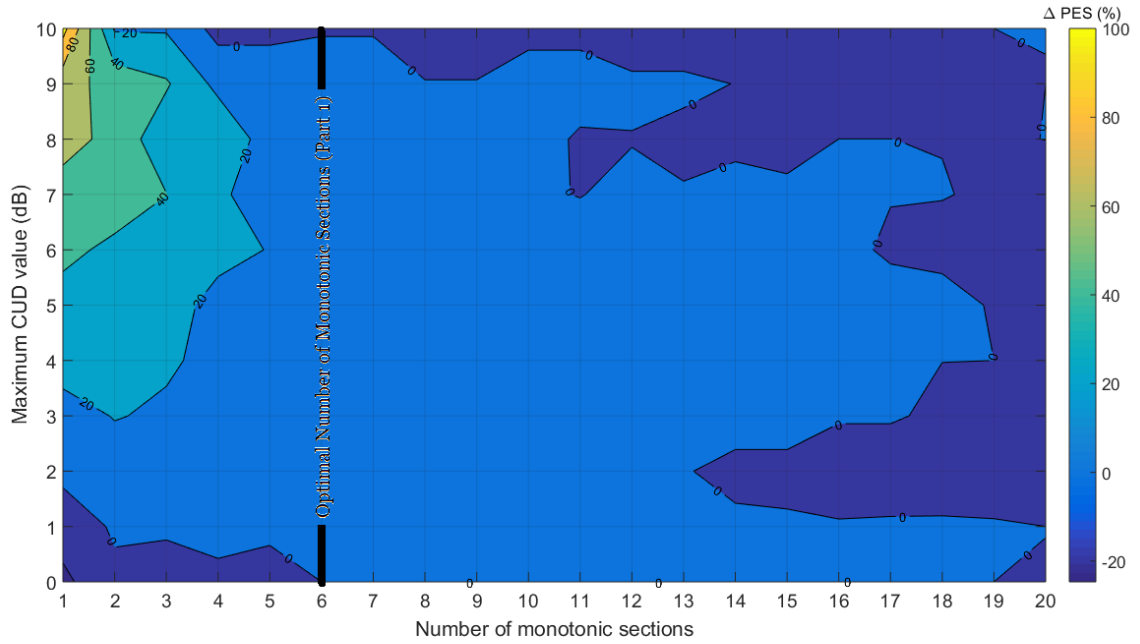
Figure 2. Same with Fig. 1 but for the WtG² coupling scheme.



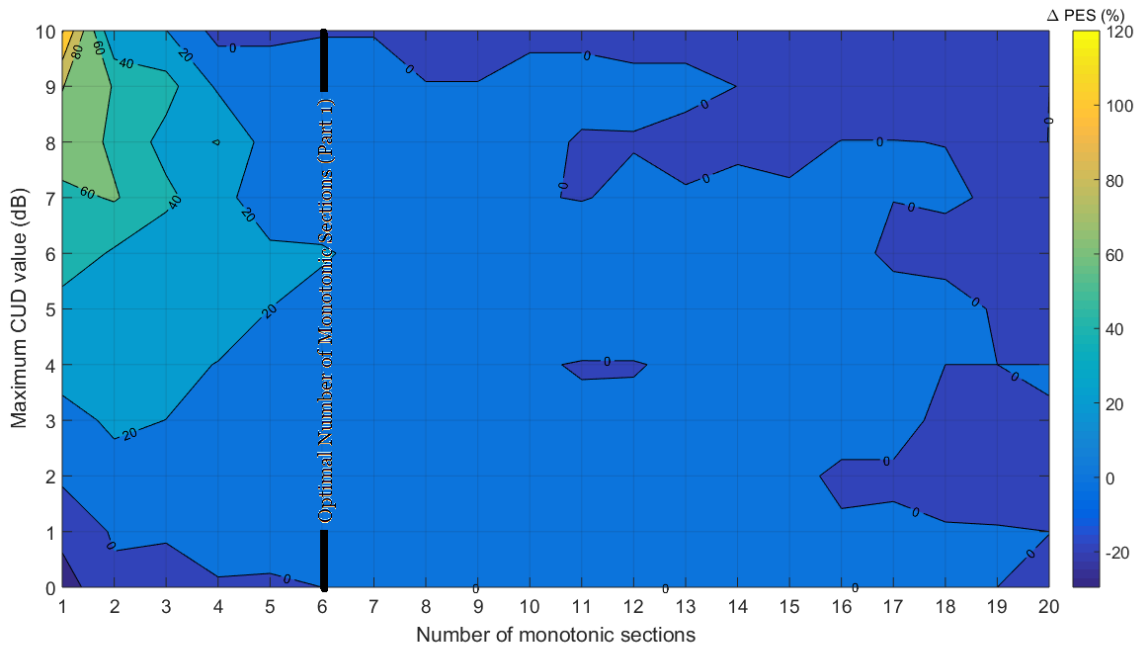
(a)



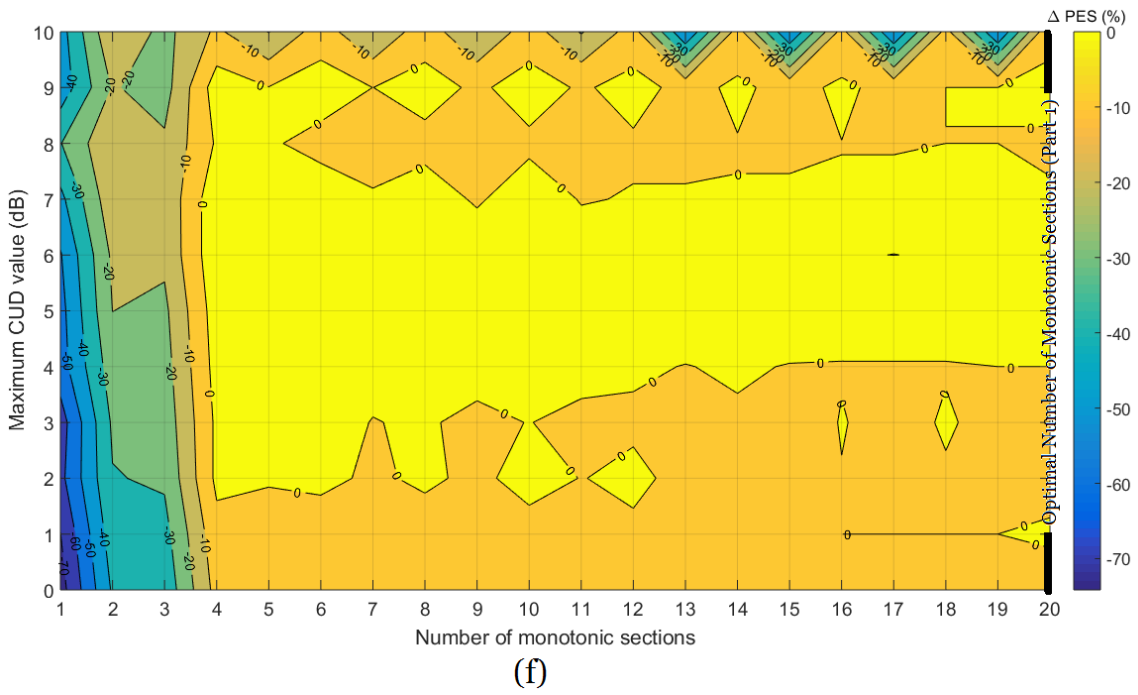
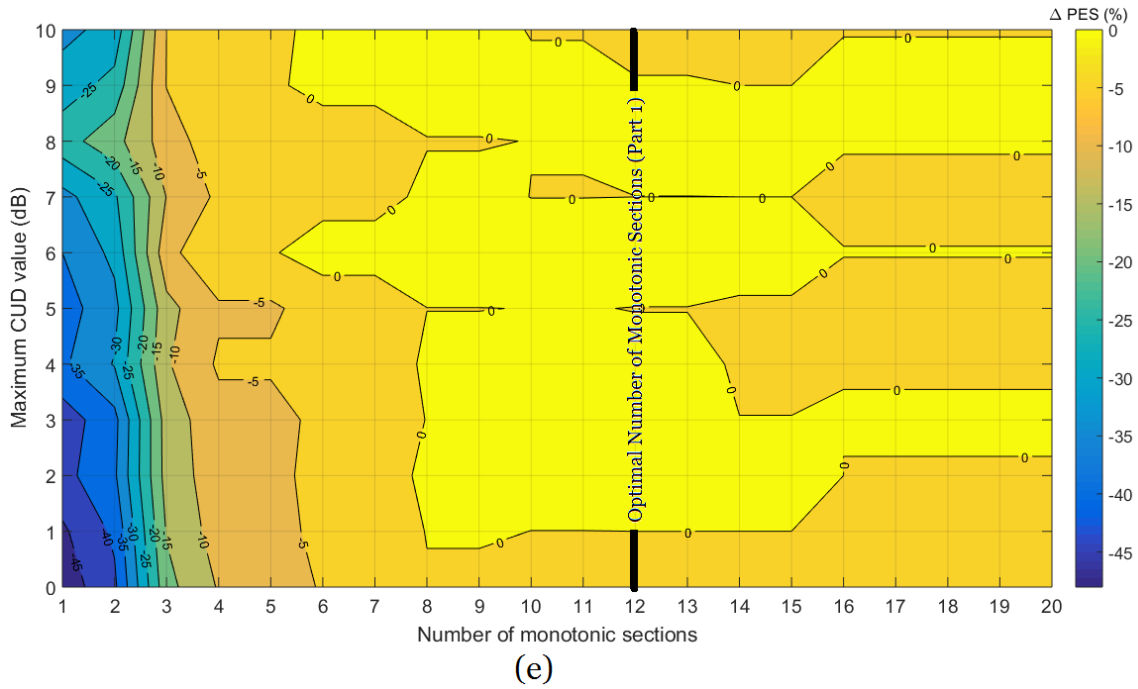
(b)

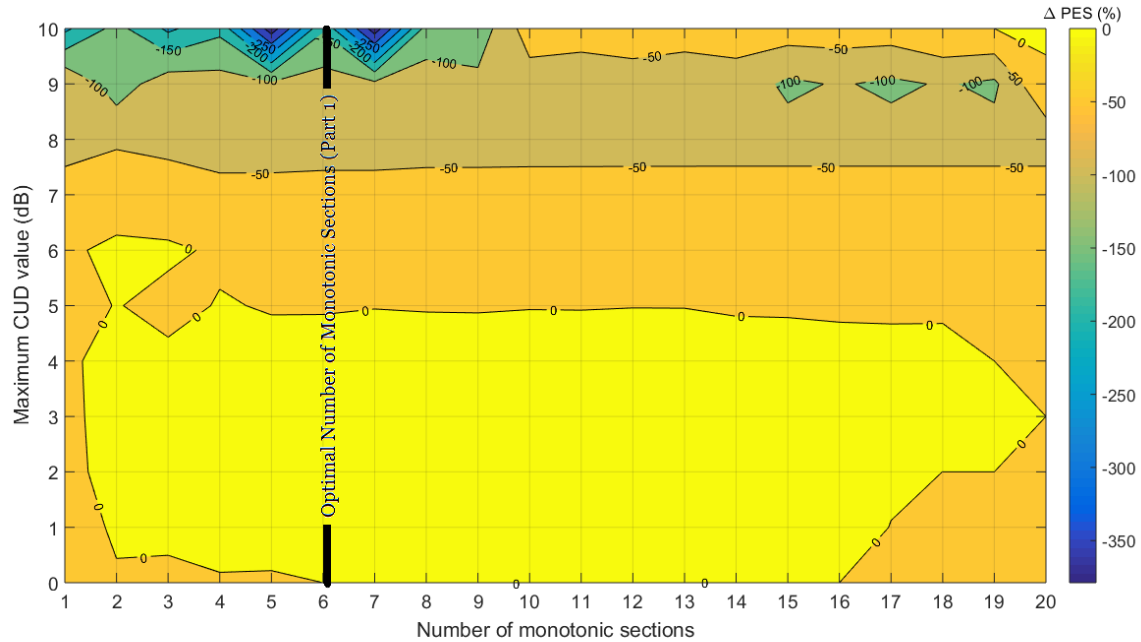


(c)

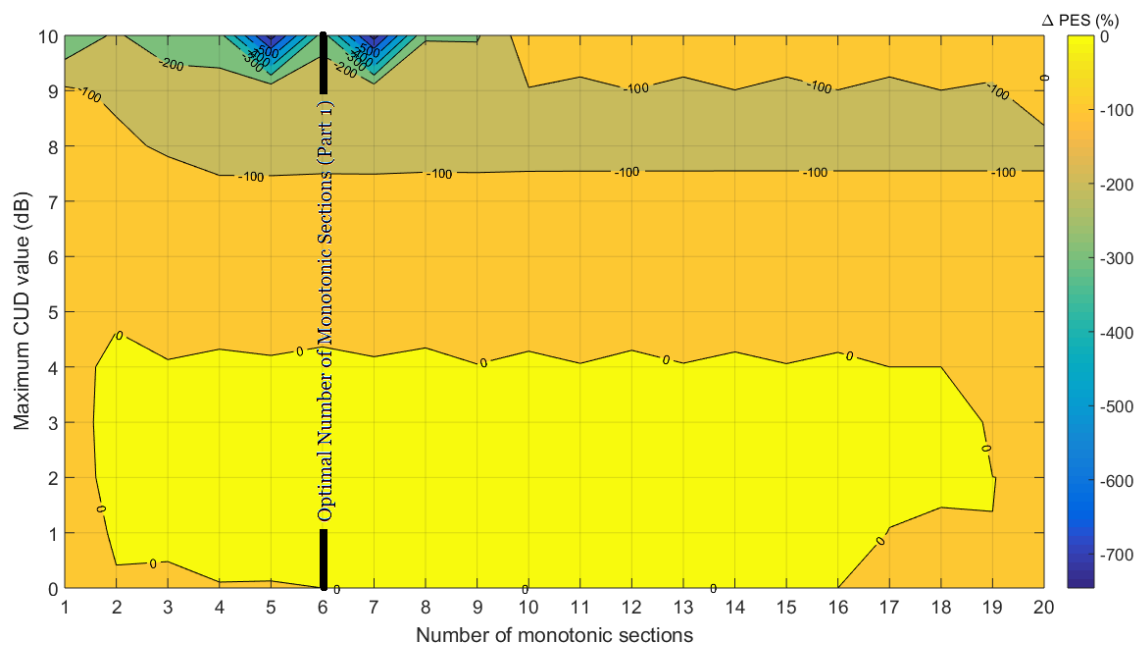


(d)





(g)



(h)

Figure 3. Same with Fig. 1 but for the WtG^3 coupling scheme.

From Figs. 1(a)-(h), 2(a)-(h) and 3(a)-(h), several interesting remarks can be pointed out:

- ΔPES presents significant fluctuations in the 24 cases examined in the aforementioned figures. In fact, its values approximately range from -1600% to 180%. However, positive ΔPES values may occur in all the cases examined indicating that there is always a careful selection of the number of monotonic sections that can mitigate possible measurement differences.

- L1PMA and L2WPMA present significant Δ PES differences even if the same OV MV BPL topology is examined, namely:
 - In the rural and “LOS” cases, L1PMA presents significantly better Δ PES results in comparison with L2WPMA ones regardless of the applied WtG coupling scheme and maximum CUD value. Δ PES differences between two piecewise monotonic data approximations may reach up to 180%. Also, analyzing the morphology of the isodynamic regions, the nature of the approximation procedure remains different between the two investigated approximations in the rural and “LOS” cases; L1PMA best approximates the data by requiring low number of monotonic sections while L2WPMA steadily approximates the same data regardless of the number of monotonic sections.
 - In urban and suburban cases, Δ PES results of L1PMA marginally exceed the respective ones of L2WPMA. Actually, the Δ PES differences between the application of L1PMA and L2WPMA may reach up to 15%. Here, both the applied methods approximate the coupling transfer function data by requiring a number of monotonic sections that ranges between a lower and an upper limit. Below the lower limit, L1PMA and L2WPMA are unable to approximate the rich multipath environments of urban and suburban cases whereas above the upper limit, L1PMA and L2WPMA cannot distinguish spectral notches from severe measurement differences due to the overfit.
- For given piecewise monotonic data approximation and OV MV BPL topology, Δ PES results remain almost the same regardless of the applied WtG coupling scheme. This is a rational event since the coupling transfer function differences among the supported WtG coupling schemes remain small due to the strong presence of the common mode [8], [14], [34].
- The definition of the optimal number of monotonic sections that has been described in [10], [21]-[23] provides an average approximation whether the maximum CUD value is known or not. As described in [10], the optimal number of monotonic sections for the indicative urban, suburban, rural, and “LOS” topologies is equal to 12, 20, 6, and 6, respectively. The line of the optimal number of monotonic sections of [10] is plotted in each figure while it runs through the areas of best Δ PES values in the vast majority of the cases examined either for L1PMA or L2WPMA.
- Also, in the vast majority of the cases examined, L1PMA can better approximate OV MV BPL coupling transfer function data than L2WPMA. This is a result that comes from: (i) the comparison of the respective colorbars next to plots; (ii) the comparison of the optimal Δ PES areas in figures; and (iii) the Δ PES results of the optimal number of monotonic sections. Hence, the main interest of the Sec. IIIB, which deals with the concept of an adaptive behavior against the measurement differences, is focused on L1PMA.

Although the improvement margins for the Δ PES values of L1PMA remain low in urban and suburban topologies when the optimal number of monotonic sections of [10] is adopted, the respective margins in rural and “LOS” cases can become significant. These latter improvements can allow L1PMA to become competitive against L2CXCVCV in rural and “LOS” cases where piecewise monotonic data approximations with monotonic

sections present certain approximation difficulties, which have been described in [10]. The solution of fully exploiting L1PMA potential passes through the proposal of an adaptive number of monotonic sections by taking under consideration an estimation of the maximum CUD value of the surrounding OV MV BPL network environment.

3.2 L1PMA with Adaptive Number of Monotonic Sections versus L1PMA with Optimal Number of Monotonic Sections and L2CXCV

If an accurate estimation of the maximum CUD value can be provided, then the potential Δ PES improvements of L1PMA through the adaptive number of monotonic sections can be significant. In fact, the adaptive number of monotonic sections comes from the localization of the best Δ PES value from the Figs. 1(a)-(h), 2(a)-(h), and 3(a)-(h) given the maximum CUD value, the examined OV MV BPL topology and the applied WtG coupling scheme. Note that greater Δ PES values imply that smaller PES can also be achieved.

In order to demonstrate the improvement potential, L1PMA Δ PES is reported in Table 1 when the optimal number of monotonic sections of [10] and the proposed adaptive number of monotonic sections are applied. To compare the performance improvement, L2WPMA Δ PES and L2CXCV Δ PES are also presented. Finally, In Table 1, all the indicative OV MV BPL topologies are examined when the WtG¹ coupling scheme is applied.

TABLE 1
 Δ PES of L1PMA with Optimal Number of Monotonic Sections, L1PMA with Adaptive Number of Monotonic Sections, L2WPMA and L2CXCV for the Indicative Urban OV MV BPL Topology when Different Maximum CUD Values Are Applied
 (Blue Font: The Best Δ PES Among the Different Piecewise Monotonic Data Approximations for Given Maximum CUD Value)

Indicative OV MV BPL Topology	Maximum CUD Value	L1PMA / Optimal Number of Monotonic Sections [10]		L2WPMA		L2CXCV	L1PMA / Adaptive Number of Monotonic Sections	
		Number of Monotonic Sections	Δ PES (%)	Number of Monotonic Sections	Δ PES (%)	Δ PES (%)	Number of Monotonic Sections	Δ PES (%)
Urban	0	12	-9.25×10^{-6}	12	-9.70×10^{-6}	-34.55	12 – 20	-9.25×10^{-6}
	1	12	-2.01×10^{-6}	12	-2.13×10^{-6}	-31.13	8 – 9	1.29×10^{-1}
	2	12	-1.08×10^{-1}	12	0.48	-28.41	10 – 11	3.20×10^{-1}
	3	12	-1.65×10^{-1}	12	0.24	-25.72	8 – 9	7.58×10^{-1}
	4	12	-5.93×10^{-1}	12	0.33	-22.32	10 – 11	2.79×10^{-1}
	5	12	5.53×10^{-1}	12	-0.02	-20.30	8 – 9	9.44×10^{-1}
	6	12	8.77×10^{-2}	12	0.81	-15.74	8 – 9	1.71
	7	12	5.15×10^{-2}	12	-5.43×10^{-4}	-17.83	8 – 9	1.31
	8	12	1.06×10^{-1}	12	0.03	-12.02	8 – 9	7.36×10^{-1}
	9	12	1.59×10^{-1}	12	0.16	-10.35	8 – 9	4.99×10^{-1}
	10	12	1.53	12	-0.72	-5.39	4	7.75
Suburban	0	20	-5.36×10^{-6}	20	-5.65×10^{-6}	-36.64	20	-5.36×10^{-6}
	1	20	2.36×10^{-6}	20	1.85×10^{-6}	-31.03	16 – 20	2.36×10^{-6}

	2	20	-5.39×10^{-6}	20	-4.44×10^{-6}	-24.43	6 – 7	3.09
	3	20	2.60×10^{-6}	20	1.34×10^{-6}	-20.47	18 – 19	1.33×10^{-1}
	4	20	-1.39×10^{-6}	20	-2.04×10^{-6}	-15.77	4	2.57
	5	20	4.96×10^{-2}	20	1.48	-11.66	10	3.11
	6	20	4.48×10^{-6}	20	4.93×10^{-6}	-5.33	4	4.90
	7	20	2.50×10^{-6}	20	1.87×10^{-6}	-7.00	4	9.06
	8	20	-4.01×10^{-6}	20	-2.64×10^{-6}	0.61	4	7.24
	9	20	-7.02×10^{-6}	20	6.10×10^{-6}	4.05	4 – 5	4.75
	10	20	-6.34×10^{-6}	20	-6.27×10^{-6}	0.80	1	10.14
Rural	0	6	-5.40×10^{-6}	6	-5.16×10^{-6}	-9.45	6 – 20	-5.40×10^{-6}
	1	6	2.72	6	5.02	2.50	6	2.72
	2	6	5.44	6	6.99	11.74	2	11.41
	3	6	4.36	6	8.87	12.03	2	20.86
	4	6	3.78	6	13.28	16.66	2	28.40
	5	6	11.43	6	-2.53	29.77	1	28.83
	6	6	18.68	6	-6.71	39.46	1	47.26
	7	6	7.39	6	-19.85	46.39	2	55.65
	8	6	13.14	6	-88.57	48.59	1	68.01
	9	6	7.82	6	-75.91	48.79	1	68.18
	10	6	-1.33	6	-155.84	68.45	1	106.96
“LOS”	0	6	-5.18×10^{-6}	6	-5.24×10^{-6}	-11.96	6 – 20	-5.18×10^{-6}
	1	6	3.91	6	5.83	2.12	6	3.91
	2	6	7.38	6	6.62	12.51	2	12.81
	3	6	4.82	6	9.88	12.90	2	23.66
	4	6	4.02	6	8.00	18.06	2	33.57
	5	6	12.88	6	-14.02	32.82	2	39.35
	6	6	22.26	6	-25.05	43.70	1	52.55
	7	6	7.69	6	-33.76	51.10	2	61.84
	8	6	14.27	6	-167.07	53.55	1	73.11
	9	6	8.64	6	-107.21	54.11	1	80.72
	10	6	-1.15	6	-252.97	76.01	1	122.29

From Table 1, it is evident that LIPMA with the adaptive number of monotonic sections achieves better Δ PES against either LIPMA with the optimal number of monotonic sections or L2WPMA or L2CXCVCV in 38 of 44 cases examined while Δ PES improvement exceeds 15% in the majority of the cases reaching up to 46.28% from the next best approximation.

In addition, it is clearly indicated that even an average estimation of the maximum CUD value can allow better LIPMA approximations. For example, in suburban case, if the occurred maximum CUD value is equal to 6dB and an estimation of the maximum CUD value ranges from 4 to 8dB, the application of less than 10 monotonic sections achieves better Δ PES values than the application of 20 monotonic sections.

Besides, the adaptive number of monotonic sections decreases as the maximum CUD value increases for given OV MV BPL topology and coupling scheme. This is a reasonable result, since the need for a more general approximation is required as the

measurement differences start to create great deviations between the theoretical and measured coupling scheme transfer function data. Anyway, this is the main reason for the approximation success of L2CXCV in rural and “LOS” case where the CUD measurement differences are added around quasi-steady OV MV BPL coupling transfer function lines.

Here, it should be noted that the adaptive number of monotonic sections depends not only on the maximum CUD value but on the CUD itself. It is expected that the adaptive number of monotonic sections will little change when maximum values of other CUDs remain below 5dB. However, the robustness of the concept of the adaptive number of monotonic sections against different CUDs of the same maximum CUD value is investigated in the following Sec.IIIC.

Finally, recognizing the previous decreasing trend of the number of monotonic sections with the respective increase of maximum CUD value, this observation may also improve the performance of L1PMA and L2WPMA when the optimal number of monotonic sections is adopted [21]-[23]. Actually, during the selection of the optimal number of monotonic sections when maximum CUD value is assumed equal to 0, the optimal number of monotonic sections is equal to the minimum value of the values that achieve the same Δ PES. For example, in urban, rural, and “LOS” cases, if the optimal number of monotonic sections was assumed equal to 20, 20, and 20, respectively, then Δ PES would be worse for the other maximum CUD values. This comes from the observation that the latter values are far from the respective values of 12, 6, and 6 that are closer to the adaptive number of monotonic sections. Anyway, this remark has already been adopted in [21]-[23].

3.3 L1PMA with Adaptive Number of Monotonic Sections for Different CUDs

The application of L1PMA with the adaptive number of monotonic sections has been examined for a specific set of CUDs in Sec. IIIB. In order to assess the Δ PES performance of L1PMA with the adaptive number of monotonic sections and to generalize the utility value of the adaptive number of monotonic sections shown in Table 1, at least one different set of CUDs with maximum CUD values ranging from 0 to 10dB should be examined.

In order to examine the performance of the adaptive number of monotonic sections, L1PMA Δ PES is reported in Table 2 when the adaptive numbers of monotonic sections of Table 1 are applied. Also, Δ PES of L1PMA with optimal number of monotonic sections, L2WPMA Δ PES and L2CXCV Δ PES are also presented. Furthermore, in Table 2, all the indicative OV MV BPL topologies are examined when the WtG¹ coupling scheme is applied and a different set of CUDs is available.

TABLE 2
 Same as Table1 but when the L1PMA Adaptive Number of Monotonic Sections of
 Table 1 and Different CUD Set Are Assumed
 (Blue Font: The Best Δ PES Among the Different Piecewise Monotonic Data
 Approximations for Given Maximum CUD Value)

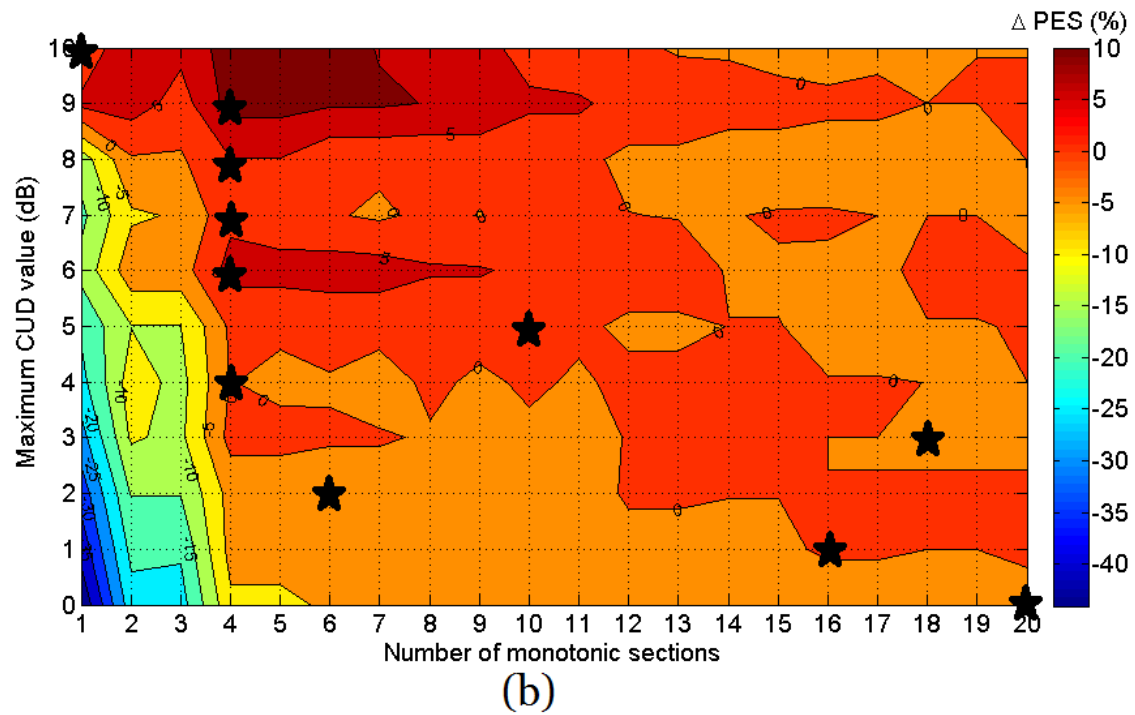
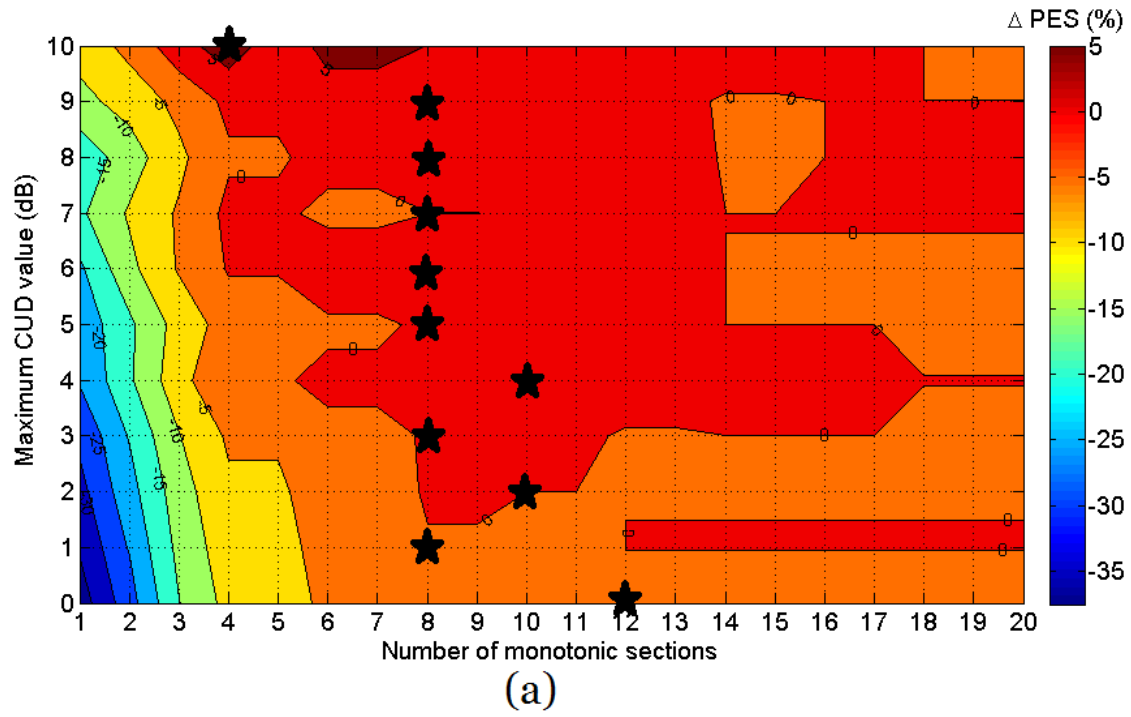
Indicative OV MV BPL Topology	Maximum CUD Value	L1PMA / Optimal Number of Monotonic Sections [10]		L2WPMA		L2CXCVCV	L1PMA / Adaptive Number of Monotonic Sections	
		Number of Monotonic Sections	Δ PES (%)	Number of Monotonic Sections	Δ PES (%)	Δ PES (%)	Number of Monotonic Sections in accordance with Table 1	Δ PES (%)
Urban	0	12	-9.25×10^{-6}	12	-9.70×10^{-6}	-34.55	12	-9.25×10^{-6}
	1	12	5.92×10^{-7}	12	2.13×10^{-7}	-31.29	8	-2.10×10^{-1}
	2	12	-6.01×10^{-7}	12	-1.08×10^{-6}	-27.21	10	-6.01×10^{-7}
	3	12	-0.11	12	0.002	-23.96	8	3.84
	4	12	0.59	12	1.09	-20.43	10	0.23
	5	12	0.02	12	0.02	-18.92	8	0.85
	6	12	1.05	12	0.95	-17.14	8	3.21
	7	12	0.41	12	-0.40	-9.17	8	-4.71×10^{-2}
	8	12	0.44	12	0.86	-12.93	8	3.02
	9	12	0.36	12	-0.29	-5.13	8	1.58
10	12	2.02	12	-2.72	-4.60	4	7.76	
Suburban	0	20	-5.37×10^{-6}	20	-5.65×10^{-6}	-36.64	20	-5.37×10^{-6}
	1	20	2.67×10^{-6}	20	1.90×10^{-6}	-30.31	16	1.61×10^{-1}
	2	20	1.15×10^{-6}	20	1.39×10^{-6}	-24.02	6	-1.81
	3	20	-1.62×10^{-6}	20	-2.90×10^{-6}	-17.43	18	-1.62×10^{-6}
	4	20	-5.35×10^{-6}	20	-5.11×10^{-6}	-14.19	4	1.54×10^{-1}
	5	20	0.09	20	0.0092	-10.80	10	5.29×10^{-1}
	6	20	3.39×10^{-6}	20	4.21×10^{-6}	-7.40	4	6.74
	7	20	-8.42×10^{-6}	20	-7.92×10^{-6}	-1.29	4	3.78
	8	20	3.44×10^{-6}	20	4.20×10^{-6}	-14.22	4	4.84
	9	20	3.65×10^{-6}	20	3.59×10^{-6}	15.99	4	11.75
10	20	-7.73×10^{-7}	20	-9.60×10^{-7}	12.75	1	14.01	
Rural	0	6	-5.40×10^{-6}	6	-5.16×10^{-6}	-9.45	6	-5.40×10^{-6}
	1	6	1.80	6	4.61	2.52	6	1.80
	2	6	1.12	6	14.68	10.36	2	7.67
	3	6	8.34	6	8.31	24.86	2	22.33
	4	6	14.90	6	6.18	36.42	2	41.63
	5	6	0.10	6	-12.16	33.26	1	36.76
	6	6	13.91	6	-19.70	46.90	1	53.02
	7	6	-3.99	6	-47.91	37.42	2	4.55
	8	6	19.46	6	0.95	59.28	1	54.27
9	6	13.62	6	-56.98	81.93	1	61.88	

	10	6	18.72	6	-478.80	63.82	1	62.07
“LOS”	0	6	-5.19×10^{-6}	6	-5.24×10^{-6}	-11.96	6	-5.19×10^{-6}
	1	6	1.92	6	4.81	2.09	6	1.92
	2	6	1.91	6	15.54	11.49	2	8.73
	3	6	8.78	6	5.87	27.21	2	24.89
	4	6	17.95	6	-1.73	40.70	2	47.23
	5	6	-0.21	6	0.10	36.94	2	9.44
	6	6	14.53	6	-43.35	48.60	1	57.51
	7	6	-4.73	6	-93.50	41.57	2	2.51
	8	6	21.35	6	-14.51	65.35	1	62.47
	9	6	15.02	6	-122.39	91.15	1	67.07
	10	6	20.23	6	-178.44	70.56	1	66.92

Comparing the Δ PES results of Table 2 with the respective ones of Table 1 and PES results of [10], several general thoughts concerning the concept of the adaptive number of monotonic sections can be expressed:

- It is clearly shown that the performance of L1PMA has significantly been enhanced since the adoption of the concept of the adaptive number of monotonic sections. Indeed, L1PMA with adaptive number of monotonic sections presents better Δ PES results in comparison with the respective ones of L1PMA with the optimal number of monotonic sections even though an arbitrary set of CUDs has been chosen for the evaluation. The performance increase of L1PMA with adaptive number of monotonic sections is based on the need for more general approximations as the maximum CUD value increases and the examined OV MV BPL topology lacks of frequent and short branches across its BPL transmission path.
- Comparing the performance of piecewise monotonic data approximations in Table 1 and 2 with Table 2-5 of [10], the performance improvement of L1PMA with the adaptive number of monotonic sections is evident. In fact, L1PMA with the adaptive number of monotonic sections achieves to give the best approximations in urban and suburban cases while manages to enhance its approximation efficiency in rural and “LOS” cases. Especially, in the case of indicative rural and “LOS” BPL topologies, it should be noted that L2CXCVC was competing without an opponent when L2WPMA and L1PMA with the optimal number of monotonic sections were applied. Anyway, L2CXCVC better mitigates measurement differences of rural and “LOS” cases when maximum CUD value exceeds 6dB.

Schematically, the highest mitigating performance of L1PMA with the adaptive number of monotonic sections is presented in Figs. 4(a)-(d) where Δ PES is plotted versus the maximum CUD value and the number of monotonic sections for the indicative urban, suburban, rural and “LOS” case, respectively. In these figures, WtG¹ coupling scheme is as well as the optimal number of monotonic sections in each case is drawn as black stars in accordance with Table 2.



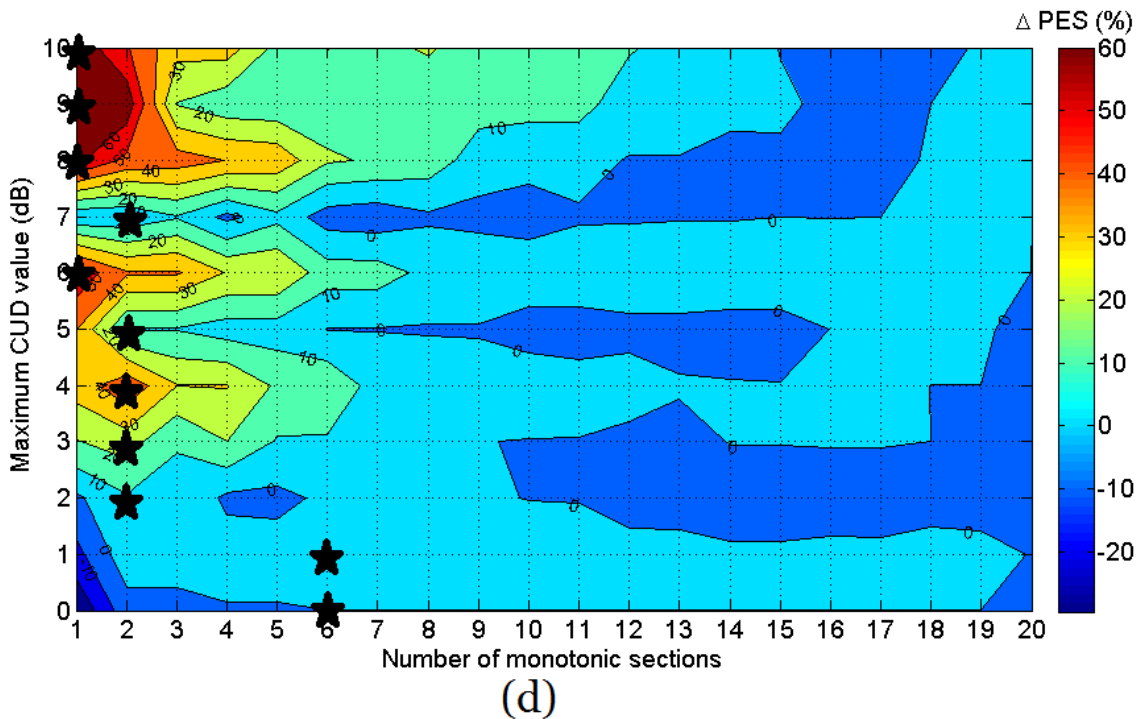
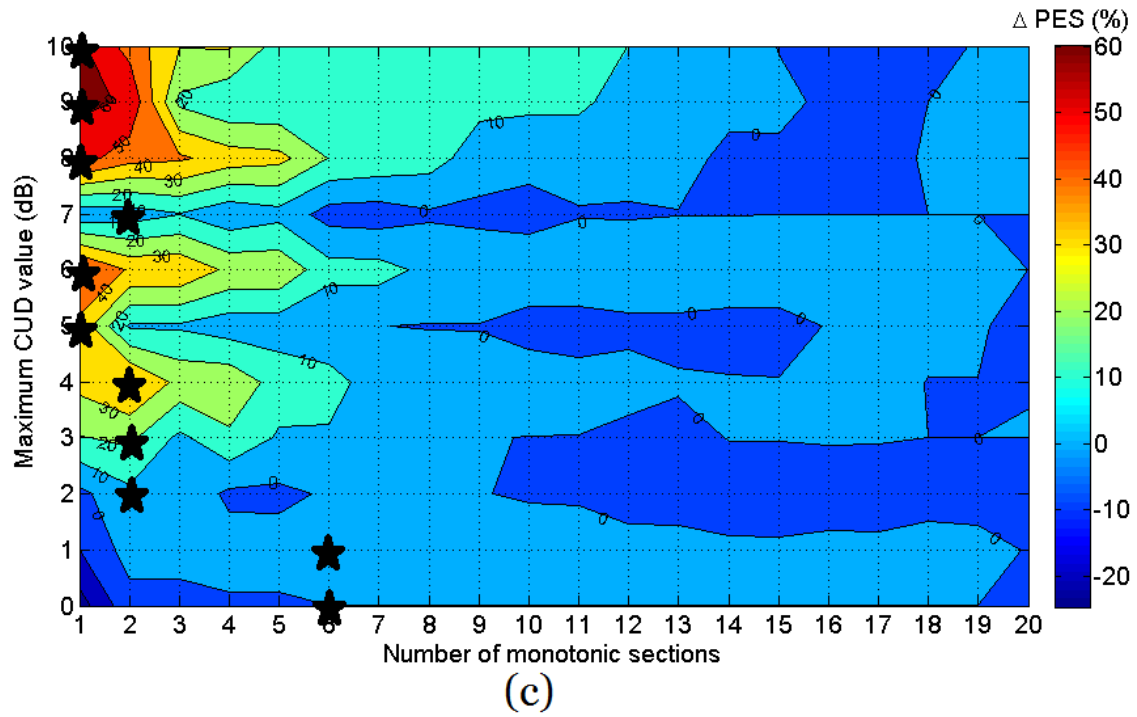


Figure 4. Δ PES is plotted for various indicative OV MV BPL topologies with respect to the maximum CUD value and number of monotonic sections for the CUD of Table 2 (WtG¹ coupling scheme is applied). The black stars indicate the adaptive number of monotonic sections for given OV MV BPL topology and maximum CUD value. (a) Urban case / L1PMA. (b) Suburban case / L1PMA. (c) Rural case / L1PMA. (d) “LOS” case / L1PMA.

The improved Δ PES performance of L1PMA with the adaptive number of monotonic sections is also illustrated by the distribution of the number of monotonic sections in Figs. 4(a)-(d). Even though the adaptive number of monotonic sections comes from the numerical analysis of Δ PES results for the set of CUDs of Table 1, the distribution of the adaptive number of monotonic sections, which is illustrated in Figs. 4(a)-(d) with the black stars, is proven to be very accurate for the set of CUDs of Table 2. Indeed, black stars are located in the isodynamic regions of the best Δ PES in the majority of the cases examined. Especially, the adaptive number of monotonic sections in rural and “LOS” cases are in the center of the best Δ PES isodynamic regions, which have significant and frequent changes, exploiting all the mitigating potential of L1PMA against the occurred measurement differences.

Among the future steps of the research concerning the application of piecewise monotonic data approximations in BPL networks, the efficiency of Topology Identification Methodology (TIM) of [22] and Fault and Instability Identification Methodology (FIIM) of [23] needs to be reviewed by taking into account the new findings during the application of L1PMA. Also, other piecewise data approximation methods can be comparatively benchmarked so that better mitigation performance against measurement differences can be established in the future works. Finally, further research and new solutions regarding L1PMA application need to be released in order to explain the better L2CXCV mitigation behavior in rural and “LOS” cases when maximum CUD values exceed 6dB.

Conclusions

In this companion paper, L1PMA efficiency against the measurement differences, which occur during the determination of OV MV BPL coupling transfer functions, has significantly been improved through the adoption of the adaptive number of monotonic sections concept. The behavior of measurement differences has been modeled by continuous uniform distributions (CUDs) with various maximum CUD values.

Although the adaptive number of monotonic sections had been defined in an initial arbitrary CUD set with maximum CUD values ranging from 0 to 10dB, the L1PMA mitigation performance against measurement differences has critically been enhanced even though a different arbitrary CUD set has been chosen for the Δ PES evaluation. In fact, the concept of the adaptive number of monotonic sections is based on the need for more general approximations as the maximum CUD value increases and the examined OV MV BPL topologies lack of frequent and short branches.

The comparative Δ PES benchmark among L1PMA with adaptive number of monotonic sections, L1PMA with optimal number of monotonic sections, L2WPMA with optimal number of monotonic sections and L2CXCV has revealed that the concept of the adaptive number of monotonic sections improves the overall L1PMA performance as follows: (i) L1PMA achieves the best measurement difference mitigation in urban and suburban case without competition. (ii) L1PMA dynamically deals with the measurement differences in rural and “LOS” case when their maximum CUD values remain below 6dB. (iii) Although the performance difference between L1PMA and L2CXCV has drastically been reduced by the use of the adaptive number of monotonic sections, L2CXCV still better approximates rural and “LOS” cases when maximum CUD values exceed 6dB.

Finally, the more effective identification and restoration of the measurement differences during the OV MV BPL coupling transfer function determination may significantly help towards a more stable and self-healing power system.

Conflicts of Interest

The author declares that there is no conflict of interests regarding the publication of this paper.

References

- [1] A Homeplug, Technology Gains Momentum, 2013, [Online]. Available: <http://www.businesswire.com> (Accessed on 11/30/2016)
- [2] Homeplug, AVWhitepaper, 2007, [Online]. Available: <http://www.homeplug.org/techresources/resources/> (Accessed on 11/30/2016)
- [3] Homeplug, AV2Whitepaper, 2011, [Online]. Available: <http://www.homeplug.org/techresources/resources/> (Accessed on 11/30/2016)
- [4] A. G. Lazaropoulos and P. G. Cottis, "Transmission characteristics of overhead medium voltage power line communication channels," *IEEE Trans. Power Del.*, vol. 24, no. 3, pp. 1164-1173, Jul. 2009.
- [5] A. G. Lazaropoulos and P. G. Cottis, "Capacity of overhead medium voltage power line communication channels," *IEEE Trans. Power Del.*, vol. 25, no. 2, pp. 723-733, Apr. 2010.
- [6] A. G. Lazaropoulos and P. G. Cottis, "Broadband transmission via underground medium-voltage power lines-Part I: transmission characteristics," *IEEE Trans. Power Del.*, vol. 25, no. 4, pp. 2414-2424, Oct. 2010.
- [7] A. G. Lazaropoulos and P. G. Cottis, "Broadband transmission via underground medium-voltage power lines-Part II: capacity," *IEEE Trans. Power Del.*, vol. 25, no. 4, pp. 2425-2434, Oct. 2010.
- [8] A. G. Lazaropoulos, "Broadband transmission characteristics of overhead high-voltage power line communication channels," *Progress in Electromagnetics Research B*, vol. 36, pp. 373-398, 2012. [Online]. Available: <http://www.jpier.org/PIERB/pierb36/19.11091408.pdf> (Accessed on 11/30/2016)
- [9] A. G. Lazaropoulos, "Capacity Performance of Overhead Transmission Multiple-Input Multiple-Output Broadband over Power Lines Networks: The Insidious Effect of Noise and the Role of Noise Models," *Trends in Renewable Energy*, vol. 2, no. 2, pp. 61-82, Jan. 2016. DOI: 10.17737/tre.2016.2.2.0023
- [10] A. G. Lazaropoulos, "Power Systems Stability through Piecewise Monotonic Data Approximations – Part 1: Comparative Benchmarking of L1PMA, L2WPMA and L2CXCVC in Overhead Medium-Voltage Broadband over Power Lines Networks," *Trends in Renewable Energy*, vol. 3, no. 1, pp. 2-32, Jan. 2017. DOI: 10.17737/tre.2017.3.1.0029
- [11] A. G. Lazaropoulos, "Factors Influencing Broadband Transmission Characteristics of Underground Low-Voltage Distribution Networks," *IET Commun.*, vol. 6, no. 17, pp. 2886-2893, Nov. 2012.
- [12] A. G. Lazaropoulos, "Towards broadband over power lines systems integration: Transmission characteristics of underground low-voltage distribution power

- lines,” *Progress in Electromagnetics Research B*, 39, pp. 89-114, 2012. [Online]. Available: <http://www.jpier.org/PIERB/pierb39/05.12012409.pdf> (Accessed on 11/30/2016)
- [13] A. G. Lazaropoulos, “Broadband transmission and statistical performance properties of overhead high-voltage transmission networks,” *Hindawi Journal of Computer Networks and Commun.*, 2012, article ID 875632, 2012. DOI: 10.1155/2012/875632
- [14] A. G. Lazaropoulos, “Towards modal integration of overhead and underground low-voltage and medium-voltage power line communication channels in the smart grid landscape: model expansion, broadband signal transmission characteristics, and statistical performance metrics (Invited Paper),” *ISRN Signal Processing*, vol. 2012, Article ID 121628, 17 pages, 2012. DOI: 10.5402/2012/121628
- [15] A. G. Lazaropoulos, “Review and Progress towards the Common Broadband Management of High-Voltage Transmission Grids: Model Expansion and Comparative Modal Analysis,” *ISRN Electronics*, vol. 2012, Article ID 935286, pp. 1-18, 2012. DOI: 10.5402/2012/935286
- [16] A. G. Lazaropoulos, “Review and Progress towards the Capacity Boost of Overhead and Underground Medium-Voltage and Low-Voltage Broadband over Power Lines Networks: Cooperative Communications through Two- and Three-Hop Repeater Systems,” *ISRN Electronics*, vol. 2013, Article ID 472190, pp. 1-19, 2013. DOI: 10.1155/2013/472190
- [17] A. G. Lazaropoulos, “Green Overhead and Underground Multiple-Input Multiple-Output Medium Voltage Broadband over Power Lines Networks: Energy-Efficient Power Control,” *Springer Journal of Global Optimization*, vol. 2012 / Print ISSN 0925-5001, pp. 1-28, Oct. 2012.
- [18] P. Amirshahi and M. Kavehrad, “High-frequency characteristics of overhead multiconductor power lines for broadband communications,” *IEEE J. Sel. Areas Commun.*, vol. 24, no. 7, pp. 1292-1303, Jul. 2006.
- [19] T. Sartenaer, “Multiuser communications over frequency selective wired channels and applications to the powerline access network” Ph.D. dissertation, Univ. Catholique Louvain, Louvain-la-Neuve, Belgium, Sep. 2004.
- [20] T. Calliacoudas and F. Issa, ““Multiconductor transmission lines and cables solver,” An efficient simulation tool for plc channel networks development,” presented at the *IEEE Int. Conf. Power Line Communications and Its Applications*, Athens, Greece, Mar. 2002.
- [21] A. G. Lazaropoulos, “Best L1 Piecewise Monotonic Data Approximation in Overhead and Underground Medium-Voltage and Low-Voltage Broadband over Power Lines Networks: Theoretical and Practical Transfer Function Determination,” *Hindawi Journal of Computational Engineering*, vol. 2016, Article ID 6762390, 24 pages, 2016. DOI:10.1155/2016/6762390.
- [22] A. G. Lazaropoulos, “Measurement Differences, Faults and Instabilities in Intelligent Energy Systems –Part 1: Identification of Overhead High-Voltage Broadband over Power Lines Network Topologies by Applying Topology Identification Methodology (TIM),” *Trends in Renewable Energy*, vol. 2, no. 3, pp. 85 – 112, Oct. 2016. DOI: 10.17737/tre.2016.2.3.0026
- [23] A. G. Lazaropoulos, “Measurement Differences, Faults and Instabilities in Intelligent Energy Systems – Part 2: Fault and Instability Prediction in Overhead High-Voltage Broadband over Power Lines Networks by Applying Fault and

- Instability Identification Methodology (FIIM),” *Trends in Renewable Energy*, vol. 2, no. 3, pp. 113 – 142, Oct. 2016. DOI: 10.17737/tre.2016.2.3.0027
- [24] I. C. Demetriou and M. J. D. Powell, “Least squares smoothing of univariate data to achieve piecewise monotonicity,” *IMA J. of Numerical Analysis*, vol. 11, pp. 411-432, 1991.
- [25] I. C. Demetriou and V. Koutoulidis, “On Signal Restoration by Piecewise Monotonic Approximation”, in *Lecture Notes in Engineering and Computer Science: Proceedings of The World Congress on Engineering 2013*, London, U.K., Jul. 2013, pp. 268-273.
- [26] I. C. Demetriou, “An application of best L1 piecewise monotonic data approximation to signal restoration,” *IAENG International Journal of Applied Mathematics*, vol. 53, no. 4, pp. 226-232, 2013.
- [27] I. C. Demetriou, “L1PMA: A Fortran 77 Package for Best L1 Piecewise Monotonic Data Smoothing,” *Computer Physics Communications*, vol. 151, no. 1, pp. 315-338, 2003.
- [28] I. C. Demetriou, “Data Smoothing by Piecewise Monotonic Divided Differences,” *Ph.D. Dissertation*, Department of Applied Mathematics and Theoretical Physics, University of Cambridge, Cambridge, 1985.
- [29] I. C. Demetriou, “Best L1 Piecewise Monotonic Data Modelling,” *Int. Trans. Opt Res.*, vol. 1, no. 1, pp. 85-94, 1994.
- [30] C. de Boor, *A Practical Guide to Splines*. Revised Edition, NY: Springer-Verlag, Applied Mathematical Sciences, vol. 27, 2001.
- [31] M. Holschneider, *Wavelets. An Analysis Tool*, Oxford: Clarendon Press, 1997.
- [32] I. C. Demetriou, “Algorithm 863: L2WPMA, a Fortran 77 package for weighted least-squares piecewise monotonic data approximation,” *ACM Transactions on Mathematical Software (TOMS)*, vol. 33, no.1, pp. 6, 2007.
- [33] I. C. Demetriou, “L2CXCVC: A Fortran 77 package for least squares convex/concave data smoothing,” *Computer physics communications*, vol. 174, no.8, pp. 643-668, 2006.
- [34] A. G. Lazaropoulos, “Designing Broadband over Power Lines Networks Using the Techno-Economic Pedagogical (TEP) Method – Part II: Overhead Low-Voltage and Medium-Voltage Channels and Their Modal Transmission Characteristics,” *Trends in Renewable Energy*, vol. 1, no. 2, pp. 59-86, Jun. 2015. DOI: 10.17737/tre.2015.1.2.006

Article copyright: © 2017 Athanasios G. Lazaropoulos. This is an open access article distributed under the terms of the [Creative Commons Attribution 4.0 International License](https://creativecommons.org/licenses/by/4.0/), which permits unrestricted use and distribution provided the original author and source are credited.



Optimization of Raw Material Composition in an Agricultural Biogas Plant

Lili Mézes¹, Attila Bai^{2,*}, Dávid Nagy², István Cinka², Zoltán Gabnai²

1: Institute of Water- and Environmental Management, Faculty of Agricultural and Food Sciences and Environmental Management, University of Debrecen, Debrecen, Hungary

2: Department of Business Economics, Institute of Applied Economics, Faculty of Economics and Business, University of Debrecen, Debrecen, Hungary

Received November 3, 2016; Accepted December 1, 2016; Published January 1, 2017

We analyzed the operation of a typical agricultural biogas plant in Hungary. Our aim was to optimize the composition of substrates for the biogas production and make a correct recommendation for completing feedstock recipes by considering the raw materials and technologies analyzed. The calculations were based on a very detailed database (including the daily operating data of 1673 days). Distribution of the biogas yields in summer and winter periods was normal based on the One-Sample Kolmogorov-Smirnov test, while the variance of data was homogeneous based on the Levene-test. Factor analysis of the biogas yield was performed with the Kaiser-Meyer-Olkin Measure of Sampling Adequacy probe (0.616) and the Bartlett's Test. According to the objectivity of our LP (linear program) model, we believe that a significant excess biogas yield (18-66%) could be achieved by the use of our model compared to the actual measured data. Although the amount of corn silage, grass silage, and the extract – as variables – was minimal in the recipe, they played a crucial role in the total biogas yield of the recipe because of their significantly higher organic matter contents and specific biogas yields. Our results could provide a reliable foundation for optimizing of the recipe in biogas plants with raw material base similar to the analyzed plants.

Keywords: Biogas; Optimization; Heterosis Effect; Feedstock; Substrate

Introduction

Agriculture faces some major inter-connected challenges in delivering food security at a time of increasing pressures from population growth, changing consumption patterns and dietary preferences, and post-harvest losses. At the same time, there are growing opportunities and demands for the use of biomass to provide additional renewables, energy for heat, power and fuel, pharmaceuticals and green chemical feedstocks [1]. However, the worldwide potential of bioenergy is limited, because all land is multifunctional, and the land is also needed for food, feed, timber and fiber production, and for nature conservation and climate protection [2].

Fuchsz and Kohlheb (2015) [3] examined the environmental effects of anaerobic digestion (AD) plants, which operate with the same power production capacity, but use different raw materials during the full life circle. Their results showed that, from the perspective of greenhouse gas (GHG) emission, biogas production from energy crops

cannot be regarded negatively, and having the lowest CO₂ emissions (CO₂ absorber: -188 g/kWhe) of the three investigated AD plants. At the same time, energy-crop-only-based biogas production has the worst acidification potential because of the high fossil fuel demand in growing and transporting the raw materials. In addition, agricultural waste utilization for energy purposes is not always the best solution because of its high GHG emission; therefore, for environmental reasons, it is not always worth high-tech investment. The biogas plant that processes low-energy-density agricultural wastes produced 7.7% of its full-life-cycle CO₂ emissions during its construction phase, compared with a 0.9% ratio for the biogas plant processing only energy crops. Interestingly, co-fermentation turned out to be the best option with regard to the energy efficiency, although its environmental consequences are moderate.

Present agricultural GHG reduction projects in Hungary cannot contribute to achieving long term GHG reduction goals to the same degree as that can be experienced in other sectors due to food market insecurities, food production limitations, and decreasing exchange quotation of GHG emissions. Consequently, climate-friendly agricultural investments have more advantageous returns than in other sectors [4].

The construction and operation of a biogas plant is a combination of economic and technical considerations [5]. Environmental conditions such as pH, temperature, substrate type, total solid (TS) and volatile solid (VS) content of the substrate, hydraulic retention time (HRT), and acclimation periods, are the main factors affecting both the inhibition level in an anaerobic process under different total ammonium nitrogen (TAN) concentrations and the rate of biogas production [6].

Obtaining the maximum biogas yield, by fully digesting the biogas substrate, would require a long retention time of the substrate inside the digester and a correspondingly large digester size. It is thus important to ensure a stable and continuous supply of feedstock with suitable quality and quantities. Feedstock conditioning offers the significant potential for process optimization, and increases digestion rates and biogas yields [5]. Co-digestion of different materials may enhance the anaerobic digestion process due to better carbon and nutrient balances, and applying organic wastes also provides nutrients in excess [7].

The most used substrate in co-fermentation with biogas crops is pig or cow manure [8]. Grasses, including straws from wheat, rice, and sorghum, are a plentiful supply of biomass, most of which is produced as a waste product by food production [9]. Harvesting time can also significantly affect the composition of the substrate, and thus impact the biogas yield of plants [10, 11]. Co-digestion of animal manure with various biomass substrates increases the biogas yield and offers a number of advantages for the management of manure and organic wastes [12] and for mitigation of greenhouse gas (GHG) emissions [13]. Wu *et al.* (2010) [14] concluded that significant increases in volumetric biogas production can be achieved by adding carbon rich agricultural residues to the co-digestion process with swine manure. Cuetos *et al.* (2008) [15] observed that co-digestion of mixtures stabilizes the feed to the bioreactor, thereby improving the C/N ratio and decreasing the concentration of nitrogen. Cavinato *et al.* (2010) [16] studied the co-digestion of cattle manure, agricultural waste, and energy crops, where 1.10 l/day biogas production rate and 179 l/kg VS methane yield were detected and significant increase in biogas production from the co-digestion was observed. Other studies analyzed the methanogenesis processes during anaerobic digestion at different moisture levels (60–80%), it has been reported that the highest methane production rates occurred at 60–80% of humidity [17] and [18]. An important parameter in determining the size of the biogas

digester is the hydraulic retention time (HRT). The HRT is the average time interval when the substrate is kept inside the digester tank [5].

HRT is the average period that a given quantity of input material remains in the digester to be acted upon by the methanogens [19]. The disadvantage of a longer retention time is the increasing reactor size needed for a given amount of substrate to be treated [20]. A short HRT provides a good substrate flow rate, but a lower gas yield [5] and lower overall degradation [20]. Another problem for a short HRT is, that the bacteria in the digester are “washed out” faster than they can reproduce. It is therefore important to adapt the HRT to the specific decomposition rate of the used substrates. Knowing the targeted HRT, the daily feedstock input and the decomposition rate of the substrate, it is possible to calculate the necessary digester volume. The average HRT is usually varies from 20 to 40 days [5], under other results from 10 to 30 days [21], depending on the type of substrate and digestion temperature [5]. Kaosol and Sohgrathok (2012) [22] analyzed the effect of HRT on biogas production in a 15 L reactor with 10 L working volume for 10 days, 20 days, and 30 days. The results during the whole process showed that the 20-day and 30-day HRT reactors can remove COD in the range of 92.28%-94.54%, while the 10-day HRT reactor showed the lowest removal performance (i.e., 71.21%). The COD removal performances of the 20-day HRT and the 30-day HRT reactors showed no significant difference.

In practice, the anaerobic degradation rate of organic matters from animal manure and slurries is about 40% for cattle slurry and of 65% for pig slurry, respectively. The degradation rate depends at large on the feedstock type, HRT, and process temperature. The organic load is an important operational parameter, which indicates how much organic dry matter can be fed into the digester per volume and time unit [5]).

Braun *et al.* (2006) [23] examined more than 40 agricultural biogas plants in his study. The plant sizes changed between 50 kW_{el} and 1672 kW_{el}, the reactor volume varied between 1,000 and 17,000 m³. Therefore, the HRT changed significantly with the analyzed agricultural biogas plants. The organic load varied from 2.92 to 4.61 m³/Vr*day.

Menardo *et al.* (2011) [24] analyzed four mesophilic (41°C) agricultural biogas plants. The digester volume changed between 4990 and 12000 m³, HRT varied from 51 to 105 days, while organic loading rate (OLR) was between 0.85 and 2.25 kgVs/m³*day.

The potential biogas yield relies not only on the VS content, but also on the degradability of those solids in an anaerobic environment [25]. Furthermore, both of these VS parameters depend on the OLR and HRT [26]. Menardo *et al.* (2011) [24] applied Pearson “R” correlation coefficient analyses in his study and showed the parameters that were most correlated to the biogas yields of digestate samples were the OLR of the original biogas plant and the samples’ TS and VS contents.

Many anaerobic digesters have various feedstock sources, which can cause fluctuations of the chemical composition in the reactor. As a result from poorly monitored systems, most anaerobic digesters are currently run at a less-than-optimum loading rate to prevent instability occurring in the digester. This instability often inhibits methanogens [27] and results in a decrease of the biogas yields.

Our hypothesis was that the quantity and quality of raw materials (dry or wet, organic material content, etc.) have an impact on the biogas and methane yields. We would like to prove the connection and correlation between the feedstock and the biogas yields, and to take into account the constraints often encountered in practice. We also analyzed the effect of seasonal differences on biogas yields. Our aim was to optimize the composition of substrates for biogas production and make a correct recommendation for

completing feedstock recipes based on based on the raw materials and technologies analyzed.

Regarding the comparative analysis of actual and optimized feedstock recipes, our aim was to analyze the recipe's exact composition and biogas yield, based on the different feedstock quantities. We aimed to determine via linear program (LP) modelling (1) the recipes' potential reserves which can be suitable for yield-boosting effect and (2) the level of heterosis effect during co-fermentation compared to the biogas yield of single raw material.

Materials and Methods

The most important feature of the biogas plant studied between 2012-2016, is that it uses predominantly by-products generated in a nearby farm, providing a significant advantage for the feedstock management due to the predictable quantity and quality, and cost saving. Currently, the farm produces crops on 4,000 hectares of arable land including raw materials usable for biogas production (such as corn silage and grass silage). However, the main goal of the production is to provide food for the animal sector. The latter includes 2,000 dairy cows and almost 1,200 sows with progeny (~20,000 piglets/year).

The raw material base for the mesophilic fermentation in the biogas plant is made up of various materials. The liquid part of the substrate consists of pig and cattle waste slurry, in addition to the whey and dairy sludge from the nearby cheese factory to be disposed in the biogas plant. The purpose of the biogas plant is the disposal of these continually generated unmarketable and environmentally dangerous products. In the remaining fermentation space of the fermenter – in order to enhance the biogas yield – corn silage, grass silage, solid separated digestate, and manure are added, which have a significant dry matter content.

The majority of the raw materials fed daily consists of four liquid components: cattle slurry, pig slurry, whey, and sludge. The utilization of the total amount of these materials is especially important because of storage limits, and thus the limiting factors of their daily consumption must be taken into account during optimizing the process. Technical problems that were caused by the slurry happened a few times. The amount of incoming slurry had the significant fluctuations, causing either reduced amount fed in or (usually) higher proportion added.

Most biogas plants utilizing agricultural by-products use different recipes for the winter and summer periods, because the two-phase feeding of ruminants results in raw materials with different quality and quantity for each period. However, the plant analyzed in this study does not prevail this seasonality. According to its operating data, approximately 94% of the summer recipe and 92% of the winter recipe were composed of the four aforementioned liquid materials (Table 1.), resulting in balanced feeds and higher biogas yields compared to the changing recipes.

The raw materials were fed in the three mesophilic digesters of total 4,500 m³ capacity from the mixers between 2012 and 2016. The amount of material fed daily varied between 55.5 and 232.5 m³, and the average daily amount of feedstock substrate was 178 m³, which was equivalent to 18.8 t/day.

Table 1. Composition of feedstock-recipe for biogas production in summer and winter periods

Used feedstocks	Summer period	Winter period
	Average (\pm SD)	Average (\pm SD)
Cattle slurry (%)	56.26 \pm 6.57	51.76 \pm 12.01
Pig slurry (%)	24.95 \pm 5.40	27.71 \pm 8.37
Silo maize (%)	1.92 \pm 1.33	2.47 \pm 1.57
Grass silage (%)	0.75 \pm 0.69	0.95 \pm 0.85
Solid separated digestate (%)	2.26 \pm 1.36	2.33 \pm 1.16
Whey (%)	6.48 \pm 2.74	5.94 \pm 2.62
Dairy sludge (%)	6.54 \pm 1.78	6.35 \pm 2.24
Cattle manure (%)	0.83 \pm 0.87	0.47 \pm 0.73

SD: standard derivation

The average amount of biogas produced monthly was 171 thousand Nm³, while the daily biogas production varied between 3,638-7,265 Nm³. The daily average of the produced biogas was 5,988.3 Nm³, and the average methane yield was 3,310.8 Nm³, from which electricity of 11,305.7 kWh/day was generated in the biogas plant. The biogas production was calculated according to the gas flow meters of the digesters to figure out the overall daily gas yield in Nm³. The quality of biogas (CH₄, CO₂, H₂S, NH₄) was analyzed with a ENVIRO-100 type gas analyzer. The average value of the methane concentration in biogas was 55%, but the maximal value (76%) indicated that a great potential is available, which can be achieved by a well-balanced, less various raw materials (Table 2.).

Table 2. Biogas quality parameters by the examined biogas plant

Biogas quality	CH ₄ (%)	CO ₂ (%)	H ₂ S (mg/kg)	O ₂ (%)
Average (\pm SD)	55.16 \pm 4.82	30.73 \pm 3.18	123.04 \pm 122.18	1.64 \pm 1.20
Min.	42.34	24.07	0.67	0.04
Max.	75.69	53.08	699.50	8.98

The average hydrogen-sulphide content of the biogas was 123 mg/kg after sulphur removal. The desulfurization was conducted with oxygen dozing, FeCl₂ addition, and biological processes. Preißler *et al.* (2010) [28] determined more rapid reduction of the H₂S content in the case of the iron (III) chloride variant. A 60% reduction of hydrogen sulphide content was achieved with the stoichiometric equal addition of iron in the case of the chlorides and the hydroxide compared with the control [28]. Based on the results, the combined sulphur-removal methods resulted in a very low (200 mg/kg >) hydrogen-sulphide content in the produced biogas.

The daily organic load (kg/d*m³) was calculated from the following equation: OLR = m * c/Vr [5]. The average hydraulic retention time (HRT) was calculated from the maximal volume of the digesters (Vr)(m³) and the amount of daily fed materials according to the following equation: HRT=Vr/V, where HRT=hydraulic retention time [days], Vr=digester volume [m³], and V=volume of substrate fed per time unit [m³/d] [19].

The operation of the plant from the biogas production point of view can be divided into three phases (Figure 1.).

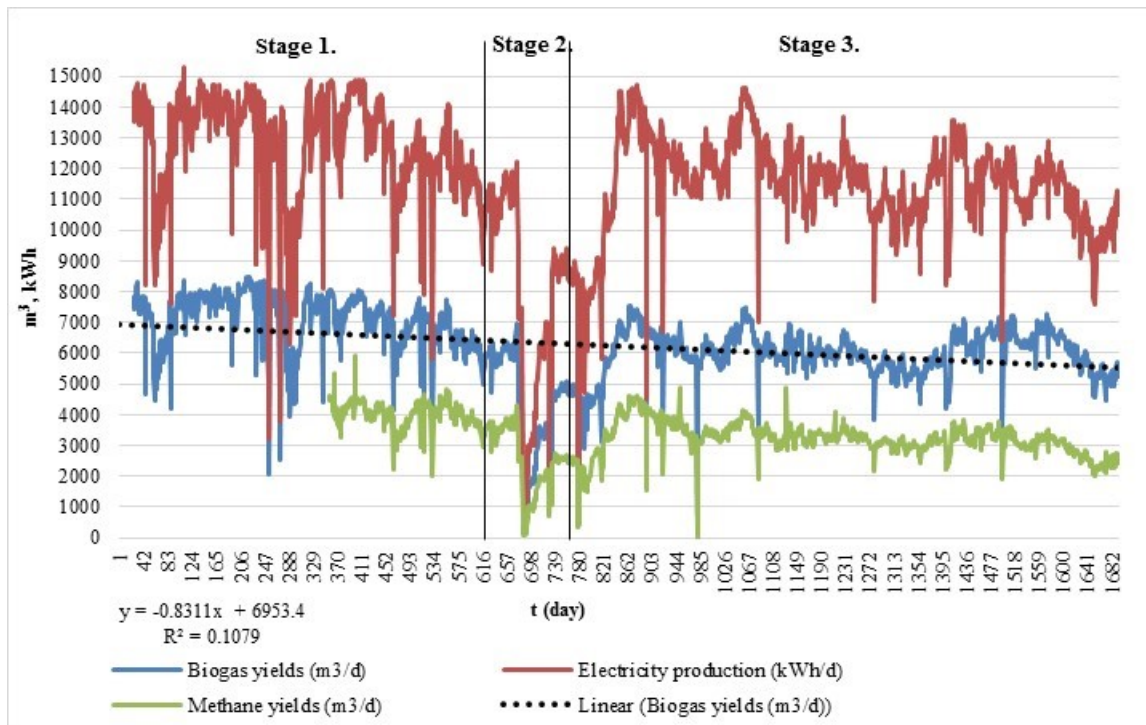


Figure 1. Biogas yields, methane yields, and electricity production in the analyzed biogas plant

During the first phase of operation (1-652. days), 59% of the daily biogas yields exceeded 7,000 m³ per day, which was basically due to the 1.5-2 times larger amount of annual consumption of corn silage and whey as raw materials. The average daily biogas production in this period was $7,007 \pm 951$ m³. The average daily proportion of corn silage and whey fed together was 11%, which is higher than the combined rate of 7% for the third stage.

In the second phase of the operation of biogas plant (653-793. days), an intense decrease was observed in production. This was due to a malfunction that forced renovation of three fermenters, only limited quantities of raw materials could have been fed and fermented during this six month.

During the third phase (794-1694. days), 94% of the daily biogas production was less than 7,000 m³ per day, and an average of $6,050 \pm 708$ m³/day biogas was produced. Comparing the raw material consumption to that of the first period, the use of cattle slurry, the extract, and the grass silage increased by 2.5%, 1.1%, and 0.4 %, respectively, and the use of manure did not change. Accordingly, the proportion of raw materials with higher biogas yield decreased significantly (whey: -2.4%, corn silage: -1.6%, pig slurry: -0.1%, dairy sludge: -0.1%). The annual changes of the recipes are shown in Table 3.

Weiland evaluated German biogas plants in 2004 [29] and 2009[30], and most plants used manure-based mixtures with a range of crops (such as maize, grass, and cereals) as the substrate. Food and vegetable wastes, potato processing residues, whey and fat trap contents were also used as co-substrates with manure. In the 2004 study, manure was the dominant substrate (75-100% share) for nearly 50% of the plants considered. About 83% of the new German agricultural biogas plants operate with a mixture of crops and manure; 15% use crops only and just 2% were operated with manure only. In this study, the biogas plant used in average 82% of animal slurry and

manure, 3% of silo maize and grass silage, 12% of food industrial wastes, and 2% of solid separated digestate.

Table 3. The quantitative distribution of raw materials used in the biogas plant

Years	2012		2013		2014		2015		2016 Aug.	
	Daily average (m ³)	%								
Cattle slurry	89.02	51%	94.14	57%	103.64	56%	108.53	56%	101.52	55%
Pig slurry	46.58	27%	41.95	25%	48.33	26%	52.99	27%	49.83	27%
Silo maize	5.89	3%	4.26	3%	3.1	2%	2.96	2%	2.52	1%
Grass silage	1.22	1%	0.93	1%	1.92	1%	2.59	1%	1.08	1%
Solid separated digestate	3.35	2%	2.21	1%	3.82	2%	4.99	3%	7.22	4%
Whey	16.15	9%	9.94	6%	10.09	5%	10.01	5%	1002	5%
Dairy sludge	11.88	7%	10.01	6%	11.71	6%	12.14	6%	13.16	7%
Cattle manure	0.00	0%	2.15	1%	2.43	1%	0.67	0%	0.33	0%
Summary	174.09	100%	165.59	100%	185.04	100%	194.88	100%	185.68	100%

Optimization

The comparative analysis of the optimized and actual recipes examined the composition and the biogas yield of the recipes by varying the quantities of different raw material feeds. The starting value of this changed between 180 m³ (long term constantly enterable quantity) and 210 m³ (maximum fed actual quantity) with 10 m³ stages. The effect of raw materials on the biogas yield – according to the technology – was calculated with a HRT of 25 days.

Our calculations aimed to show that the biogas potential behind the recipes and the significance of the heterosis effect by using LP modelling, compared to the biogas yield of single raw material. The fact, which the body of literature that we know do not contain reliable estimates on the extent of the latter mentioned effect, underlines the significance of this analysis. LP is the most appropriate tool to determine the recipe providing the maximum biogas yield by given recipe ingredients, taking into account the specific unit yields [31].

Since the exact composition of tested individual raw material is unknown and most likely not constant, the calculation used the typical values found in the literature (presented in Table 4.). The biogas yields and the yields of a single feedstock, which can be considered as characteristics, were calculated with means.

The limiting terms of the model were as follows: the specific biogas plant receives daily 100 t cattle slurry, 50 t pig slurry, and 10-10 t whey and dairy sludge, which were rounded to meet the typical daily delivery value. The other three components were the mean values of the collected daily data that increased or reduced with the variance. Another limiting condition was the maximum daily capacity of the fermenter (an average of 180 m³, maximum 210 m³). The objective function was to maximize the biogas production. The problem was solved with the use of Solver add-in software of MS Excel.

Table 4. The quality of different raw materials

Raw materials	Dry matter cont. (DM) %	Organic matter cont. (OM) %*	Biogas yields m ³ /t OM	Biogas yields m ³ /t feedstock	Density t/m ³
Cattle slurry	3.55 ⁽²⁾	75 ⁽⁵⁾	200-300 ⁽¹⁾	6.66	1
Pig slurry	4 ⁽¹⁾	75 ⁽¹⁾	300-800 ⁽³⁾	16.50	1
Silo maize	26.09 ⁽²⁾	72 ⁽⁴⁾	600-700 ⁽³⁾	122.10	0.77 ⁽⁵⁾
Grass haylage	24.77 ⁽²⁾	85 ⁽⁴⁾	560 ⁽¹⁾	117.89	0.6 ⁽⁵⁾
Dairy sludge	1.98 ⁽²⁾	85 ⁽⁴⁾	800-950 ⁽¹⁾	124.94	1
Whey	3.51 ⁽²⁾	80 ⁽⁴⁾	500-900 ⁽³⁾	19.63	1
Solid separated digestate	26.02 ⁽²⁾	85 ⁽⁴⁾	350-780 ⁽¹⁾	14.74	0.50 ⁽⁶⁾
Cattle manure	21.18 ⁽²⁾	85 ⁽⁴⁾	600-800 ⁽³⁾	126.02	0.75 ⁽⁷⁾

(1) [32]

(2) [33]

(3) [34]

(4) [32] and [33]

(5) [34] and [33]

(6) [33]

(7) [35]

The model – because of its optimizing feature and the consideration of mono-digestion biogas yields – did not consider the heterosis effect, the extent of which was calculated by dividing the theoretical (mono-digestion) biogas yield of the actual recipe pasted in the model by the measured yields of the same recipe, after classifying 1,673 pieces of data into quantitative categories and averaging them. The average of the quantitative categories corresponded to the optimized flow rates (180, 190, 200, and 210 m³).

The data have been evaluated and analyzed with the computer programs of MS Excel and SPSS 23 statistical software package. In order to test the normal distribution of the data, one-sample Kolmogorov-Smirnov test and Lilliefors-probe were used. For the simultaneous comparison of the mean values, analysis of variance was used. The significance differences between the winter and summer periods, - with and without Stage 2 phase - were analyzed by one-way analysis of variance (ANOVA) using Tukey b and Duncan tests at P>0.05 significant level. Factor analysis, - based on Kaiser-Meyer-Olkin Measure of Sampling Adequacy probe (0.616) and Bartlett's test - was applied to analyze different components under linear relationship, and to reduce the number of studied components. The relationship between the main raw materials and the biogas production was detected by a linear regression analysis. In the linear regression model, biogas yields without Stage 2 phase were considered as Y (*i.e.* dependent factor).

Results and Discussion

Technology and operational parameters of the studied biogas plant

This interval indicates the degradability of the given raw material, and the time needed for gas production to be commenced. The following are the main operational parameters of the studied agricultural biogas plant:

- Temperature: 32.0 °C
- Capacity (V): 179.8 m³/d
- Reactor value (Vr): 4,500 m³
- Hydraulic retention time (HRT) (Gruber, 2006): 25.0 d (Vr m³/Input m³*d)
- Biogas quantity: 5,988.3 Nm³/d
- Biogas quantity: 2,052,000 Nm³/a
- Amount of oTS: 0.71 Input t oTS/d
- Organic loading rate (OLR): 0.16 kg oTS* / (Vr m³*d)
- Dry matter load: 0.24 kg TS (dry matter content)/ (Vr m³*d)
- Methane concentration in biogas: 55.2 %
- Biogas productivity: 1.32 Nm³/(Vr m³*d)
- Specific biogas production: 33.3 Nm³/(Input m³*d)
- Specific biogas yield: 8.39 Nm³/(kgVs*d)
- Electricity production: 4,214,620 kWh/a
- Electricity production: 11,305.7 kWh/d

In case of the organic load, our results were lower (0.16 kg oTS /Vr m³ *d) than the average ORT in Braun *et al.* (2006) [23]. It's proven to be effective for the biogas productivity in the studied biogas plant, compared to Braun *et al.* (2006) [23] results. However, the average methane content of biogas was lower within the studied period (2012-2016).

The hydraulic retention time (HRT) had been established as 25 days based on Gruber (2006) [19] study, which is lower than the optimal value based on other publications. The Biogas Handbook suggested a minimum retention time of 30 to 40 days under mesophilic conditions. Mendaro *et al.* (2011) [24] analyzed four digestate samples in batch reactors. The methane yield was shown to be highly influenced by OLR and by feedstock quality of the biogas plant, but the HRT only showed limited effects.

Optimization of raw material composition

Descriptive statistic of biogas yields in summer and winter is shown in Table 5. Distribution of the biogas yields in summer and winter periods was normal based on One-Sample Kolmogorov-Smirnov test.

Table 5. Descriptive statistic of biogas yields in winter and summer periods

Biogas yields (m ³ /d)	N	Mean	Std. Deviation	Std. Error	95% Confidence Interval for Mean		Minimum	Maximum
					Lower Bound	Upper Bound		
Winter period	1528	6442.75	942.53	24.11	6395.45	6490.04	56.96	8481.00
Summer period	877	6427.73	964.78	32.58	6363.78	6491.66	56.96	8481.00
Total	2405	6437.27	950.53	19.38	6399.26	6475.28	56.96	8481.00

Based on Levene-test, the variance of data was homogeneous. No significance differences were detected at $P > 0.05$ significant level by ANOVA analysis for the biogas yields between the winter and summer periods, because the significance level of F-probe was 0.709. In case of the fed amount (oTS (kg/d)), no significance differences (Sig. 0.6<) was detectable between the winter and summer periods, therefore permanent and stable quality of feedstock and OLR was found in the studied agricultural biogas plant. The daily fed amount of total animal slurry and manure, silo maize, grass silage, and milk industrial wastes (m^3) differed significantly in the summer and winter periods, which was based on variance analysis (Sig. 0.00). In case of solid separated digestate (Sig. 0.494) the fed amounts were similar in all seasons.

The Stage 2 data series were excluded from the database, because it was identified as a technical error. Factor analysis and linear regression analysis were performed and then applied. Distribution of quantity of used raw materials was normal based on the Kolmogorov-Smirnov test.

Factor analysis based on the Kaiser-Meyer-Olkin Measure of Sampling Adequacy probe (0.616) and the Bartlett's Test was well applicable. Based on principal Component Analysis and Rotated Component Matrix, the biogas yields, quantity of silo maize, solid digestate, and total slurry and manure (m^3/d) could be separated in the first group. These components were determined as the biogas yield factors. The second group were classified as the acidity factors like amount of oTS (kg/d) and pH. Milk industrial wastes (m^3/d) were classified as a third group. The most important factor was the silo maize, which showed a strong linear correlation with the biogas yield. An inversely proportional relationship could be detected between the biogas yield and the quantity of solid digestate, slurry, and manure. The more slurry, manure, and digestate used in the biogas plant as raw material, there was less biogas production, and therefore decreased effectiveness of the plant. Higher ratio of organic matter content in the fed raw materials often caused lower pH, therefore increased the acidity in the digester. Factor analysis of feedstock, biogas yield, oTS, OLR and pH are detailed below:

Components

1. Biogas yield factor:

- Silo maize (m^3/d) (-0.757)
- Solid digestate (m^3/d) (0.671)
- Biogas yields (m^3/d) (-0.650)
- Total slurry and manure (m^3/d) (0.609)

2. Acidity factor:

- Amount of oTS (kg/d) (0.803)
- pH (-0.675)

3. Milk industrial wastes (m^3/d) (0.862)

Based on the regression analysis of biogas yields (m^3/d) and silo maize (m^3/d), we can build up a linear regression equation with low dependability ($R=0.38$; $R^2=0.145$). Weak correlation was observed between the biogas yields and total amount of slurry and manure (m^3/d) with linear regression analysis ($R=0.371$, $R^2=0.137$) at $P > 0.05$ significant

level. In case of applied solid digestate the dependency was also weak ($R=0.217$, $R^2=0.047$).

An average difference of 2.1 times was observed between the model and the measured values by a relative low standard deviation ($R=0.40$), however, with very different extreme values (minimum of 0.02 to a maximum of 3.07).

Taking into account the daily accurately measured values, the objectivity of the LP model, and the model considering only the individual (mono-digestion) biogas yield of the single raw materials, we believe that the heterosis effect in this recipe could result in a 110% excess yield. However, this value is only the best possible approximation, since the actual composition of raw materials used in the given biogas plant – thus their biogas yields – is not precisely known, and it may not correspond to the used average values. Considering the average standard deviation, it can be stated that the heterosis effect results in a 1.7-2.5-fold yield increase under the test conditions.

Although the amount of corn silage, grass silage and the extract – as variables – was minimal in the recipe, they played a crucial role in the total biogas yield of the recipe because of their significantly higher organic matter content and specific biogas yield (Figure 2.).

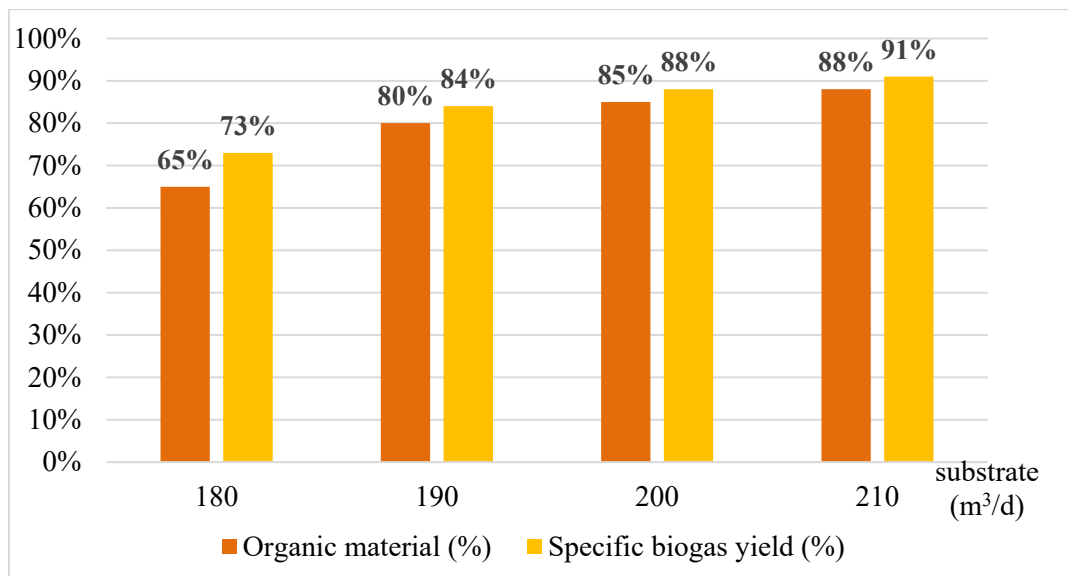


Figure 2. The correlation between organic material content and specific biogas yield

The recipe composition and the actual daily biogas yields based on the operational measures are detailed in the upper part of Table 6, while the same parameters as results of the optimization are shown in the lower part of the table. The biogas yield of the model at 180 m³ daily input level was 16% lower, while at higher input levels it was 18-66% higher than the average of the yields measured in the plant.

Table 6. The real (measured) and the optimized values regarding the recipe

Daily feedstock (m ³)	Cattle slurry	Pig slurry	Silage maize	Grass silage	Solid separate digestate	Whey	Dairy sludge	Cattle manure	Biogas yield (m ³)
Real values, measured in the biogas plant									
175-185	98.9	48.6	7.2	2.3	9.6	11.2	10.8	0.8	6496
185-195	106.2	50.9	5.5	3.8	9.5	10.3	11.9	1.1	6193
195-205	112.5	52.5	4.5	5	9.5	10.5	12.2	2.1	6110
205-215	115.1	56	4.5	4.9	8.9	10.3	14.3	2.6	6042
Results and values by the optimization									
180	100	50	2.9	0.2	3	10	10	0	5425
190	100	50	9.1	1.4	3	10	10	0	7308
200	100	50	9.1	5.1	4.9	10	10	0	8731
210	100	50	9.1	5.1	9.9	10	10	0	10046

In case of the 180 m³ per day input level, the actual recipe contained a significantly smaller proportion of the substrate with the lower biogas yield compared with the optimized 180 m³ per day capacity. Consequently corn silage, grass silage, and digestate were present in a 3.15-fold proportion (19 % compared to 6 %), so the difference of the proportion of valuable substrates was much higher than of biogas yields (6496 m³ per day compared to 5425 m³ per day).

Assuming that the raw material in the plant had more favorable parameters (like organic matter content and biogas yield) than the average, the degree of the heterosis effect was corrected upwards with the standard deviation (to 2.50). The measured and the optimized daily yield was practically identical (6496 m³ or 6445 m³), despite the divergence of the more valuable components.

The considerable surplus yield (18-66%) of the optimized recipe in case of the 190 to 210 m³ per day input volume was due to the decreased proportion of ingredients with high biogas yield in the higher input volume under the actual operating conditions and the increase of their proportion in the model. The most recommended of these was the feeding of corn silage; the LP model increased first the volume of this ingredient to the maximum level (in addition to leaving the other two substrates on minimum level), than the volume of grass silage and finally the volume of extract. Our calculations suggested that the maximum limit could be reached at 213 m³ daily input volume. If there was no limits for the variables, the model would have recommended the solely feeding of corn silage – in addition to a minimal feeding of grass silage and extract – at 210 m³ daily input level with an estimated biogas yield of 12,637 Nm³/day, which is more than double of the relevant operating data.

Against this background, we believe that a significant excess yield could be achieved with the use of our model compared to the actual measured data.

It is important to point out, that even a relatively small over-sizing of the fermenter capacity could result in a significant yield increase. In this case study, a 5.5% increase of the input volume (from 180 to 190 m³) resulted in a 35% increase of the biogas yield when using optimized recipe. However, the increasing rate of the yield – according to the law of diminishing returns – decreased significantly in case of further similar capacity increases. In turn, the actual operating data displayed the opposite

tendency, which is probably due to the fact that after recovering the breakdown in livestock farms, the operators tried to dispose the most possible volume of the accumulated slurry in the biogas plant, resulting in a higher proportion of slurry in the greater input volume. However, large-scale or long-term decline in livestock can be a serious threat not only for the security of the raw material basis, but for the utilization of unmarketable by-products of the biogas production (primarily waste heat).

CONCLUSIONS

Biogas plants serving for disposal of the slurry from livestock farms have relatively modest possibilities for increasing yield, since they are scaled for constantly processing hardly storable raw materials with modest biogas yields (a variety of slurry and food processing by-products). Optimization of this kind of feedstocks is possible, but combines with significant limitations. Because these feedstocks make up the vast majority of the recipe, the seasonality is much less important compared to other types of biogas plants. However, substrates with the high organic content (silage maize, grass silage, solid separate digestate) are responsible for most of the biogas production, so they should be considered when scaling up the fermenter.

A temporary or permanent, minor decrease in the feedstock from the livestock can make the recipe use a higher proportion of energy crops, resulting in a significant increase in the biogas production. Energy crops also have the land demand, but it's significant smaller than the crop production for feeding.

ACKNOWLEDGMENTS

This study and our research work were partly supported by the University of Debrecen, Faculty of Economics and Business Research Fund (in Hungarian: GTK Kutatási Alap).

CONFLICTS OF INTEREST

The authors declare that there is no conflict of interests regarding the publication of this paper.

REFERENCES

- [1] Popp, J., Lakner, Z., Harangi-Rákos, M., and Fári, M. (2014). The effect of bioenergy expansion: food, energy, and environment. *Renewable and Sustainable Energy Reviews*, 32, 559-578.
- [2] Popp, J., Harangi-Rákos, M., Petô, K., and Nagy, A. (2013). Bioenergy: Risks to food-, energy-and environmental Security. *APSTRACT: Applied Studies in Agribusiness and Commerce*(4/5), 121-130.
- [3] Fuchsz, M., and Kohlheb, N. (2015). Comparison of the environmental effects of manure-and crop-based agricultural biogas plants using life cycle analysis. *Journal of Cleaner Production*, 86, 60-66.
- [4] Fogarassy, C., and Nábrádi, A. (2015). Proposals for low-carbon agriculture production strategies between 2020 and 2030 in Hungary. *APSTRACT: Applied Studies in Agribusiness and Commerce*, 9(4).
- [5] für Umwelt, B. L. (2007). Biogashandbuch Bayern, Materialienband. *Augsburg, Germany*, 13-14.

- [6] Chen, Y., Cheng, J. J., and Creamer, K. S. (2008). Inhibition of anaerobic digestion process: a review. *Bioresource Technology*, 99(10), 4044-4064.
- [7] Hartmann, H., and Ahring, B. K. (2005). Anaerobic digestion of the organic fraction of municipal solid waste: influence of co-digestion with manure. *Water research*, 39(8), 1543-1552.
- [8] Linke, B., Muha, I., Wittum, G., and Plogsties, V. (2013). Mesophilic anaerobic co-digestion of cow manure and biogas crops in full scale German biogas plants: a model for calculating the effect of hydraulic retention time and VS crop proportion in the mixture on methane yield from digester and from digestate storage at different temperatures. *Bioresource Technology*, 130, 689-695.
- [9] Ward, A. J., Hobbs, P. J., Holliman, P. J., and Jones, D. L. (2008). Optimisation of the anaerobic digestion of agricultural resources. *Bioresource Technology*, 99(17), 7928-7940.
- [10] Amon, T., Amon, B., Kryvoruchko, V., Machmüller, A., Hopfner-Sixt, K., Bodiroza, V., Hrbek, R., Friedel, J., Pötsch, E., and Wagentristl, H. (2007). Methane production through anaerobic digestion of various energy crops grown in sustainable crop rotations. *Bioresource Technology*, 98(17), 3204-3212.
- [11] Amon, T., Amon, B., Kryvoruchko, V., Zollitsch, W., Mayer, K., and Gruber, L. (2007). Biogas production from maize and dairy cattle manure—influence of biomass composition on the methane yield. *Agriculture, Ecosystems & Environment*, 118(1), 173-182.
- [12] Nielsen, L. H., Hjort-Gregersen, K., Thygesen, P., and Christensen, J. Samfundsøkonomiske analyser af biogasfællesanlæg. In: *Proc., DAKOFA-konference om organisk affald*.
- [13] Møller, H. B., Sommer, S. G., and Ahring, B. K. (2004). Biological degradation and greenhouse gas emissions during pre-storage of liquid animal manure. *Journal of Environmental Quality*, 33(1), 27-36.
- [14] Wu, X., Yao, W., Zhu, J., and Miller, C. (2010). Biogas and CH₄ productivity by co-digesting swine manure with three crop residues as an external carbon source. *Bioresource Technology*, 101(11), 4042-4047.
- [15] Cuetos, M. J., Gómez, X., Otero, M., and Morán, A. (2008). Anaerobic digestion of solid slaughterhouse waste (SHW) at laboratory scale: influence of co-digestion with the organic fraction of municipal solid waste (OFMSW). *Biochemical Engineering Journal*, 40(1), 99-106.
- [16] Cavinato, C., Fatone, F., Bolzonella, D., and Pavan, P. (2010). Thermophilic anaerobic co-digestion of cattle manure with agro-wastes and energy crops: comparison of pilot and full scale experiences. *Bioresource Technology*, 101(2), 545-550.
- [17] Bouallagui, H., Cheikh, R. B., Marouani, L., and Hamdi, M. (2003). Mesophilic biogas production from fruit and vegetable waste in a tubular digester. *Bioresource Technology*, 86(1), 85-89.
- [18] Hernández-Berriel, M. C., Márquez-Benavides, L., González-Pérez, D., and Buenrostro-Delgado, O. (2008). The effect of moisture regimes on the anaerobic degradation of municipal solid waste from Metepec (Mexico). *Waste Management*, 28, S14-S20.
- [19] Gruber, W. (2007). Biogasanlagen in der Landwirtschaft. *Verbraucherschultz, Ernährung, Landwirtschaft*, 1453.
- [20] Group, B. T. (2003). BTG Anaerobic Digestion.

- [21] Jenagi, I. (2002). Production methane gas from effluent. Adelaide University, Diploma Individual Project.
- [22] Kaosol, T., and Sohgrathok, N. (2012). Influence of Hydraulic Retention Time on Biogas Production from Frozen Seafood Wastewater Using Decanter Cake as Anaerobic Co-digestion Material. *TVS*, 20, 0.20.
- [23] Braun, R., Madlener, R., and Laaber, M. Efficiency evaluation of energy crop digestion plants. In: *Proc., Proceedings of the 7th FAO/SREN Workshop "The Future of Biogas for Sustainable Energy Production in Europe"*.
- [24] Menardo, S., Gioelli, F., and Balsari, P. (2011). The methane yield of digestate: effect of organic loading rate, hydraulic retention time, and plant feeding. *Bioresource Technology*, 102(3), 2348-2351.
- [25] Schievano, A., Pognani, M., D'Imporzano, G., and Adani, F. (2008). Predicting anaerobic biogasification potential of ingestates and digestates of a full-scale biogas plant using chemical and biological parameters. *Bioresource Technology*, 99(17), 8112-8117.
- [26] Lindorfer, H., Lopez, C. P., Resch, C., Braun, R., and Kirchmayr, R. (2007). The impact of increasing energy crop addition on process performance and residual methane potential in anaerobic digestion. *Water science and technology*, 56(10), 55-63.
- [27] Pullammanappallil, P., Svoronos, S., Chynoweth, D., and Lyberatos, G. (1998). Expert system for control of anaerobic digesters. *Biotechnology and Bioengineering*, 58(1), 13-22.
- [28] Preissler, D., Drochner, U., Lemmer, A., Oechsner, H., and Jungbluth, T. (2010). Sulphur binding in biogas plants using ferric salts. *Landtechnik*, 65(3), 201-203.
- [29] Weiland, P. (2004). Erfahrungen deutscher Biogasanlagen-Ergebnisse einer bundesweiten Bewertung. *Institut für Technologie und Biosystemtechnik, Bundesforschungsanstalt für Landwirtschaft (FAL)*.
- [30] Biosystemtechnik, I. f. A. u., and Rohstoffe, F. N. (2009). *Biogas-Messprogramm 2: 61 Biogasanlagen im Vergleich*, Fachagentur Nachwachsende Rohstoffe.
- [31] Arora, J. S. (2004). *Introduction to optimum design*, Elsevier Academic Press, The University of Iowa.
- [32] Al Seadi, T. (2001). Good practice in quality management of AD residues from biogas production.
- [33] Mézes, L. (2011). *Mezőgazdasági és élelmiszeripari biogáz-termelés optimalizálása*. University of Debrecen, Debrecen, Hungary
- [34] Eder, B., Krieg, A., and Schulz, H. (2006). *Biogas-Praxis: Grundlagen, Planung, Anlagenbau, Beispiele, Wirtschaftlichkeit*, Ökobuch-Verlag.
- [35] Chadwick, D. (2005). Emissions of ammonia, nitrous oxide and methane from cattle manure heaps: effect of compaction and covering. *Atmospheric environment*, 39(4), 787-799.

Article copyright: © 2017 Lili Mézes, Attila Bai, Dávid Nagy, István Cinka, and Zoltán Gabnai. This is an open access article distributed under the terms of the [Creative Commons Attribution 4.0 International License](https://creativecommons.org/licenses/by/4.0/), which permits unrestricted use and distribution provided the original author and source are credited.



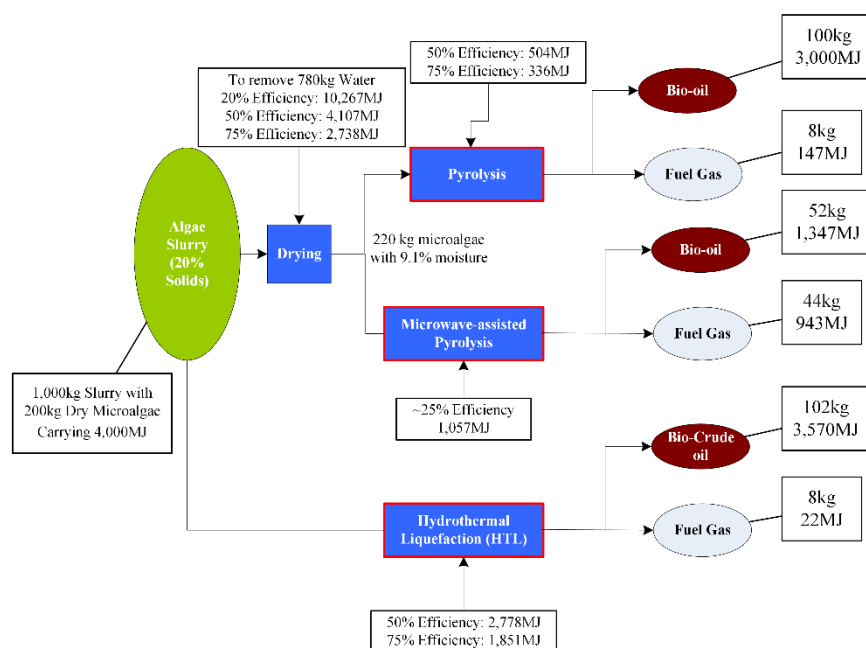
A Comparison of Energy Consumption in Hydrothermal Liquefaction and Pyrolysis of Microalgae

Bo Zhang^{1*}, Jinsheng Wu¹, Zhao Deng¹, Changyan Yang^{1,2*}, Chang Cui¹, Yigang Ding¹

1: Key Laboratory for Green Chemical Process of Ministry of Education, Hubei Key Laboratory of Novel Chemical Reactor and Green Chemical Technology, School of Chemical Engineering and Pharmacy, Wuhan Institute of Technology, Hubei, China

2: Hubei Key Laboratory for Processing and Application of Catalytic Materials, Huanggang Normal University, Hubei, China

Received December 2, 2016; Accepted December 25, 2016; Published January 1, 2017



The energy requirements for converting one tonne (1,000 kg) of *Chlorella* slurry of 20 wt% solids via fast pyrolysis, microwave-assisted pyrolysis (MAP), and hydrothermal liquefaction (HTL) were compared. Drying microalgae prior to pyrolysis by using a spray drying process with a 50% energy efficiency required an energy input of 4,107 MJ, which is higher than the energy content (4,000 MJ) of raw microalgae. The energy inputs to conduct fast pyrolysis, MAP, and HTL reactions were 504 MJ (50% efficient), 1,057 MJ (~25% efficient), and 2,776 MJ (50% efficient), respectively. The overall energy requirement of fast pyrolysis is theoretically about 1.6 times more than that of HTL. The energy recovery ratios for fast pyrolysis, MAP, and HTL of microalgae were 78.7%, 57.2%, and 89.8%, respectively. From the energy balance point of view, hydrothermal liquefaction is superior, and it achieved a higher energy recovery with a less energy cost. To improve the pyrolysis process, developing drying devices powered by renewable energies, optimizing the pyrolysis process (specifically microwave-assisted), and improving the energy efficiency of equipment are options.

Keywords: Microalgae; Energy Consumption; Pyrolysis; Hydrothermal Liquefaction (HTL); Microwave-assisted pyrolysis; Thermal Drying

Introduction

Thermochemical conversion of microalgae can be divided into pyrolysis of dry algae and hydrothermal liquefaction (HTL) of algal slurries [1]. Usually, the microalgal culture has a very dilute concentration of 0.1-1% dry solids. Currently, the proposed harvesting process is using a series of mechanical unit operations to dewater the microalgae media to a level of ~20% dry solids, which is considered as a less energy intensive processing option than completely drying microalgae for pyrolysis purpose. Drying is one of most dominant costs for algae harvest and may account for 30% of the total product costs, and the power consumption was equivalent to 15.8% of the energy of the recovered hydrocarbon [2]. Because of this energy consumption barrier, pyrolysis is considered as a kind of hopeless technologies for microalgae and only limited to laboratory investigations [3]. Meanwhile, researchers also recognized the advantages of the pyrolysis of microalgae (such as higher quality of pyrolytic bio-oil than that of cellulosic biomass) [4] and the merits of pyrolysis technology (such as lower capital cost than HTL) [5, 6].

This paper provides a simple comparison between the energy consumptions in pyrolysis of microalgae and hydrothermal liquefaction of microalgae. The purpose is not to provide a complete evaluation to these conversion technologies, but to give an idea how the energy consumption impacted the conversion processes of microalgae, and what would be the possible solutions.

Methodology

Microalgae

The composition analysis and properties of *Chlorella sp.* are summarized in Table 1. An engineered *Chlorella sp.* was assumed to be grown autotrophically, and had following components: 25% fatty acids, 50% protein, 15% polysaccharide, and 10% ash. For calculation, one tonne (1,000 kg) of *Chlorella* slurry at 20°C with 20 wt% solids and 80 wt% water (*i.e.* 200 kg dry algal cells and 800 kg water) was selected as the baseline. Cell concentration of 20 wt% has been used in multiple technical reports published by US national laboratories [7, 8]. This kind of algal slurries can be obtained via a series of dewatering unit operations such as settling, dissolved air flotation, and centrifugation. The energy content of microalgae is ~20 MJ/kg, so this microalgal slurry carried 4,000 MJ.

Table 1. Composition analysis and properties of *C. vulgaris* [9-12]

Protein (wt%)	34-58.1	Specific heat (kJ/kg·K)*	1.57
Polysaccharide (wt%)	9.42-15.5	Molecular weight (g/mol)*	360
Lipid (wt%)	1.04-15.6	HHV (MJ/kg)	19.3-21.2
C (wt%)	44.5-50.2	Volatile matter (wt%)	51.8-75.2
H (wt%)	6.2-7.2	Fixed carbon (wt%)	9-32.1
N (wt%)	6.4-10.9	Ash (wt%)	9.6-11.4
O (wt%)	24.6-40.7		

* [13]

Fast pyrolysis and microwave-assisted pyrolysis processes

Prior to pyrolysis, the microalgal slurry (1,000 kg) was dried with a spray dryer to 220 kg with a 9.1% moisture. Spray drying could generate *Chlorella* powders consisted of globular particles with a diameter of approximately 50-80 μm (*i.e.* 0.05-0.08 mm, approximately 270- 200 mesh) [14], which is fine enough for fast pyrolysis. Fast pyrolysis of microalgal powders were conducted in a fluidized bed reactor at 500°C with a heating rate of 600 °C/s. Pyrolytic product yields were assumed to be following: the bio-oil yield was 50 wt%, the yield of water solubles was 15 wt%, gaseous products counted for 4 wt%, and the biochar yield was 28 wt%. The gaseous products consisted of 22.2 vol% H₂, 34.9 vol% CH₄, 38.6 vol% CO₂, and 4.3 vol% C₂H₆ [11].

For microwave-assisted pyrolysis, microalgae could be air-dried by using solar dryers (Figure 1), because microwave pyrolysis doesn't require the finely ground feed [15, 16]. Microwave-assisted pyrolysis was assumed to be conducted in a pilot scale system, which could process large chunks of dry microalgae [17]. Pyrolytic product yields were assumed to be following: the bio-oil yield is 26 wt%, the yield of water solubles was 24 wt%, gaseous products counted for 22 wt%, and the biochar yield is 28 wt% [10].

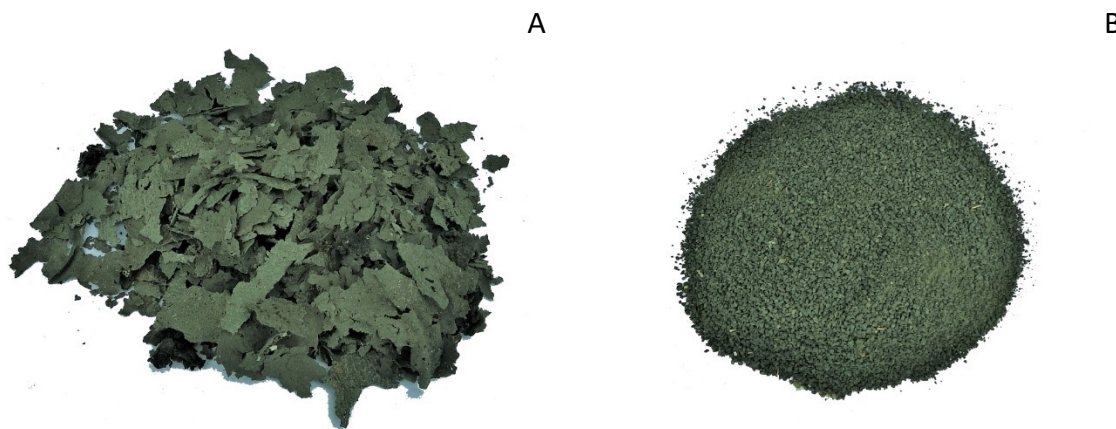


Figure 1. Naturally dried microalgae (A) and ground microalgae (B)

Hydrothermal liquefaction (HTL)

The microalgal slurry of 20 wt% solids was pumped to the HTL reactor, and hydrothermally treated in subcritical water at 2,500-3,000 psia and 350°C. The HTL process yielded 4 wt% gases, 51 wt% bio-crude oil, and 43 wt% aqueous organics and ash [5]. The non-condensable gases had following composition: 42 vol% CO₂, 50 vol% NH₃, 7 vol% CH₄, and 1 vol% ethane [18]. The non-condensable gases were mixed with natural gas and sent to a steam boiler for power generation. The predominately organic liquid phase is sent to catalytic upgrading, and the predominately aqueous phase is sent to wastewater cleanup for carbon recovery. Solids that can be removed by filtration might be recycled back to the algae ponds as nutrients [14]. The conditions and product yields for pyrolysis and HTL processes used in this study are summarized in Table 2.

Table 2. Conditions and product yields of pyrolysis and hydrothermal liquefaction of microalgae

	Fast Pyrolysis (500°C)	Microwave-assisted Pyrolysis	HTL (350°C)
Reaction temperature	500°C	-	350°C
Pressure	Atmospheric pressure	Atmospheric pressure	2500-3000 psia
Bio-oil (wt%)	50	26	51
Water (wt%)	15	24	-
Biochar yield (wt%)	28	28	-
Gaseous products (wt%)	4	22	4

Calculation

Specific heat of microalgae

According to a scientific report that studied the thermo-chemical properties of six species of microalgae, the specific heat (c_p) of microalgae was determined as 1.2 - 2 kJ/kg·K [13]. Meanwhile, to calculate the specific heat of microalga from its composition, following assumptions were applied: ash is SiO₂ with a specific heat of 733 J/kg·K or 0.175 cal/g·°C, the specific heat of polysaccharides is same as that of glucose (0.3 cal/g·°C), the specific heat of fatty acids is same as that of stearic acid (0.55 cal/g·°C), and the specific heat of protein is same as that of quinolone (0.352 cal/g·°C). Thus, the specific heat of *Chlorella sp.* was determined via Eqn. 1 as 0.376 cal/g·°C or 1.57 kJ/kg·K.

Specific heat of microalga (c_p , microalgae)

$$=10\% \times 0.175 + 25\% \times 0.55 + 50\% \times 0.352 + 15\% \times 0.3 = 0.376 \text{ cal/g} \cdot ^\circ\text{C} \quad \text{Eqn. 1}$$

Energy for thermal drying of microalgal slurry

The feedstock for pyrolysis is typically quoted at <10 wt% moisture and requires thermal drying. To thermally dry one tonne of microalgal slurry (20°C) to 9.1% moisture, 780 kg water needs to be evaporated at 100°C. Water has a specific heat of 4.187 kJ/kg·K and latent heat (at 100°C) of 2256.9 kJ/kg [19].

Energy required for water evaporation:

$$=780 \times 4.187 \times (100-20) + 780 \times 2256.9 = 2,022 \text{ MJ} \quad \text{Eqn. 2}$$

To evaporate 780 kg water from 1 tonne algal slurry, it will require at least 2,021,650 kJ, which is approximately 2,022 MJ or 562 kWh. This energy consumption is about 18.6 days of electricity usage of an American household [20]. Because the whole slurry shall be heated by the thermal dryer, the energy input for heating up rest water and microalgae can be calculated via following equations:

Energy required for heating 20 kg water to 100°C:

$$=20 \times 4.187 \times (100-20) = 6,699.2 \text{ kJ} = 1.86 \text{ kWh} \quad \text{Eqn. 3}$$

Energy required for heating 200 kg microalgae to 100°C:

$$=200 \times 1.57 \times (100-20) = 25,120 \text{ kJ} = 6.98 \text{ kWh} \quad \text{Eqn. 4}$$

The total energy for thermal drying of 1,000 kg microalgal slurry shall be equal to the sum of equations 2 through 4.

The total energy for thermal drying of 1,000 kg microalgal slurry:

$$=2,021,650.8 \text{ kJ} + 6,699.2 \text{ kJ} + 25,120 \text{ kJ} = 2,053 \text{ MJ} = 570 \text{ kWh} \quad \text{Eqn. 5}$$

However, the overall thermal efficiency of spray dryers is only 20-50% [21]. Hence, if a dryer with 50% efficiency was used for drying the microalgal slurry, the total energy input for the drying process is 4,107 MJ or 1140 kWh. If the thermal efficiency can be improved to 75% [22], the energy requirement reduced to 2,737,960 kJ (2738 MJ) or 760 kWh.

Energy required for fast pyrolysis of microalgae

It's reported that the energy required to achieve thermal conversion (*i.e.* pyrolysis) of six different microalgae at 500°C was found to be approximately 1 MJ/kg [13]. Because only dry microalgal samples were used in their study, the energy required to evaporate moisture must be considered too.

$$\begin{aligned} &\text{Energy required for evaporation of 20 kg water:} \\ &= 20 \times 4.187 \times (100 - 20) + 20 \times 2256.9 = 51,837 \text{ kJ} = 23.6 \text{ kWh} \end{aligned} \quad \text{Eqn. 6}$$

$$\begin{aligned} &\text{Energy required for pyrolyzing 200 kg microalgae:} \\ &= 200 \times 1 \text{ MJ/kg} = 200 \text{ MJ} = 200,000 \text{ kJ} = 55.6 \text{ kWh} \end{aligned} \quad \text{Eqn. 7}$$

$$\begin{aligned} &\text{Total energy required for pyrolysis of 220 kg microalgae} \\ &= 51,837 \text{ kJ} + 200,000 \text{ kJ} = 251,837 \text{ kJ} = 252 \text{ MJ} = 70 \text{ kWh} \end{aligned} \quad \text{Eqn. 8}$$

If a pyrolyzer with 50% energy efficiency was used, the total energy input for the pyrolysis of microalgae rose to:

$$= 251,837 \text{ kJ} \div 50\% = 503,674 \text{ kJ} = 504 \text{ MJ} = 140 \text{ kWh} \quad \text{Eqn. 9}$$

Energy output from fast pyrolysis products

Pyrolyzing 200 kg dry microalgae yielded 100 kg bio-oil, 30 kg water, 8 kg gases, and 56 kg biochar. The microalgal bio-oil was assumed to have a higher heating value of 30 MJ/kg, so the energy output from the bio-oil is 3,000 MJ (3,000,000 kJ = 833 kWh). According to the composition of the gaseous products (22.2 vol% H₂, 34.9 vol% CH₄, 38.6 vol% CO₂, and 4.3 vol% C₂H₆), the gas phase had an average molecular weight:

$$\text{MW} = 2 \times 0.222 + 16 \times 0.349 + 44 \times 0.386 + 30 \times 0.043 = 24 \text{ g/mol}$$

Eqn. 10

So, total gaseous products were 333.3 mol and 7,466.7 L (7.5 m³) at normal temperature & pressure conditions, including 1.665 m³ H₂, 2.61 m³ CH₄, 2.89 m³ CO₂, and 0.32 m³ C₂H₆. The higher heating values of H₂, CH₄, and C₂H₆ are 12.769 MJ/m³, 39.781 MJ/m³, and 69.693 MJ/m³ [23]. The energy output from the gases:

$$= 12.769 \times 1.665 + 39.781 \times 2.61 + 69.693 \times 0.32 = 147.4 \text{ MJ} = 41 \text{ kWh} \quad \text{Eqn. 11}$$

Because microalgal biochar is normally used as the soil amendment, total energy output from pyrolysis of 200 kg microalgae is 3,147.4 MJ (3,147,400 kJ or 874 kWh).

Energy required for microwave-assisted pyrolysis of microalgae

Energy requirement for microwave-assisted pyrolysis was only experimentally determined for a benchtop system that converted 30-60 g dry microalgae. Based on their results, it required 317 kJ to pyrolyze 60 g microalgae to the bio-oil with a 404 kJ energy content and gases with a 283 kJ energy content [24]. The experiments in [24] were performed in a microwave oven, which normally is less than 60% efficient [25]. If scaling up this microwave oven linearly to a system processing 200 kg microalgae with the same efficiency, the microwave-assisted pyrolysis requires an energy input of 1,056,667 kJ (1,057 MJ or 293.5 kWh), producing the bio-oil of 52 kg with a 1346,666 kJ (1347 MJ or 374 kWh) energy content and gases of 44 kg with a 943,333 kJ (943 MJ or 262 kWh) energy content.

Energy required for HTL of microalgae

One tonne (1,000 kg) of microalgal slurry was processed via HTL at 350°C. According to the steam table, the specific enthalpies of water (saturated liquid) at 20°C and

350°C (~17 MPa/2,500 psia) are 83.9 kJ/kg and 1,690 kJ/kg, respectively [26]. Energy required for heating 800 kg water from 20°C to 350°C:

$$= 800 \times (1690 - 83.9) = 1,284,880\text{kJ} = 1,285\text{MJ} = 357\text{kWh} \quad \text{Eqn. 12}$$

Energy required for heating 200 kg microalgae from 20°C to 350°C:

$$= 200 \times 1.57 \times (350 - 20) = 103,620\text{kJ} = 104\text{MJ} = 29\text{kWh} \quad \text{Eqn. 13}$$

The total energy required for heating this 1,000 kg microalgal slurry to 350°C is 1,389 MJ or 386 kWh. If an electric heater with a 50% efficiency was used for this duty, the total energy required for HTL of microalgae is 2,778 MJ (772 kWh). If a 75% thermal efficiency can be applied, the total energy required for HTL is 1,851 MJ or 514 kWh.

Energy output from HTL products

Since the yield of bio-crude oil was 51%, and thus the process yielded 102 kg bio-crude with a 35 MJ/kg heating value [27]. Total energy recovered in the bio-crude oil was 3,570 MJ.

The gaseous products (42 vol% CO₂, 50 vol% NH₃, 7 vol% CH₄, and 1 vol% ethane) had an average molecular weight:

$$\text{MW} = 44 \times 0.42 + 17 \times 0.5 + 16 \times 0.07 + 30 \times 0.01 = 28.1\text{g/mol}$$

Eqn. 14

So, total gaseous products were 285 mol and 6,377 L (6.4 m³) at normal temperature & pressure conditions, including 2.7 m³ CO₂, 3.2 m³ NH₃, 0.45 m³ CH₄, and 0.06 m³ C₂H₆. The higher heating values of CH₄, and C₂H₆ are 39.781 MJ/m³ and 69.693 MJ/m³. The energy output from the combustible gases:

$$= 39.781 \times 0.45 + 69.693 \times 0.06 = 22\text{MJ} = 6\text{kWh} \quad \text{Eqn. 15}$$

Results and Discussion

To compare the energy consumption of different conversion technologies for microalgae, a 1,000 kg microalgal slurry was used as the baseline, and assumed to be processed with fast pyrolysis, microwave-assisted pyrolysis, and hydrothermal liquefaction processes. The energy requirements for the drying process and conversion reactors are summarized in Table 3. The energy present in original microalgae, the bio-oil or bio-crude, and gases is also summarized in Table 3.

Table 3. Breakdown of energy consumption during pyrolysis and liquefaction of microalgae (1,000 kg slurry with 20% solids at 20°C)

Energy (MJ)	Fast Pyrolysis (500°C)	Microwave-assisted Pyrolysis	HTL (350°C)
Energy in microalgae (20 MJ/kg)	4,000	4,000	4,000
Drying	4,107 ^a	4,107 ^a	N/A
Supporting conversion reaction	504 ^a	1,057 ^b	2,778 ^a
Total energy input	4611	5,164	2,778
Bio-oil	3000	1347	3570
Gas	147	943	22
Total energy in products	3147	2290	3592
Energy recovery	78.7%	57.2%	89.8%

a: 50% efficiency

b: 25% efficiency

The original 1,000 kg microalgal slurry with 200 kg dry microalgal cells carried 4,000 MJ energy. If drying this slurry to a moisture content of 9.1% by using a spray dryer with a 75% efficiency, the energy requirement for the dryer was 2,738 MJ. One advantage of spray drying for microalgae is to directly generate fine powders for the need of pyrolysis. However, the spray dryers generally have 20-50% efficiency, resulting in increased energy inputs of 4,107-10,267 MJ. Obviously, the efficiency of the drying system plays a very important role. If a drying system powered by renewable energies could be introduced into this process, the pyrolysis of microalgae will be more attractive.

The energy requirements for microalgae conversion were various for different techniques. Fast pyrolysis required the lowest amount of heat, because the process was considered to be conducted under the optimal conditions. Microwave-assisted pyrolysis was scaled up from a bench-top system with a low energy efficiency, and showed an energy requirement of ~1,000 MJ for converting 200 kg dry microalgae. Because pyrolyzing 200 kg microalgae requires an energy input of 252 MJ, the actual efficiency of this microwave pyrolysis system was approximately 25%. Meanwhile, hydrothermally liquefying 1,000 kg microalgal slurry needed ~2,778 MJ (50% efficient). The energy need for HTL was less than that of drying wet microalgae, because the evaporation process was avoided and HTL reactions happened in saturated water.

The product yields of fast pyrolysis and HTL were optimal numbers, which were projected from recent experimental studies and shall be realized in the near future. Both optimized pyrolysis and HTL processes should produce ~50 wt% bio-oil or bio-crude oil with a higher heating value of 30-30 MJ/kg, which is the main energy carrier for both processes. The combustible gas yields from both processes were relatively low and less than 4 wt%. The energy recovery ratios from microalgae were 78.7% and 89.8% for fast pyrolysis and HTL, respectively. Because microalgae have a high ash content, resulting in a significant amount of ash and metals in the microalgal biochars. Normally, the microalgal biochars are considered as a good soil amendment.

The microwave-assisted pyrolysis process used for this study was not optimized, and produced large quantities of gases and less bio-oil products than fast pyrolysis or HTL. The energy recovery ratio for microwave-assisted pyrolysis was only 57.2%. Microalgae are a poor microwave absorber too, so other materials like char and activated carbon are often added to help microwave absorption [28].

From the energy balance point of view, hydrothermal liquefaction is superior, and it could achieve the higher energy-recovery ratio with a lower energy cost.

Meanwhile, the pyrolysis of microalgae might still have its chance. The major advantage of microwave-assisted pyrolysis is that it can process feedstock with a large particles size even chunks, because of the unique heating approach. If the efficiency of microwave-assisted pyrolysis can be improved to that of fast pyrolysis, and solar drying can be applied to solve the negative energy issue (as shown in Figure 2), the pyrolysis of microalgae will be more promising.

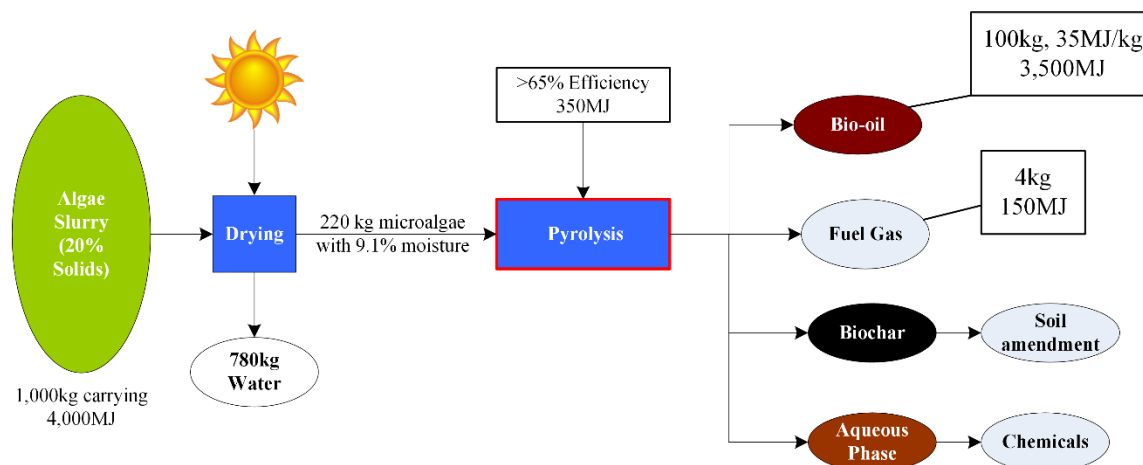


Figure 2. Proposed ideal pyrolysis process for microalgae

CONCLUSIONS

The energy requirements for converting one tonne (1,000 kg) of *Chlorella* slurry of 20 wt% solids via fast pyrolysis, microwave-assisted pyrolysis (MAP), and hydrothermal liquefaction (HTL) were compared. Drying microalgae prior to pyrolysis by using a spray drying process with 20%, 50%, and 75% energy efficiency required energy inputs of 10,267 MJ, 4,107 MJ, and 2,738 MJ, respectively. The energy inputs to conduct fast pyrolysis, MAP, and HTL reactions were 504 MJ (50% efficient), 1,057 MJ (~25% efficient), and 2,776 MJ (50% efficient), respectively. The microalgal feed contained 4,000 MJ, and the energy recovery ratios for fast pyrolysis, MAP, and HTL of microalgae were 78.7%, 57.2%, and 89.8%, respectively. From the energy balance point of view, hydrothermal liquefaction is superior, and it achieved a higher energy recovery with a less energy cost. To improve the pyrolysis process, developing drying devices powered by renewable energies, optimizing the pyrolysis process, and improving the energy efficiency of equipment are options.

ACKNOWLEDGMENTS

We are grateful for the support from the School of Chemical Engineering and Pharmacy at the Wuhan Institute of Technology.

CONFLICTS OF INTEREST

The authors declare that there is no conflict of interests regarding the publication of this paper.

REFERENCES

- [1] Yang, C., Li, R., Cui, C., Liu, S., Qiu, Q., Ding, Y., Wu, Y., and Zhang, B. (2016). Catalytic hydroprocessing of microalgae-derived biofuels: a review. *Green Chemistry*, 18(13), 3684-3699. DOI: 10.1039/c6gc01239f
- [2] Chen, Y., Wu, Y., Hua, D., Li, C., Harold, M. P., Wang, J., and Yang, M. (2015). Thermochemical conversion of low-lipid microalgae for the production of liquid

- fuels: challenges and opportunities. *RSC Advances*, 5(24), 18673-18701. DOI: 10.1039/c4ra13359e
- [3] Elliott, D. C. (2016). Review of recent reports on process technology for thermochemical conversion of whole algae to liquid fuels. *Algal Research*, 13, 255-263. DOI: 10.1016/j.algal.2015.12.002
- [4] Raheem, A., Wan Azlina, W. A. K. G., Taufiq Yap, Y. H., Danquah, M. K., and Harun, R. (2015). Thermochemical conversion of microalgal biomass for biofuel production. *Renewable and Sustainable Energy Reviews*, 49, 990-999. DOI: 10.1016/j.rser.2015.04.186
- [5] Saber, M., Nakhshiniev, B., and Yoshikawa, K. (2016). A review of production and upgrading of algal bio-oil. *Renewable and Sustainable Energy Reviews*, 58, 918-930. DOI: 10.1016/j.rser.2015.12.342
- [6] Yang, C., Li, R., Cui, C., Wu, J., Ding, Y., Wu, Y., and Zhang, B. (2017). The Pyrolysis of Duckweed over a Solid Base Catalyst: Py-GC/MS and TGA Analysis. *Energy Sources, Part A: Recovery, Utilization, and Environmental Effects*, 39 (2), 177-183. DOI: 10.1080/15567036.2016.1214641
- [7] Jones, S. B., Zhu, Y., Anderson, D. M., Hallen, R. T., Elliott, D. C., Schmidt, A., Albrecht, K., Hart, T., Butcher, M., and Drennan, C. (2014). *Process design and economics for the conversion of algal biomass to hydrocarbons: whole algae hydrothermal liquefaction and upgrading*, Pacific Northwest National Laboratory.
- [8] Jones, S. B., Zhu, Y., Snowden-Swan, L. J., Anderson, D., Hallen, R. T., Schmidt, A. J., Albrecht, K., and Elliott, D. C. (2014). Whole Algae Hydrothermal Liquefaction: 2014 State of Technology. Pacific Northwest National Laboratory (PNNL), Richland, WA (US).
- [9] Du, Z., Li, Y., Wang, X., Wan, Y., Chen, Q., Wang, C., Lin, X., Liu, Y., Chen, P., and Ruan, R. (2011). Microwave-assisted pyrolysis of microalgae for biofuel production. *Bioresource Technology*, 102(7), 4890-4896. DOI: 10.1016/j.biortech.2011.01.055
- [10] Borges, F. C., Xie, Q., Min, M., Muniz, L. A. R., Farenzena, M., Trierweiler, J. O., Chen, P., and Ruan, R. (2014). Fast microwave-assisted pyrolysis of microalgae using microwave absorbent and HZSM-5 catalyst. *Bioresource Technology*, 166, 518-526. DOI: 10.1016/j.biortech.2014.05.100
- [11] Gong, X., Zhang, B., Zhang, Y., Huang, Y., and Xu, M. (2014). Investigation on Pyrolysis of Low Lipid Microalgae *Chlorella vulgaris* and *Dunaliella salina*. *Energy & Fuels*, 28(1), 95-103. DOI: 10.1021/ef401500z
- [12] Thangalazhy-Gopakumar, S., Adhikari, S., Chattanathan, S. A., and Gupta, R. B. (2012). Catalytic pyrolysis of green algae for hydrocarbon production using H+ZSM-5 catalyst. *Bioresource Technology*, 118, 150-157. DOI: 10.1016/j.biortech.2012.05.080
- [13] Grierson, S., Strezov, V., Ellem, G., McGregor, R., and Herbertson, J. (2009). Thermal characterisation of microalgae under slow pyrolysis conditions. *Journal of Analytical and Applied Pyrolysis*, 85(1-2), 118-123. DOI: 10.1016/j.jaap.2008.10.003
- [14] Lin, L. (1985). Microstructure of spray-dried and freeze-dried microalgal powders. *Food Structure*, 4(2), 17.
- [15] Zhang, B., Yang, C., Moen, J., Le, Z., Hennessy, K., Wan, Y., Liu, Y., Lei, H., Chen, P., and Ruan, R. (2010). Catalytic Conversion of Microwave-assisted

- Pyrolysis Vapors. *Energy Sources, Part A: Recovery, Utilization, and Environmental Effects*, 32(18), 1756-1762. DOI: 10.1080/15567030902842285
- [16] Yang, C., Zhang, B., Moen, J., Hennessy, K., Liu, Y., Lin, X., Wan, Y., Lei, H., Chen, P., and Ruan, R. (2010). Fractionation and characterization of bio-oil from microwave-assisted pyrolysis of corn stover. *Int J Agric & Biol Eng*, 3(3), 54-61. DOI: 10.3965/j.issn.1934-6344.2010.03.054-061
- [17] Ruan, R., Chen, P., Hemmingsen, R., Morey, V., and Tiffany, D. (2008). Size matters: small distributed biomass energy production systems for economic viability. *International Journal of Agricultural and Biological Engineering*, 1(1), 64-68. DOI: 10.3965/j.issn.1934-6344.2008.01.064-068
- [18] Elliott, D. C., Hart, T. R., Schmidt, A. J., Neuenschwander, G. G., Rotness, L. J., Olarte, M. V., Zacher, A. H., Albrecht, K. O., Hallen, R. T., and Holladay, J. E. (2013). Process development for hydrothermal liquefaction of algae feedstocks in a continuous-flow reactor. *Algal Research*, 2(4), 445-454. DOI: 10.1016/j.algal.2013.08.005
- [19] Doran, P. M. (2013). *Bioprocess engineering principles*, Academic Press.
- [20] U.S. EIA (2016). How much electricity does an American home use? <https://www.eia.gov/tools/faqs/faq.cfm?id=97&t=3>. (Accessed on 12/26/2016)
- [21] Earle, R. L. (2013). *Unit operations in food processing*, Elsevier.
- [22] APV (2000). APV Dryer Handbook. http://userpages.umbc.edu/~dfrey1/ench445/apv_dryer.pdf. (Accessed on 12/26/2016)
- [23] Waldheim, L., and Nilsson, T. (2001). Heating value of gases from biomass gasification. *Report prepared for: IEA bioenergy agreement, Task, 20*.
- [24] Zhang, R., Li, L., Tong, D., and Hu, C. (2016). Microwave-enhanced pyrolysis of natural algae from water blooms. *Bioresource Technology*, 212, 311-317. DOI: 10.1016/j.biortech.2016.04.053
- [25] Holladay, M. (2014). All About Microwave Ovens. <http://www.greenbuildingadvisor.com/blogs/dept/musings/all-about-microwave-ovens>. (Accessed on 12/26/2016)
- [26] Perry, R. H., and Green, D. W. (1999). *Perry's chemical engineers' handbook*, McGraw-Hill Professional.
- [27] Biller, P., Sharma, B. K., Kunwar, B., and Ross, A. B. (2015). Hydroprocessing of bio-crude from continuous hydrothermal liquefaction of microalgae. *Fuel*, 159, 197-205. DOI: 10.1016/j.fuel.2015.06.077
- [28] Xie, Q., Addy, M., Liu, S., Zhang, B., Cheng, Y., Wan, Y., Li, Y., Liu, Y., Lin, X., Chen, P., and Ruan, R. (2015). Fast microwave-assisted catalytic co-pyrolysis of microalgae and scum for bio-oil production. *Fuel*, 160, 577-582. DOI: 10.1016/j.fuel.2015.08.020

Article Copyright: © 2017 Bo Zhang, Jinsheng Wu, Zhao Deng, Changyan Yang, Chang Cui, and Yigang Ding. This is an open access article distributed under the terms of the [Creative Commons Attribution 4.0 International License](https://creativecommons.org/licenses/by/4.0/), which permits unrestricted use and distribution provided the original author and source are credited.



Characterization, Modification and Application of Biochar for Energy Storage and Catalysis: A Review

Shuangning Xiu, Abolghasem Shahbazi,* and Rui Li

Department of Natural Resources and Environmental Design, North Carolina A & T State University, 1601 East Market Street, Greensboro, NC 27411, United State

Received January 6, 2017; Accepted February 6, 2017; Published February 7, 2017

Biomass can be converted to biofuels and bioproducts via thermochemical processes. Biochar is one of the major products of thermochemical conversion of biomass. The efficient use of biochar is critical to improving the economic viability and environmental sustainability of biomass conversion technologies. Applications of biochar for both agricultural and environmental benefits (e.g. as soil amendment, for inorganic pollutant removal) have been studied and reviewed extensively. However, biochar for energy storage materials and catalytic applications has not been widely reviewed in the recent past. This review aims to present the more significant recent advances in several biochar utilizations such as catalysts and supercapacitors. Discussions on biochar production technologies, chemistry, properties, characteristics, and advanced functionalization techniques are provided. It also points out barriers to achieving improvements in the future.

Keywords: *Biochar; Hydrochar; Catalysis; Supercapacitor; Thermochemical conversion of biomass; Mechanism of biochar formation; Feedstock choice; Characterization; Biochar modification*

Introduction

Energy crisis, environmental pollution, and global warming are serious problems that are of great concerns throughout the world. Sustainable development requires discovering economically viable and environmentally friendly energy sources with the aim of solving these problems.

One important aspect of such research is to synthesize a range of materials that can be used to resolve many of the challenges encountered (e.g., environmental pollution and global warming). For example, materials with catalytic functionalities can be developed to convert renewable sources to fuel or chemicals. Absorbents or catalytic materials can be developed to capture CO₂ or remove pollutants. Materials with high storage capacities can be produced for the storage of low-cost clean renewable energy (such as solar, wind, and bioenergy) [1]. Carbon-based materials have attracted considerable interest in many energy-related applications, such as energy storage in supercapacitors and Li-ion batteries, catalysis/electrocatalysis, absorption, and gas separation and storage, due to their abundance, chemical and thermal stability, processability, and the possibility of tuning their textural and structural characteristics to fulfill the requirements of specific applications.

Different routes have been used to synthesize carbon-based materials, such as chemical vapor deposition, arc discharge synthesis, and carbonization of synthetic or natural polymers. However, these methods usually require tedious synthetic methods as well as organic solvents and electrochemical treatment. In addition, they often rely on relatively expensive fossil fuel-based precursors, the use of metal catalysts, and complicated apparatus involving high processing temperatures, none of which are environmentally and economically sustainable. These drawbacks lead to high production cost and limit the large-scale production and commercialization of such carbon materials. Alternatively, thermochemical conversion (*e.g.* pyrolysis and hydrothermal carbonization) of biomass is a promising route, offering low-cost, low temperature, and environmentally friendly production of novel carbon materials from natural precursors without the need to use toxic chemicals [2].

Biomass is a naturally abundant renewable resource that has great potential as a raw carbon material for synthesizing various carbon materials [2]. Considerable attention has been given to lignocellulosic biomass such as agricultural residues, woody biomass and energy crops [3]. Recently, biochar, a product from biomass thermochemical conversion, has received increasing attention for the use in several applications due to the cheap, abundant, and sustainable advantages. The most common biochar application is soil amendment to mitigate greenhouse gas emission and improve soil health. Recent developments in activation procedures and/or precursors allow a better control over the pore structure and surface property. These characteristics have widened the use of biochar to more demanding applications, including use biochar as a precursor for making catalysts, energy storage, gas storage and contaminant adsorbents. These new high-value applications are still in their infancy, and further research and development are needed to reach commercialization.

This review addresses the opportunities and advantages of using new technologies to convert biomass into biochar-based functional materials with applications in energy storage and catalysis. Discussions on biochar production technologies, chemistry, properties, characteristics and advanced methods to modify its structure and properties are also provided.

Biochar Production

Overview of the biochar production technologies

Research to date has shown biochar to be a carbonaceous solid consisting of an aromatic, furanic, and aliphatic backbone and numerous oxygen defects. The international Biochar Initiative defines biochar as “a solid material obtained from the thermochemical conversion of biomass in an oxygen-limited environment” [4]. Biochar is produced in solid form by dry carbonization, pyrolysis or gasification of biomass, and in slurry form by hydrothermal carbonization (HTC) of biomass under pressure. Typical operating conditions and char yields of different thermochemical processes are shown in Table 1 [5]. An advantage of the thermochemical process is that it is relatively simple, usually requiring only one reactor, thus having a low capital cost.

Pyrolysis is the most common method to produce biochar, which can be categorized into slow pyrolysis and fast pyrolysis depending on the heating rate and residence time. Slow pyrolysis, also called conventional carbonization, produces biochar by heating biomass at a low heating rate for a relatively long residence time (up to several

days). According to the literature, the production of biochar from carbonization of biomass can be dated back for centuries [6].

Table 1. Different thermochemical processes and typical char yields from these processes

Process	Temperature (°C)	Residence Time	Char Yield (wt%)
Slow Pyrolysis	400-600	min to days	20-50
Fast Pyrolysis	400-600	~1 s	10-20
Gasification	800-1000	5-20 s	~10
Hydrothermal Carbonization	160-350	1-12 h	30-60

On the other hand, fast pyrolysis involves the rapid thermal decomposition of organic compounds by heat in the absence of oxygen, which results in the production of biochar, bio-oil, and gaseous products. Fast pyrolysis produces biochar at a high heating rate (above 200 °C/min) and short residence time (less than 10 s). The major differences between the two pyrolysis methods are the yields of biochar and bio-oil: Fast pyrolysis favors a high yield of bio-oil, while slow pyrolysis favors a high yield of biochar.

Gasification is different from general pyrolysis processes. For gasification, the biomass is converted into primarily a gaseous mixture (containing CO, H₂, CO₂, CH₄, and smaller quantities of higher hydrocarbons) by supplying a controlled amount of oxidizing agent under high temperature (greater than 700°C). The resulting gas mixture is known as synthetic gas or syngas. The typical biochar yield of gasification averages about 10 wt% of biomass [7].

Hydrothermal carbonization (HTC) is also called wet pyrolysis, direct liquefaction, hydrothermal upgrading/pyrolysis, and solvolysis. The use of water as a solvent obviates the need to dry biomass and permits reactions to be carried out at lower temperatures in comparison with pyrolysis. HTC of biomass takes place in water at elevated temperatures (160–350 °C). Since the water temperature is above 100°C, the reaction pressure also must be elevated (more than 1 atm) to maintain the water in a liquid form. Low-temperature HTC can mimic the natural coalification of biomass, although the reaction rate is higher and the reaction time is shorter compared to the hundreds of years of slow natural coalification of biomass. Char yield of low-temperature biomass HTC varies from 30% to 60% depending on the feedstock properties, reaction temperature, and pressure [8]. Since HTC requires water, this may be a cost-effective biochar production method for feedstocks with high moisture content.

The char produced from HTC often is called hydrochar. It is important to differentiate biochar from hydrochar because the chemical and physical properties differ significantly from each other. Chemical properties of biochars from gasification or pyrolysis were compared to hydrochars from HTC in the publication of [9]. The observations showing that hydrochars have lower proportions of aromatic compounds than biochars (less stable) but are rich in functional groups (higher cation exchange capacity) than biochars [9].

Mechanism of biochar formation in the biomass thermochemical conversion process

Biomass undergoes series of chemical reactions that are highly complicated and partially understood during the biochar or hydrochar production. The understanding of

the mechanism involved in biochar formation is essential in order to make it possible to tune the morphology, functionality, and porosity of the resulting biochar.

The overall mechanism of biochar formation consists indirectly of the pyrolysis/HTC mechanisms of the main biomass components, namely, cellulose, hemicellulose, and lignin. However, the reaction mechanisms of these two processes are different, which have been studied by many investigators [10, 11]. The HTC occurred in an aqueous medium which involves complex sequences of reactions including solvolysis, dehydration, decarboxylation, hydrogenation of functional groups, etc. The hemicelluloses were partly undergoing hydrolysis at lower temperatures and results in the formation of biochar/hydrochar through polymerization (water solubility homogenous reaction). For pyrolysis, the reaction mechanism is characterized by decreasing degrees of polymerization through homogeneous reactions in the gas phase. A number of pyrolysis mechanisms of cellulose, hemicellulose, and lignin have been proposed in [12, 13].

Several factors can influence the production and properties of biochar, of which the reaction temperature and the nature of biomass feedstock are the main factors [14]. The properties of biochar can be tuned by modifying the thermochemical operating conditions such as temperature, substrate concentration, residence time, and catalysts. Further studies are required to develop efficient catalysts for the conversion of biomass to biochar with the desired functional groups and porous structure.

Feedstock for biochar production

A number of lignocellulosic biomass materials have been used as feedstocks for pyrolysis and HTC. For example, Minowa *et al.* [15] tested twenty species of forest and agricultural residues with different lignin, hemicellulose, and cellulose contents. However, animal wastes and aquatic materials with low lignin and cellulose contents have not been studied as extensively as the high lignin and cellulose content biomass due to their difficult handling conditions. Besides, Giant Miscanthus as a bioenergy feedstock has gained importance in the recent few years [16].

Managing animal and crop wastes from agriculture poses a significant environmental burden that leads to pollution of ground and surface waters [17, 18]. These wastes, as well as other biomass, are usable resources for biochar production. Not only can energy be obtained in the production process, but the volume and weight of these wastes are significantly reduced, which is an important aspect of managing agricultural wastes [19].

Biomass with different chemical compositions (*i.e.* different contents of hemicellulose, cellulose, and lignin) are thought to have a significant impact on the biochar surface composition, reactivity with the chemical activating agent, and yields. A detailed comparative study on biochar produced from different feedstocks will be of great importance to identify common features and develop appropriate protocols for biochar-based materials production. Furthermore, it will be of immense interest to develop a correlation between the surface characteristics of biochar and composition of starting material with the change in thermochemical parameters.

Biochar Characterization

Physical, chemical, and mechanical properties of biochars can vary with production conditions and raw feedstock. It is very important to characterize biochar because its characterization plays a vital role in determining their applications in industry and environment.

Proximate, elemental composition and Inorganic fraction characterization

The proximate analysis can provide the weight fractions of moisture, volatile matter, ash, and fixed carbon. There are standardized methods for performing a proximate analysis (ASTM, ISO, DIN, and SB) [20]. Apart from the proximate analysis, the elemental composition of biochar are usually determined using analytical devices, such as an elemental analyzer. The principal elements of biochar are C, H, and O, with N sometimes included. The exact content differs greatly depending on the nature of the biomass feedstock. Usually, the carbon content of a typical biochar is in the range of 45-60 wt %, the hydrogen content 2-5 wt %, and the oxygen content about 10-20% [21].

In addition to the proximate and the bulk elements, various inorganic elements present in biochar also substantially influence its properties. Several analytical techniques can be applied to characterize the inorganic elements: inductively coupled plasma atomic emission spectroscopy (ICP-AES), X-ray fluorescence (XRF), and X-ray diffraction (XRD). ICP-AES can be used to determine the absolute concentrations of the inorganic elements (K, Mg, Ca, Na, Si, Al, Fe, Mn, etc.). XRF is often used to determine the inorganic (ash) compositions in terms of weight fraction of oxides and XRD can be used to identify the crystalline minerals in ash [22, 23]. The contents and species of inorganic elements are highly dependent on the nature of the biomass feedstock and reaction conditions (*e.g.*, temperature).

Textural characterization and morphology

The structure of biochar can be analyzed using a broad suite of analytical techniques. Scanning electron microscopy (SEM) and transmission electron microscopy (TEM) are techniques commonly used for the general characterization of biochar (*e.g.*, particle structure and surface topography) [24]. X-ray diffraction (XRD), Raman spectroscopy, and energy dispersive X-ray (EDX) spectroscopy are the most widely used methods for the characterization of the biochar microstructure [25]. Surface area and pore structure can be analyzed by using the Brunauer, Emmett, and Teller (BET) method, in which N₂ and CO₂ are the most widely used sorbate gas [20]. It is also suitable for the characterization of the biochar textural features, such as surface area and porosity. In addition to the above-mentioned routine characterization methods, there are also some in-depth characterization techniques used to understand the biochar fine structure. For example, solid-state ¹³C nuclear magnetic resonance (NMR) is a commonly used technique for carrying out comparisons that do not rely on peak ratios [26, 27]. As it has already been mentioned in the earlier sections, the biochars produced in pyrolysis usually exhibit very different structures than those obtained from the HTC process.

Surface functionality characterization

The surface functionality can be characterized by X-ray photoemission spectroscopy (XPS), FTIR, and temperature programmed desorption (TPD) techniques [28- 30]. The detailed surface chemistry of biochar, surface functionalities, and

composition can be obtained from these technologies. Surface functional groups play an important role in the application of biochars as functional materials, *e.g.*, catalysts, adsorbents, and electrode materials. The surface chemistry of biochar is very variable due to its highly heterogeneous composition. The main contribution to the reactivity of biochar is the fact that the surface usually exhibits a range of hydrophilic and hydrophobic functional groups both acidic and basic [31].

Although substantial progress has been made in the development of different techniques for the analyses of the structure, composition, and surface chemistry of biochar, future research efforts are required in order to explore the existence of various categories of biochar with unique molecular compositions and physical architectures. Future investigation into the effects of both charring conditions, such as charring duration and heating rates, as well as the nature of biomass (wood and grass) on the properties and yields of individual biochar categories may help refine the present classification scheme.

Biochar Modification

Tuning of surface properties

Typical biochars produced from a thermochemical conversion process present limited polar oxygenated surface groups such as C–O, C=O, and OH and possess very limited porosity and surface area (usually $<150 \text{ m}^2/\text{g}$) [32]. These inherent disadvantages limit the wide application of biochar as a useful functional material. For example, an abundant surface functionality is highly desirable for biochar destined to be used as a catalyst or adsorbent, because it may provide more active sites for catalysis or pollutant adsorption. Porosity and large surface areas are favorable for biochar used as an energy storage material or catalyst because they facilitate high mass transfer fluxes and high active loading.

Therefore, in order to enhance the performance of functionalized biochar materials, a suitable modification process is essential. The flexibility of biochar materials is that such groups can be easily tuned, and this offers a promising platform for synthesizing various functional materials. A number of functional materials synthesized through the functionalization/modification of the biochar materials are shown in Table 2.

Table 2. Typical functionalization/modification processes for tuning surface properties of biochar materials

Functionalization /Modification process	Surface functional group (characteristics)	Applications
Surface Oxidation	C=O, OH, and COOH	Pollutant removal; soil remediation
Surface Amination	NH ₂	Pollutant removal; CO ₂ capture
Surface Sulfonation	SO ₃ H	Solid acid catalyst
Surface and Pore structure modification	Porous biochar materials	Energy storage; CO ₂ capture; catalyst support
Surface recombination	Biochar support nanostructure	Energy storage; CO ₂ capture; catalyst

Surface oxidation is the most widely used method for creating oxygenated functional groups on the surface of biochar. Several types of oxygenated functional groups, such as carboxyl, phenolic hydroxyl, lactones, and peroxides, can be formed by surface oxidation treatments [33]. Oxygenated functional groups such as C=O, OH, and COOH are important for enhancing biochar performance in various applications. For example, Xu *et al.* found that surface OH and COOH groups can greatly enhance the adsorption capacity when biochar is used as an adsorbent for heavy-metal removal [34]. Hydrogen peroxide (H₂O₂), ozone (O₃), potassium permanganate (KMnO₄), and nitric acid (HNO₃) are the most frequently used surface oxidation reagents [35-37].

Besides oxygenated functional groups, basic amino groups on the surface of biochar have also been shown to greatly improve its performance in applications such as CO₂ capture and pollutant adsorption [38]. Surface amination is one of the most widely used methods to introduce amino groups into biochar. Ammonia (NH₃) treatment at high temperatures is a conventional surface amination technique that has been used extensively for decades [39]. Alternatively, chemical modification using some amino containing reagents is an environmentally friendly method also used for the surface amination of biochar. Compared to NH₃ treatment and chemical modification, the direct pyrolysis/HTC of nitrogen-rich biomass is a more sustainable method for the preparation of N-enriched biochar, because it does not require the use of NH₃ or expensive chemical reagents.

Sulfonic groups (SO₃H) are the main functional group in solid acidic materials. These are widely used as alternatives to liquid acids for the catalyzation of many chemical reactions [40]. Surface sulfonation of biochar using concentrated sulfuric acid or its derivatives (*e.g.*, oleum and chlorosulfonic acid) is the most commonly used method for the preparation of biochar-based solid acids [41].

Pore structure tailoring

One limitation of the biochar materials is that they often possess only a small number of micropores with a small surface area compared to conventional activated carbon. For applications in energy storage in supercapacitor, catalysis/electrocatalysis, and CO₂ capture or H₂ storage, controlled porosity and a high surface area are highly desirable. Thus, to facilitate their application in these fields, a variety of techniques have been developed to control the porosity and increase the surface area of biochar.

One of the most commonly used techniques for tuning the pore structure of biochar is in situ catalytic pore formation during biomass pyrolysis. The process is catalyzed by certain chemicals typically an acid, strong base or a salt, such as ZnCl₂ and H₃PO₄ [42-44]. The chemicals are impregnated into the biomass prior to pyrolysis at a temperature of 450-900 °C. H₃PO₄ activation can not only introduce microspores but also P-containing functional groups into biochar, which can greatly improve the performance of the biochar materials in electrochemical energy storage. It has been found that ZnCl₂ can greatly increase the surface area and porous volume of the biochar produced [43].

In addition to in situ catalytic pore formation during biomass pyrolysis, pore structure tailoring through post activation also were used to tailor the pore structure. Two steps are commonly involved in the post activation process: (1) direct pyrolysis/HTL of the biomass to produce original biochar with a very low pore volume and surface area and (2) activation of the biochar using physical or chemical methods to improve its porous structure and surface area. Post activation mainly includes physical activation with different oxidizing gases (*e.g.*, air, O₂, CO₂, steam or their mixtures) and chemical

activation with KOH, NaOH, H₃PO₄ or ZnCl₂. In the physical activation process, a carbon precursor is first exposed to pyrolysis in an inert atmosphere at 400-900 °C to eliminate the bulk of volatile matter, followed by partial gasification using an oxidizing gas at 350-1000 °C. The chemical activation process consists of the heat-treatment of a mixture of the carbon precursor and the activating agent at a temperature normally in the 450-900 °C range [45]. In addition to conventional physical and chemical activation, some other approaches, such as templating, also have the potential to introduce porosity into biochar, although to date no such reports on biochar pore structure tailoring have appeared [46]. Two stage activation processes consisting of chemical activation step followed by physical activation have also been used to further enhance the porosity development and tune the pore structure [47].

Biochar nanocomposites

Controlled synthesis of carbonaceous nanocomposites has become a hot research area, due to their improved hybrid properties with high potential values in many fields. As a result of the recombination of specific nanostructures on their surfaces, biochar-based nanocomposites can be imparted with hybrid properties that in turn open up potential applications in many fields. The final nanocomposites have been shown to be utile in many application fields, including catalysis, fuel cells, drug delivery, and bio-imaging [48].

Two main methodologies are identified for the synthesis of such biochar-based nanocomposites: post-modification and in situ synthesis. The post-modification method implies coating of performed nanostructures (*e.g.*, silica sphere, Fe₃O₄) or incorporation of inorganic nanostructures onto biochar materials (*e.g.*, Ag, Au, Pt, and Pd) [48-51]. The in situ synthesis method implies of loading of metal nanoparticles directly to the biochar via a simple one step approach [8].

Application of Biochar Materials

The most promising feature of the biochar-based material is that it's sustainable and easily scalable allowing the production of different functionalized carbon and hybrid nanostructures with a range of practical applications. To date, the application of biochar was primarily focused on using biochar as a soil amendment. New state of the art applications of biochar is emerging, although most of the applications are still in their infancy. These applications include but not limited to energy production, agriculture, carbon sequestration, wastewater treatment, biorefinery, etc. Since many of the review articles have summarized the advances of activated carbon or biochar materials in environmental protection, and agriculture applications, we will not cover this topic in detail in this review. Here, we briefly summarize recent progress and the state of art in applications of biochar in catalysis and energy storage.

Catalytic application

Biochar containing SO₃H groups, also called biochar-based solid acids, represents a type of metal-free catalyst that is ubiquitously used in a wide variety of chemical reactions. The biochar-based solid acids have been demonstrated to be efficient catalysts for various acid-catalyzed reactions, such as the esterification of organic acids in an aqueous medium, acylation of alcohols and amines, and the alkylation of aromatics, as

well as the hydrolysis of biomass itself [52]. Biodiesel production through esterification is a typical reaction catalyzed by solid acids.

It is well-known that the performance of metal nanoparticle catalysts is greatly affected by their supporting materials. Biochar materials have been straightforwardly studied as supports to stabilize metal nanoparticles for different catalytic applications due to their high surface areas and functionalities, such as syngas cleaning and conversion of syngas into liquid hydrocarbons via Fischer-Tropsch synthesis [53]. Table 3 summarizes the recent studies on biochar catalytic applications.

Table 3. Biochar unitization for catalytic applications

Application	Biochar type	Effect	Reference
Syngas cleaning	Pine bark (950°C)	Tar reduction	[54]
Syngas cleaning	Ni-Fe catalyst supported on rice husk biochar	In-situ catalytic conversion of tar	[55]
Syngas cleaning	Acidic surface activated carbon from switchgrass	Tar, NH ₃ , H ₂ S removal	[56]
Fischer-Tropsch synthesis of syngas into liquid hydrocarbons	Biochar-based iron nanoparticle from pine wood pyrolysis	High efficiency of converting syngas into liquid hydrocarbon	[57]
Methane reforming	Pt-Ru alloy nanoparticles supported on HTC biochar of furfural	Hydrocarbon catalytic oxidations; heterogeneous catalysis	[58]
Biodiesel production	Biochar-derived acid catalyst prepared by sulfonating biochar with concentrated sulfuric acid	Transesterification of canola oil with alcohol and oleic acid due to high surface area and acid density	[59]
Biodiesel production	Biochar-based catalysts made from peanut hulls, pine residues, and wood chips	High efficiency in esterification of free fatty acids of vegetable oil and animal fat with methanol and high reusability due to their particle strength hydrophobicity, high surface area, and sulfonic acid group density.	[60]
Hydrolysis of biomass	Biochar sulfonic acid catalysts prepared from bamboo, cotton, and starch	High turnover number values for cellulose hydrolysis due to the multifunctional action of strong -SO ₃ H, -COOH, and -OH groups	[61]
Catalysis of various oxidation and reduction reactions	Carbonaceous nanofibers (CNFs) prepared through a template-directed HTC process	Displayed the persistent catalytic ability in a continuous-flow mode	[62]
Acylation reaction	Starch biochar-silica composites bearing SO ₃ H as the heterogeneous catalysts	Reactants with NH ₂ , OH, SH groups can be quickly acylated to yield target products with very high yields.	[63]

As shown in Table 3, biochar-based catalysts demonstrate favorable catalytic performance in various reactions. Besides, it can be recycled for several runs without significant loss of activity. However, it has relative low efficiency and low abrasive resistance compared with the commercial catalyst. In addition, the inorganic species in biochar may cause catalyst poisoning, thus decreasing the catalytic activity in some organic or electrochemical reactions [64]. Therefore, there is a need to develop new and sustainable ways to tailor the physicochemical properties of such catalysts in order to adopt them for specific applications.

Energy storage application (Supercapacitor)

Supercapacitor, an energy storage device, has received attention to harvest energy due to its high-power density, long cycle life, and quick charge/discharge capability [65]. Supercapacitor can be used as uninterruptible power sources in electric vehicles, digital communications system, etc. The microstructure of supercapacitor electrodes has a great influence on supercapacitor performance. Carbon material with high surface area and rich porous structure are the primary raw materials for making supercapacitors due to its wide availability and low environmental impacts [66]. Producing attractive, high quality carbon material at low cost is critical for the development of the supercapacitor industry [67]. Table 4 listed some recent research activities regarding to the fabrication of supercapacitors using biochar from different feedstocks.

Table 4. Supercapacitor performance of electrodes made from various precursors

Material	Surface area (m ² /g)	Capacitance (F/g)	Reference
Activated carbon from rubber wood sawdust	<920	8-139	[68]
Carbon nanotubes(CNTs) from oil palm fruit bunches	1656	111	[69]
Nanoporous carbons from sunflower seed shell	2509	311	[70]
Functional microporous conducting carbon from dead leaves	3404	273	[71]
Templated carbon from acrylonitrile	1680	340	[72]

Results indicated that the use of biochar is promising as an electrode due to its low cost and satisfactory performance. One of the great challenges in the development of supercapacitor technology is the relatively high cost when compared to other energy devices. Thus, future research should be directed towards the development of biochar-based functional materials with high charge capacity and minimum equivalent series resistance in a cost-effective way. One-step synthesis without an additional activation process to obtain high density carbon or composite materials would be beneficial for the compact design of high power energy sources.

CONCLUSIONS

Recent advances in the biochar production, formation mechanism, and characterization are discussed in detail in this review. It is essential to modify the surface functionality and the porosity of biochar in order to enhance the performance of biochar materials for various applications. Processes used for turning the surface functionalities and pore structure of biochar, including surface oxidation, amination, sulfonation, pore structure modification, and recombination, are summarized and discussed. Abundant functional groups (e.g., C=O, -COOH, NH₂, and SO₃H), metal nanoparticles and inorganic nanostructures can be introduced onto the biochar surface. This allows the production of materials with different functionalized carbon and hybrid nanostructures for a range of practical applications. Recent progress and the state of art in applications of biochar in catalysis and energy storage are reviewed. Biochar-based catalysts exhibit favorable catalytic properties in a variety of reactions. In addition, the development of novel biochar materials, such as carbon nanotubes, functional microporous carbon, and activated carbons remain a primary choice for the construction of electrodes for commercial supercapacitor due to its low cost and satisfactory performance. Overall, the use of biochar as sustainable high-value materials seems to have a very promising future, and biochar properties need to be further improved and tailored for the appropriate applications.

ACKNOWLEDGMENTS

This research was supported by a grant from the USDA-CSREES-Evans-Allen Project, Grant No. NCX-303-5-17-130-1.

CONFLICTS OF INTEREST

The authors declare that there is no conflict of interests regarding the publication of this paper.

REFERENCES

- [1] Boo Linares, N., Silvestre-Albero, A. M., Serrano, E., Silvestre-Albero, J., Garcia Martinez, J. (2014). Mesoporous materials for clean energy technologies. *Chem. Soc. Rev.* 43, 7681– 7717. DOI: 10.1039/c3cs60435g
- [2] Hu, B.; Wang, K.; Wu, L.; Yu, S.-H.; Antonietti, M.; Titirici, M.-M. (2010) Engineering carbon materials from the hydrothermal carbonization process of biomass. *Adv. Mater.* 22, 813– 828. DOI: 10.1002/adma.200902812
- [3] Xie, J., Hse, C., Shupe T., Hu, T. (2015). Physicochemical characterization of lignin recovered from microwave-assisted delignified lignocellulosic biomass for use in biobased materials. *Journal of Applied Polymer Science*, DOI: 10.1002/APP.42635
- [4] Initiate IB. (2012). Standardized product definition and product testing guidelines for biochar that is used in soil. *International Biochar Initiative*. <http://www.biochar->

- international.org/sites/default/files/Guidelines_for_Biochar_That_Is_Used_in_Soil_Final.pdf (Accessed on 2/2/2017)
- [5] Qian, K.; Kumar, A.; Zhang, H.; Bellmer, and Huhnke, R. (2015) Recent advances in utilization of biochar. *Renewable and Sustainable Energy Reviews*. 42, 1055-1064. DOI: 10.1016/j.rser.2014.10.074
- [6] Namaalwa, J.; Sankhayan, P. L.; Hofstad, O. (2007) A dynamic bio-economic model for analyzing deforestation and degradation: An application to woodlands in Uganda. *Forest Policy Economics* 9, 479– 495. DOI: 10.1016/j.forpol.2006.01.001
- [7] Meyer, S.; Glaser, B.; Quicker, P. (2011). Technical, economical, and climate-related aspects of biochar production technologies: A literature review. *Environ. Sci. Technol.* 45, 9473– 9483. DOI: 10.1021/es201792c
- [8] Titirici M-M; White RJ; Falco C; Sevilla M. Black perspectives for a green future: hydrothermal carbons for environment protection and energy storage. (2012). *Energy Environ. Sci.* 5, 6796-6822. DOI: 10.1039/C2EE21166A
- [9] Wiedner, C.; Rumpel, C.; Steiner, A.; Pozzi, R.; Maas, B. Glaser. (2013) Chemical evaluation of chars produced by thermochemical conversion (gasification, pyrolysis and hydrothermal carbonization) of agro-industrial biomass on a commercial scale. *Biomass Bioenergy*, 59, 264–278. DOI: 10.1016/j.biombioe.2013.08.026
- [10] Xiu S.; Shahbazi A. (2012) Bio-oil Production and Upgrading Research: A Review. *Renewable and Sustainable Energy Reviews*, 16(7), 4406-4414. DOI: 10.1016/j.rser.2012.04.028
- [11] Kambo, H.S.; Dutta, A. (2015) A comparative review of biochar and hydrochar in terms of production, physical-chemical properties and applications. *Renewable and Sustainable Energy Reviews* 45, 359-378. DOI: 10.1016/j.rser.2015.01.050
- [12] Shen, D. K.; Gu, S. (2009) The mechanism for thermal decomposition of cellulose and its main products. *Bioresour. Technol.* 100, 6496– 6504. DOI: 10.1016/j.biortech.2009.06.095
- [13] Peters, B. (2011). Prediction of pyrolysis of pistachio shells based on its components hemicellulose, cellulose and lignin. *Fuel Process. Technol.* 92, 1993– 1998. DOI: 10.1016/j.fuproc.2011.05.023
- [14] Antal, M. J.; Grønli, M. (2003). The art, science, and technology of charcoal production. *Ind. Eng. Chem. Res.* 42, 1619–1640. DOI: 10.1021/ie0207919
- [15] Minowa, T.; Kondo, T.; Sudirjo, S.T. (1998) Thermochemical liquefaction of Indonesian biomass residues. *Biomass & Bioenergy*, 14(5-6), 517-524. DOI: 10.1016/S0961-9534(98)00006-3
- [16] Xiu S.; Zhang B.; Shahbazi A. (2011). Biorefinery Processes for Biomass Conversion to Liquid Fuel. In: *Biofuel's Engineering Process Technology*; Marco A.D. Bernardes, Ed.; InTech, pp: 167-190.
- [17] Carpenter, S. R.; Caraco, N. F.; Correll, D. L.; Howarth, R.W.; Sharpley, A.N., Smith, V. H. (1998) Nonpoint pollution of surface waters with phosphorus and nitrogen. *Ecological Applications* 8, 559–568. DOI: 10.1890/1051-0761(1998)008[0559:NPOSWW]2.0.CO;2
- [18] Matteson, G. C; Jenkins, B. M. (2007) Food and processing residues in California: Resource assessment and potential for power generation. *Bioresour. Technol.*, 98, 3098–3105. DOI: 10.1016/j.biortech.2006.10.031
- [19] Cantrell, K.; Ro, K.; Mahajan, D.; Anjom, M.; Hunt, P.G. (2007) Role of thermochemical conversion in livestock waste-to-energy treatments: Obstacles and

- opportunities. *Industrial and Engineering Chemistry Research* 46, 8918–8927. DOI: 10.1021/ie0616895
- [20] Joan J., Manyà. (2012) Pyrolysis for biochar purposes: A review to establish current knowledge gaps and research needs. *Environmental Science & Technology*, 46, 7939–7954. DOI: 10.1021/es301029g
- [21] Brown, T. R.; Wright, M. M.; Brown, R. C. (2011). Estimating profitability of two biochar production scenarios: slow pyrolysis vs fast pyrolysis. *Biofuels, Bioprod. Biorefin.* 5, 54– 68. DOI: 10.1002/bbb.254
- [22] Liao, C.; Wu, C.; Yan, Y. (2007). The characteristics of inorganic elements in ashes from a 1MW CFB biomass gasification power generation plant. *Fuel process. Technol.*, 88, 149–156. DOI: 10.1016/j.fuproc.2005.06.008
- [23] Li, R.; Zhang, B.; Xiu, S.N.; Wang, H., Wang, L.J.; Shahbazi, A. (2015). Characterization of Solid Residues Obtained from Supercritical Ethanol Liquefaction of Swine Manure. *American Journal of Engineering and Applied Sciences*, 8.4: 465–470.
- [24] Brewer, C.E.; Schmidt-Rohr, K.; Satrio, J.A.; Brown, R.C. (2009). Characterization of biochar from fast pyrolysis and gasification systems. *Environ. Prog. Sustainable Energy*, 28, 386–396. DOI: 10.1002/ep.10378
- [25] Spokas, K. A.; Novak, J. M.; Masiello, C. A.; Johnson, M. G.; Colosky, E. C.; Ippolito, J. A.; Trigo, C. (2014). Physical disintegration of biochar: An overlooked process. *Environ. Sci. Technol. Lett.* 1, 326–332. DOI: 10.1021/ez500199t
- [26] Sharma, R. K.; Wooten, J. B.; Baliga, V. L.; Lin, X.; Geoffrey Chan, W.; Hajaligol, M. R. (2004). Characterization of chars from pyrolysis of lignin. *Fuel* 83, 1469–1482. DOI: 10.1016/j.fuel.2003.11.015
- [27] Freitas, J. C. C.; Bonagamba, T. J.; Emmerich, F. G. (2001). Investigation of biomass and polymer-based carbon materials using ^{13}C high-resolution solid-state NMR. *Carbon* 39, 535– 545. DOI: 10.1016/S0008-6223(00)00169-X
- [28] Mukome, F. N. D.; Zhang, X.; Silva, L. C. R.; Six, J.; Parikh, S. J. (2013). Use of chemical and physical characteristics to investigate trends in biochar feedstocks. *J. Agric. Food Chem.* 61, 2196–2204. DOI: 10.1021/jf3049142
- [29] Gao, Y.; Wang, X.H.; Yang, H.P.; Chen, H.P. (2012). Characterization of products from hydrothermal treatments of cellulose. *Energy*, 42, 457–465. DOI: 10.1016/j.energy.2012.03.023
- [30] Qian, L.; Chen, B. (2014). Interactions of aluminum with biochars and oxidized biochars: Implications for biochar aging process. *J. Agric. Food Chem.* 62, 373–380. DOI: 10.1021/jf404624h
- [31] Lehmann, J.; Joseph, S. (2009). *Biochar for environmental management: science and technology*; Earthscan: London.
- [32] Liu, W.J.; Zeng, F.X.; Jiang, H.; Zhang, X.S. (2011). Preparation of high adsorption capacity bio-chars from waste biomass. *Bioresour. Technol.* 102, 8247–8252. DOI: 10.1016/j.biortech.2011.06.014
- [33] Li, Y.; Shao, J.; Wang, X.; Deng, Y.; Yang, H.; Chen, H. (2014). Characterization of modified biochars derived from bamboo pyrolysis and their utilization for target component (furfural) adsorption. *Energy Fuels* 28, 5119– 5127. DOI: 10.1021/ef500725c
- [34] Xu, D.; Zhao, Y.; Sun, K.; Gao, B.; Wang, Z.; Jin, J.; Zhang, Z.; Wang, S.; Yan, Y.; Liu, X.; Wu, F. (2014). Cadmium adsorption on plant- and manure-derived biochar

- and biochar-amended sandy soils: Impact of bulk and surface properties. *Chemosphere*, 111, 320–326. DOI: 10.1016/j.chemosphere.2014.04.043
- [35] Anfruns, A.; García-Suárez, E. J.; Montes-Morán, M. A.; Gonzalez-Olmos, R.; Martin, M. J. (2014). New insights into the influence of activated carbon surface oxygen groups on H₂O₂ decomposition and oxidation of pre-adsorbed volatile organic compounds. *Carbon*, 77, 89–98. DOI: 10.1016/j.carbon.2014.05.009
- [36] Wu, L.; Sitamraju, S.; Xiao, J.; Liu, B.; Li, Z.; Janik, M. J.; Song, C. (2014). Effect of liquid-phase O₃ oxidation of activated carbon on the adsorption of thiophene. *Chem. Eng. J.*, 242, 211–219. DOI: 10.1016/j.cej.2013.12.077
- [37] Gokce, Y.; Aktas, Z. (2014). Nitric acid modification of activated carbon produced from waste tea and adsorption of methylene blue and phenol. *Appl. Surf. Sci.*, 313, 352–359. DOI: 10.1016/j.apsusc.2014.05.214
- [38] Adelodun, A. A.; Lim, Y. H.; Jo, Y. M. (2014). Stabilization of potassium-doped activated carbon by amination for improved CO₂ selective capture. *J. Anal. Appl. Pyrolysis*, 108, 151–159. DOI: 10.1016/j.jaap.2014.05.005
- [39] Shafeeyan, M. S., Wan Daud, W. M. A., Houshmand, A., Arami-Niya, A. (2012). The application of response surface methodology to optimize the amination of activated carbon for the preparation of carbon dioxide adsorbents. *Fuel*, 94, 465–472. DOI: 10.1016/j.fuel.2011.11.035
- [40] Takagaki, A.; Tagusagawa, C.; Hayashi, S.; Hara, M.; Domen, K. (2010) Nanosheets as highly active solid acid catalysts for green chemical syntheses. *Energy Environ. Sci.* 3, 82. DOI: 10.1039/B918563A
- [41] Dehkhoda, A. M., West, A. H., Ellis, N. (2013). Biochar based solid acid catalyst for biodiesel production. *Appl. Catal., A.*, 382, 197–204. DOI: 10.1016/j.apcata.2010.04.051
- [42] Taberna, P.-L., Gaspard, S. (2014). CHAPTER 9. Nanoporous Carbons for High Energy Density Supercapacitors. In: *Biomass for Sustainable Applications: Pollution Remediation and Energy*, S. Gaspard, and M. C. Ncibi, eds., The Royal Society of Chemistry, pp: 366–399. DOI:10.1039/9781849737142-00366
- [43] Sun, L.; Tian, C.; Li, M.; Meng, X.; Wang, L.; Wang, R.; Yin, J.; Fu, H. (2013). From coconut shell to porous graphene-like nanosheets for high-power supercapacitors. *J. Mater. Chem. A*, 1, 6462–6470. DOI: 10.1039/C3TA10897J
- [44] Hulicova-Jurcakova, D.; Puziy, A. M.; Poddubnaya, O. I.; Suárez-García, F.; Tascón, J. M. D.; Lu, G. Q. (2009). Highly stable performance of supercapacitors from phosphorus-enriched carbons. *J. Am. Chem. Soc.*, 131, 5026–5027. DOI: 10.1021/ja809265m
- [45] Sevilla, M.; Mokaya, R. (2014). Energy storage applications of activated carbons: supercapacitors and hydrogen storage. *Energy & Environmental Science*, 7, 1250–1280. DOI: 10.1039/C3EE43525C
- [46] Gaspard, S., Passe-Coutrin, N., Durimel, A., Cesaire, T., and Jeanne-Rose, V. (2014). CHAPTER 2 Activated Carbon from Biomass for Water Treatment. In: *Biomass for Sustainable Applications: Pollution Remediation and Energy*, S. Gaspard, and M. C. Ncibi, eds., The Royal Society of Chemistry, pp: 46–105. DOI: 10.1039/9781849737142-00046
- [47] Hu, Z.; Guo, H.; Srinivasan, M.P.; Yaming, N. (2003). A Simple Method for Developing Mesoporosity in Activated Carbon. *Sep. Purif. Technol.* 31, 47–52. DOI: 10.1016/S1383-5866(02)00148-X

- [48] Hu, B.; Yu, S.H.; Wang, K.; Liu, L.; Xu, X.W. (2008). Functional carbonaceous materials from hydrothermal carbonization of biomass: an effective chemical process. *Dalton Trans.*, 5414-5423. DOI: 10.1039/B804644C
- [49] Sun, X.M; Li, Y.D. (2004). Colloidal carbon spheres and their core/shell structures with noble-metal nanoparticles. *Angew Chem., Int. Ed.*, 43, 597–601. DOI: 10.1002/anie.200352386
- [50] Qian, H. S.; Antonietti, M.; Yu, S. H. (2007). Hybrid “Golden Fleece”: Unique approaches for synthesis of uniform carbon nanofibres and silica nanotubes embedded/confined with high population of noble metal nanoparticles and their catalytic performance. *Adv. Funct. Mater.*, 17, 637–643.
- [51] Hu, B.; Zhao, Y.; Zhu, H.Z.; Yu, S.H. (2011). Selective chromogenic detection of thiol-containing biomolecules using carbonaceous nanospheres loaded with silver nanoparticles as carrier. *ACS nano*, 5 (4), 3166-3171. DOI: 10.1021/nm2003053
- [52] Zhou, C.H., Xia, X., Lin, C.X., Tong, D.S., Beltramini, J. (2011). Catalytic conversion of lignocellulosic biomass to fine chemicals and fuels. *Chem. Soc. Rev.* 40, 5588-5617. DOI: 10.1039/C1CS15124J
- [53] Wang, S., Wang, H., Yin, Q., Zhu, L., Yin, S. (2014). Methanation of bio-syngas over a biochar supported catalyst. *New J. Chem.* 38, 4471– 4477. DOI: 10.1039/C4NJ00780H
- [54] Mani, J.R; Kastner, A; Juneja. (2013). Catalytic decomposition of toluene using a biomass derived catalyst. *Fuel Process Technol*, 114, 118–125. DOI: 10.1016/j.fuproc.2013.03.015
- [55] Shen, Y.; Zhao, P.; Shao, Q.; Ma, D.; Takahashi, F.; Yoshikawa, K. (2014). In-situ catalytic conversion of tar using rice husk char-supported nickel-iron catalysts for biomass pyrolysis/gasification. *Appl Catal B: Environ*, 152–153, 140–151. DOI: 10.1016/j.apcatb.2014.01.032
- [56] Bhandari, P.N.; Kumar, A.; Huhnke, R.L. (2013). Simultaneous removal of toluene (model tar), NH₃, and H₂S, from biomass-generated producer gas using biochar-based and mixed-metal oxide catalysts. *Energy Fuels*, 28, 1918–1925. DOI: 10.1021/ef4016872
- [57] Yan, Q.; Wan, C.; Liu, J.; Gao, J.; Yu, F.; Zhang, J. (2013). Iron nanoparticles in situ encapsulated in biochar-based carbon as an effective catalyst for the conversion of biomass-derived syngas to liquid hydrocarbons. *Green Chem*, 15, 1631–1640. DOI: 10.1039/C3GC37107G
- [58] Matosa, J.; Rosalesa, M.; Rezan, D.C., Titiricib, M.M. (2010). Methane conversion on Pt–Ru nanoparticles alloy supported on hydrothermal carbon. *Appl. Catal., A*, 386, 140-146. DOI: 10.1016/j.apcata.2010.07.047
- [59] Dehkhoda, A.M.; Ellis, N. (2013). Biochar-based catalyst for simultaneous reactions of esterification and transesterification. *Catal Today*, 207, 86–92. DOI: 10.1016/j.cattod.2012.05.034
- [60] Kastner, J.R.; J. Miller; D.P. Geller; J. Locklin; L.H. Keith; T. Johnson. (2012). Catalytic esterification of fatty acids using solid acid catalysts generated from biochar and activated carbon. *Catal Today*, 190, 122–132. DOI: 10.1016/j.cattod.2012.02.006
- [61] Wu, Y.; Fu, Z.; Yin, D.; Xu, Q.; Liu, F.; Lu, C.; Mao, L. (2010). Microwave-assisted hydrolysis of crystalline cellulose catalyzed by biomass char sulfonic acids. *Green Chem*, 12, 696-700. DOI: 10.1039/B917807D

- [62] Liang, H.W.; Zhang, W.J.; Ma, Y.N.; Cao, X.; Guan, Q.F., Xu, W.P.; Yu, S.H. (2011). Highly Active Carbonaceous Nanofibers: A Versatile Scaffold for Constructing Multifunctional Free-Standing Membranes. *ACS Nano*, 5 (10), 8148–8161. DOI: 10.1021/nn202789f
- [63] Gupta, P.; Paul, S. (2011). Amorphous carbon-silica composites bearing sulfonic acid as solid acid catalysts for the chemoselective protection of aldehydes as 1,1-diacetates and for N-, O- and S-acylations. *Green Chem.* 13, 2365-2372. DOI: 10.1039/C0GC00900H
- [64] Bhandari, P. N.; Kumar, A.; Bellmer, D. D.; Huhnke, R. L. (2014). Synthesis and evaluation of biochar-derived catalysts for removal of toluene (model tar) from biomass-generated producer gas. *Renewable Energy*, 66, 346– 353. DOI: 10.1016/j.renene.2013.12.017
- [65] Xiao, Y.H.; Zhang, A.Q.; Liu, S.J. Zhao, J.H.; Fang, S.M. Jia, D.Z. (2012). Free-standing and porous hierarchical nanoarchitectures constructed with cobalt cobaltite nanowalls for supercapacitors with high specific capacitances. *J Power Sources*, 219, 140–146. DOI: 10.1016/j.jpowsour.2012.07.030
- [66] Liu, M.C.; Kong, L.B.; Zhang, P.; Luo, Y.C.; Kang, L. (2012). Porous wood carbon monolith for high-performance supercapacitors. *Electrochim Acta*, 60, 443–448. DOI: 10.1016/j.electacta.2011.11.100
- [67] Zhang, L.; Zhao, X.S. (2009). Carbon-based materials as supercapacitor electrodes. *Chemical Society Reviews*, 38, 2520-2531. DOI: 10.1039/B813846J
- [68] Taer, E.; Deraman, M.; Tali, I.A., Awitdrus, A.; Hashmi, A.; Umar, A.A. (2011). Preparation of a Highly Porous Binderless Activated Carbon Monolith from Rubber Wood Sawdust by a Multi-Step Activation Process for Application in Supercapacitors. *International journal of electrochemical science* 6(8):3301-3315.
- [69] Basri, N.H.; M. Deraman; S. Kanwal; I.A. Talib; J.G. Manjunatha; A.A. Aziz. (2013). Supercapacitors using binderless composite monolith electrodes from carbon nanotubes and pre-carbonized biomass residues. *Biomass Bioenergy*, 59, 370–379. DOI: 10.1016/j.biombioe.2013.08.035
- [70] Li, X.; Xing, W.; Zhou, S.P.; Zhou, J.; Li, F.; Qiao, S.Z.; Lu, G.Q. (2011). Preparation of capacitor's electrode from sunflower seed shell. *Bioresour. Technol.* 102(2):1118-1123. DOI: 10.1016/j.biortech.2010.08.110
- [71] Biswal, M.; Banerjee, A.; Deo, M.; Ogale, S. (2013). From dead leaves to high energy density supercapacitors. *Energy Environ. Sci.* 6, 1249-1259. DOI: 10.1039/C3EE22325F

Article copyright: © 2017 Shuangning Xiu, Abolghasem Shahbazi, and Rui Li. This is an open access article distributed under the terms of the [Creative Commons Attribution 4.0 International License](https://creativecommons.org/licenses/by/4.0/), which permits unrestricted use and distribution provided the original author and source are credited.





CALL FOR PAPERS

Trends in Renewable Energy

ISSN Print: 2376-2136 ISSN online: 2376-2144

<http://futureenergysp.com/index.php/tre/>

Trends in Renewable Energy (TRE) is an open accessed, peer-reviewed semi-annual journal publishing reviews and research papers in the field of renewable energy technology and science. The aim of this journal is to provide a communication platform that is run exclusively by scientists. This journal publishes original papers including but not limited to the following fields:

- ✧ Renewable energy technologies
- ✧ Catalysis for energy generation, Green chemistry, Green energy
- ✧ Bioenergy: Biofuel, Biomass, Biorefinery, Bioprocessing, Feedstock utilization, Biological waste treatment,
- ✧ Energy issues: Energy conservation, Energy delivery, Energy resources, Energy storage, Energy transformation, Smart Grid
- ✧ Environmental issues: Environmental impacts, Pollution
- ✧ Bioproducts
- ✧ Policy, etc.

We publish the following article types: peer-reviewed reviews, mini-reviews, technical notes, short-form research papers, and original research papers.

The article processing charge (APC), also known as a publication fee, is fully waived for the Trends in Renewable Energy.

Call for Editorial Board Members

We are seeking scholars active in a field of renewable energy interested in serving as volunteer Editorial Board Members.

Qualifications

Ph.D. degree in related areas, or Master's degree with a minimum of 5 years of experience.

All members must have a strong record of publications or other proofs to show activities in the energy related field.

If you are interested in serving on the editorial board, please email CV to

editor@futureenergysp.com.